X-RAY DIFFRACTION STUDIES OF THE SOLID—LIQUID TRANSITION OF SODIUM

DISSERTATION

Presented in Partial Fulfillment of the Requirements
for the Degree Doctor of Philosophy in the
Graduate School of The Ohio State
University

By

BERNARD ANDREW KULP, B. E. E., M. Sc.

*****

The Ohio State University
1955

Approved by:

Adviser
Department of Physics and Astronomy

ACKNOWLEDGMENTS

I wish to acknowledge first the help and guidance of Dr. Shaw throughout my post graduate studies and particularly with this problem. He has contributed significantly to my education and research training. I wish also to thank Mr. Carl McWirt and the members of the Physics Shop for aiding in the mechanical construction of the apparatus and equipment, Mr. Harold Recher for assisting me in taking the data, and the other members of the X-Ray Laboratory.

I also acknowledge the many inspiring discussions with Dr. Speiser of the Department of Metallurgy during the course of the experiments, and his interest and criticism of this dissertation, and Dr. Preston Harris of the Department of Chemistry for aid in the x-ray diffraction studies of the sample.

Finally, I wish to thank my wife, Ruth, for her patience and perseverence during my school career, and for the excellent typing of this dissertation.

TABLE OF CONTENTS

LIST OF FIGURES

LIST OF TABLES

X-RAY DIFFRACTION STUDIES OF THE SOLID—LIQUID TRANSITION OF SODIUM

By

BERNARD ANDREW KULP

I INTRODUCTION

It is well established that the heat motion of the atoms of a crystal affect the diffracted intensity of x-rays. In general, for high-melting substances at room temperature or substances far from their melting points, this effect may not be noticeable. However, as the temperature is raised to the melting point, the intensity of reflection decreases until the line disappears at the melting point. The pattern of the crystalline state of the material thus passes to the pattern for the liquid state.

Debye[1] was the first to calculate the effect of thermal vibrations on the scattering power of a crystal. His first work considered the atoms to be independent of each other. Later calculations by Debye and Waller[2] have

[1] Debye, P., Ann. d. Physik, 43, 49(1914).

[2]Waller, I., Zeit. f. Physik, 17, 398(1923).
51, 213(1928).

resulted in a theory for the effect of temperature on the intensity of the x-ray diffraction lines that is well borne out by experiment. In general, the width of the line is not changed by the thermal vibrations, but the intensity is diminished. The theory is expected to hold rigorously for cubic crystals, of one kind of atom and at temperatures not too near the melting point.

As far as the author knows, no experiments have been designed to study the intensity of an x-ray diffraction line through the melting point. For the experiments to be described here, apparatus was designed and constructed to follow accurately the intensity of a powder diffraction line from a solid as it was carried through the melting range. Metallic sodium was chosen as the material to be investigated for several reasons: The melting point is in an experimentally convenient temperature region so that an emulsion in an inert oil could be easily prepared; the scattering power for x-rays is high while the absorption is fairly low; the catalyzer for heterogeneous nucleation (NaOH) is easily formed; sodium is a "simple" metal whose structure is well known; and lastly this metal has received a great deal of attention from the theorists and its

properties are perhaps best understood of all the metals. It seemed sufficient to study the intensity of one line, so the 110 line at $2\theta = 29.5^{\circ}$ for $CuK\alpha$ radiation was used.

Early in the studies, it was established that in order to obtain reproducible results, the sample had to be in the form of small particles isolated from each other, so that they did not coalesce on melting. The rate of crystal growth of sodium is very high, so that once melted, it was impossible to solidify a bulk sample in a condition to give a powder pattern. The sample used throughout the experiments consisted of a dispersion of sodium in mineral oil. There was a 50 percent solid content in the dispersion and a particle size range with the maximum size of the order of 2 microns (10^{-4} cm.) in diameter. The melting characteristics of such a sample are not expected to differ greatly from the melting characteristics of a bulk sample. The solidification characteristics, however, should, and do, show some very unusual effects, directly ascribable to the particle size and surface coating of the droplets in the dispersion.

II APPARATUS AND EQUIPMENT

The apparatus designed and constructed for the work consisted of a high voltage power supply with voltage and current regulators and a thermostatically controlled sample chamber together with a proportional counter x-ray detector

with associated amplifiers and counting equipment.

2.1 High Voltage Power Supply

A high voltage power supply for the copper target Machlett A-2 diffraction tube was designed and built. The unit consists of a single high voltage source and two current sources with separate controls and regulators, so that two x-ray tubes may be operated simultaneously without interference. The design is based upon that of a similar power supply built by James Collenge[3] and described by him. Sufficient difference in the design and construction of this unit makes a short description worthwhile. Figure 1 shows the overall schematic of the supply. The voltage is regulated by means of a series tube in the high voltage line and the current is regulated by means of a series impedance in the primary circuit of the filament transformers.

[3] Collenge, J. P., Thesis, M.S., Ohio State University(1949).

Line power is supplied to the various components of the power supply through a series of switches and interlocks. The status of the various components is indicated by pilot lights. Figure 2 shows the circuit diagram for the power and safety circuits and the location of the variacs and terminal strips. The main power switch and the protective current relays are located at the rear of the

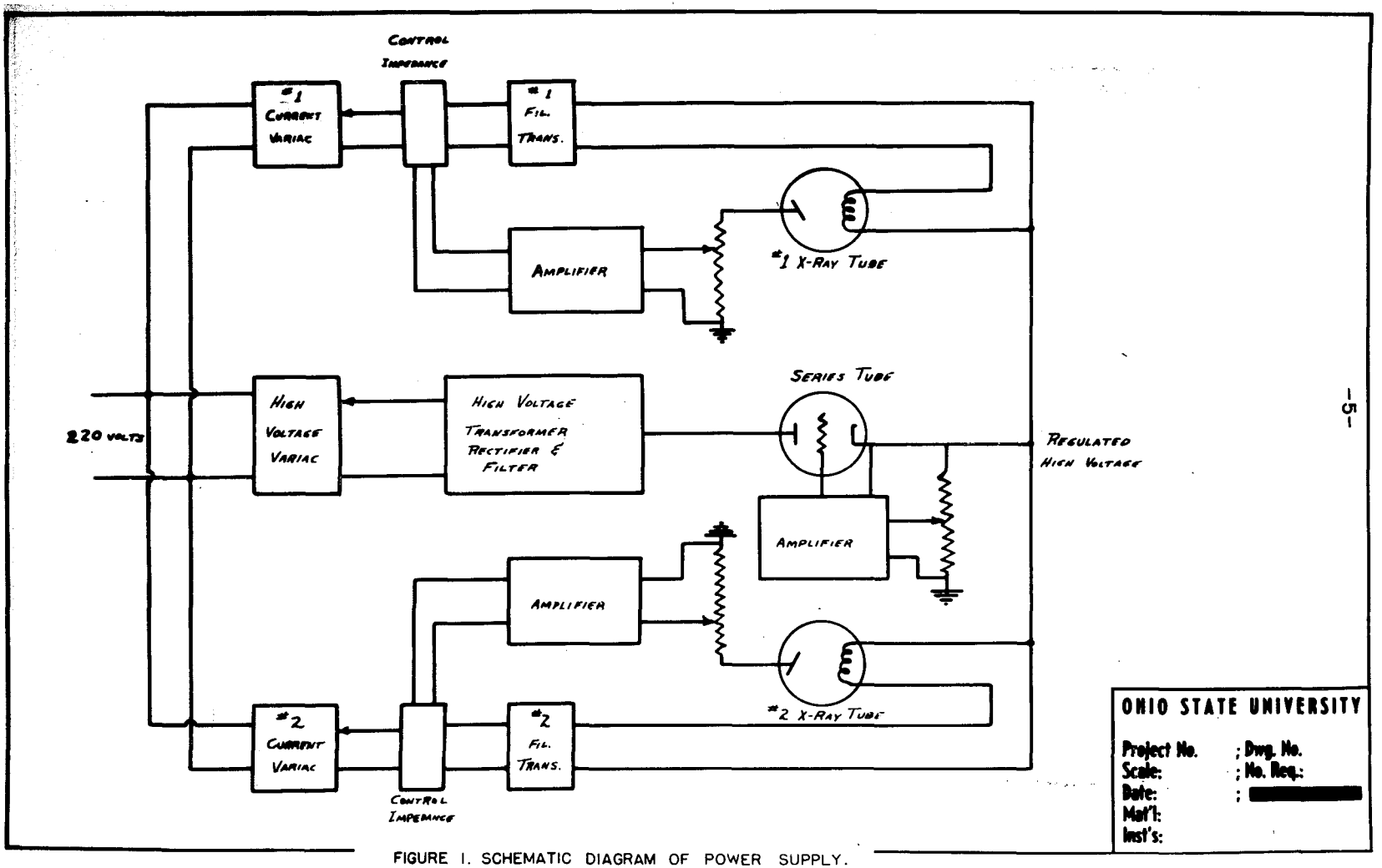

FIGURE 1. SCHEMATIC DIAGRAM OF POWER SUPPLY.

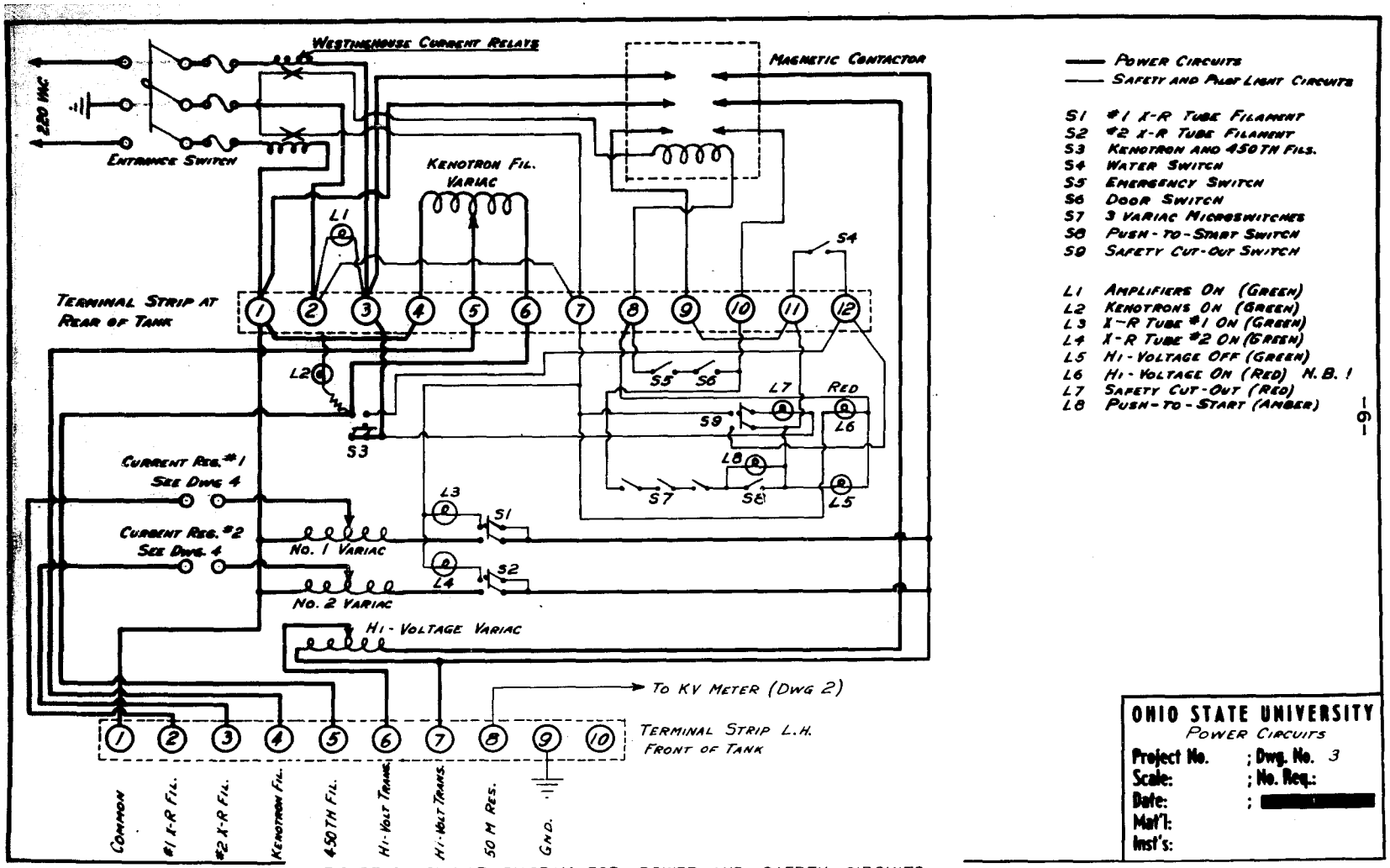

FIGURE 2. CIRCUIT DIAGRAM FOR POWER AND SAFETY CIRCUITS.

cabinet. The kenotron filament variac, the magnetic contractor and a terminal strip are located on this same panel, but facing the inside of the cabinet. All other controls are located on the front panel with the amplifiers. Figure 3 is a picture of the cabinet showing the front panel.

The high voltage transformer, rectifiers and filter, as well as the filament transformers and the high voltage sampling resistor are located in an oil-filled tank in the base of the cabinet. Figure 4 shows the layout of this tank, and Figure 5 the circuit diagram.

The high voltage and the filament leads leave the tank through micanite tubes to the series-regulator-tube chassis which is mounted inside a corona shield about 12 inches above the tank. High voltage connections are made to the cabinet through special connectors. Figure 6 shows a side view of the cabinet with the corona shield in place and the side panel removed.

2.2 Voltage Regulator, A: General

The voltage regulator is of the series-tube type used by Pepinsky and Jermotz[4]. The circuit diagram is shown in Figure 7 and the chassis layout in Figure 8. A sample of the high voltage is taken from a voltage divider consisting

---

[4] Pepinsky, R. and Jermotz, P., Rev. Sci. Instr., 19, 247(1948).

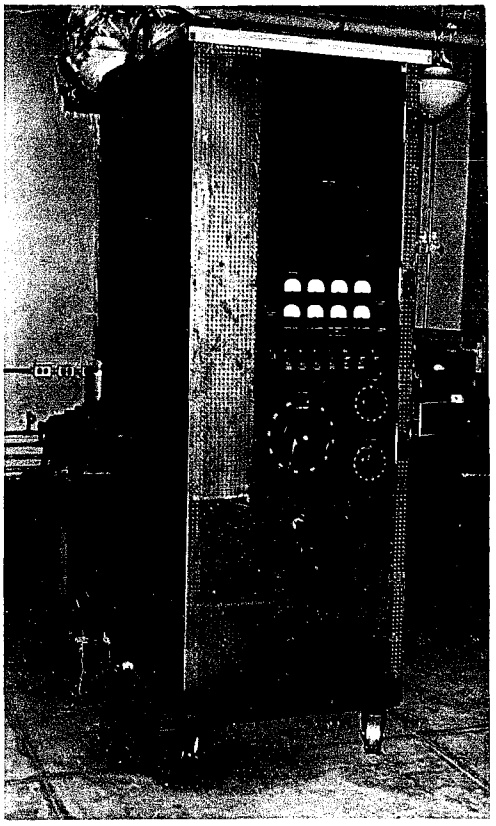

FIGURE 3. FRONT VIEW OF POWER SUPPLY.

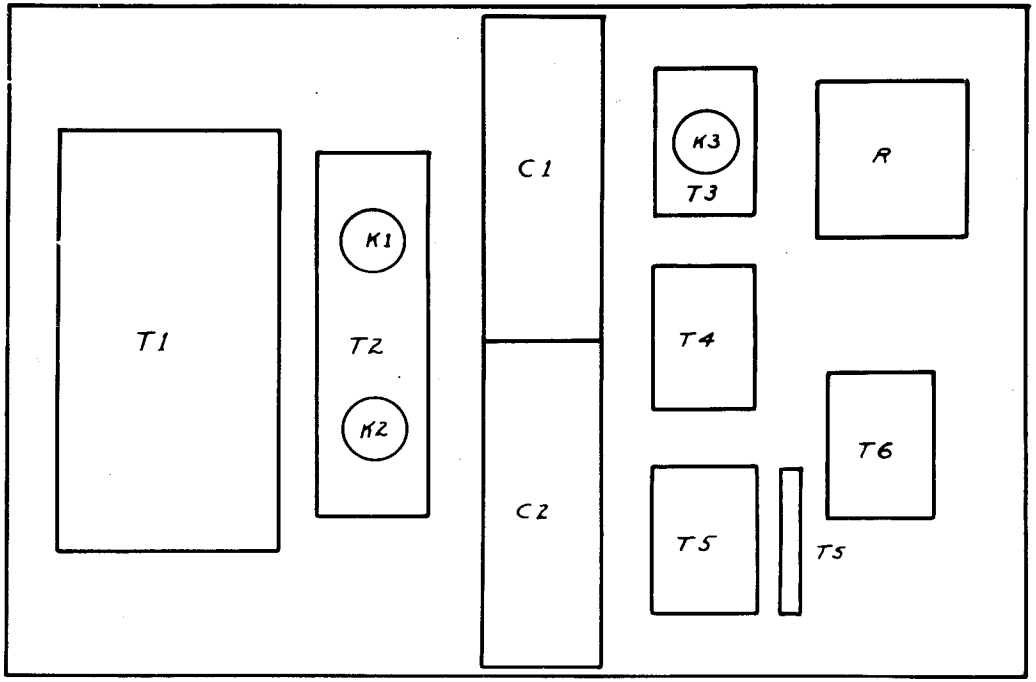

T1 High Voltage Trans.
T2 Rectifier Fil. Trans.
T3 Current Limiting Tube Fil. Trans.
T4 Regulator Tube Fil. Trans
T5, T6 X-Ray Tube Fil. Trans.
K1, K2 Rectifier Tubes
K3 Current Limiting Tube
C1, C2 Condensers
R Resistor Stack
TS Terminal Strip

161

FIGURE 4 HIGH VOLTAGE TANK LAYOUT.

OHIO STATE UNIVERSITY	
Project No.	; Dwg. No.
Scale:	; No. Req.:
Date:	; [redacted]
Mat'l:	
Inst's:	

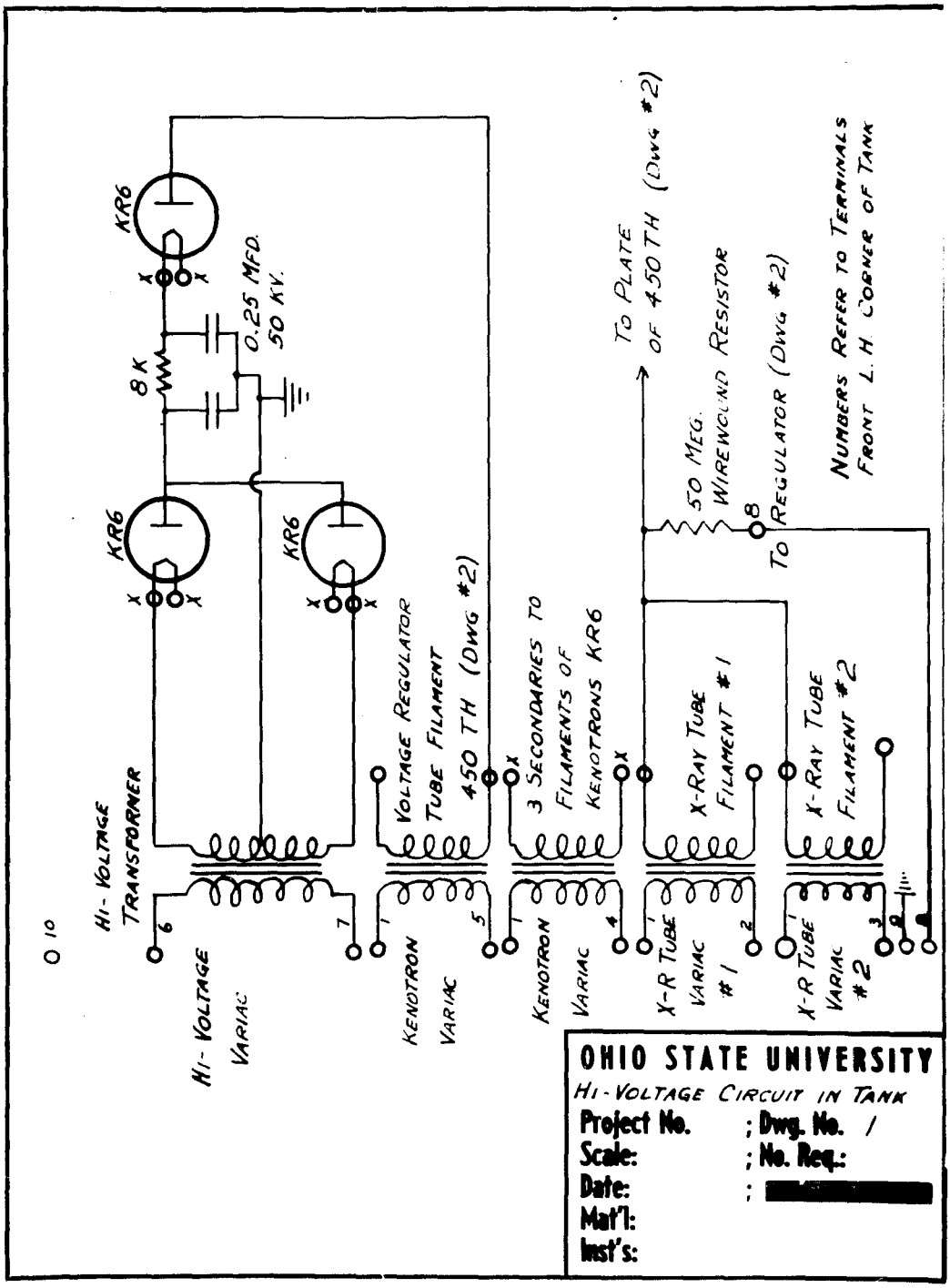

FIGURE 5. CIRCUIT DIAGRAM FOR UNREGULATED HIGH VOLTAGE SOURCE.

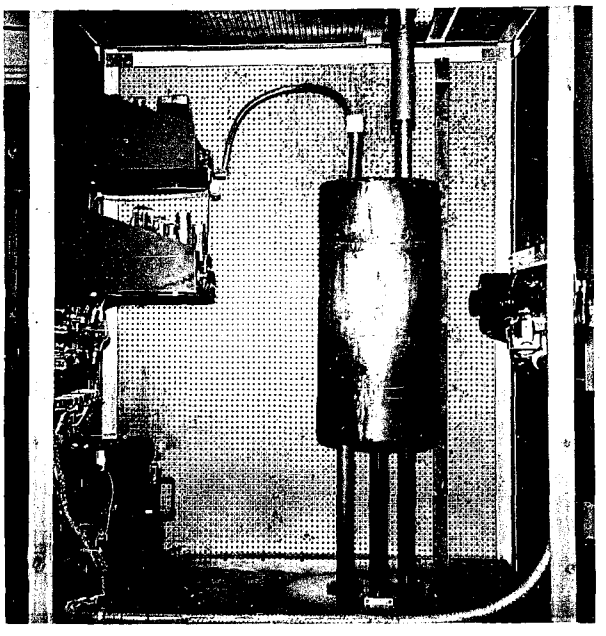

FIGURE 6. SIDE VIEW OF POWER SUPPLY.

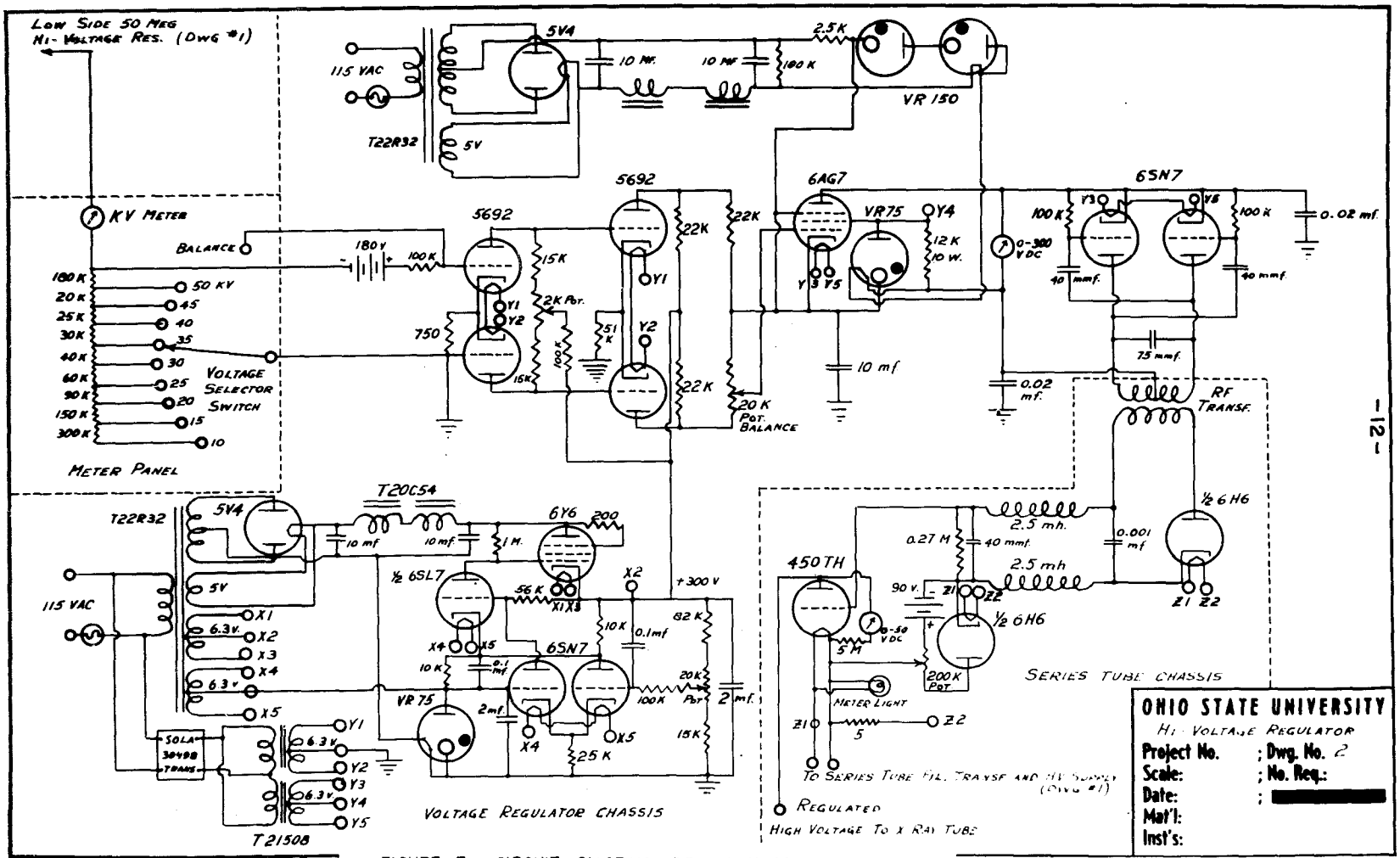

FIGURE 7. CIRCUIT DIAGRAM OF VOLTAGE REGULATOR.

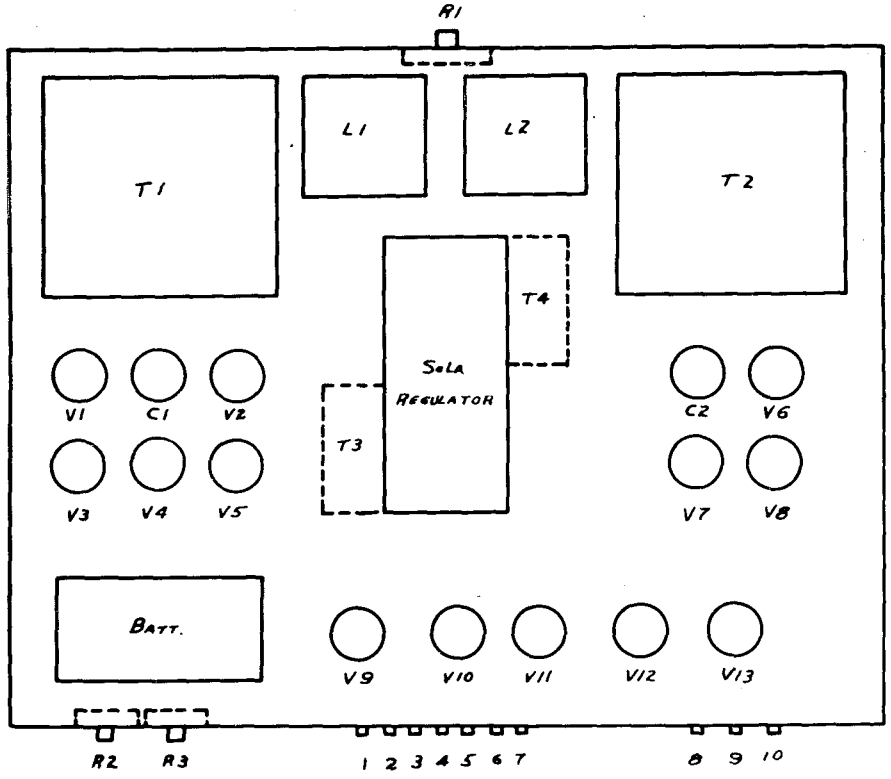

FIGURE 8. CHASSIS LAYOUT OF VOLTAGE REGULATOR.

T1, T2	Power Transformer
T3, T4	Filament Transformer
L1, L2	Filter Choke
C1, C2	Filter Condenser
V1, V6	5V4
V2	6Y6
V3, V12	0A3
V4, V13	6SN7
V5	6SL7
V7, V8	0D3
V9, V10	5692
V11	6AG7
R1	Balancing Potentiometer
R2	B+ Voltage Control
R3	Gain Control
1, 2	110 Volts AC
3	Ground
4	Balance
5	50 Megohm Resistor
6	Meter (−)
7	Meter (+)
8, 9, 10	Output to rf Transformer

1/3

OHIO STATE UNIVERSITY

Project No. ; Dwg. No.
Scale: ; No. Req.:
Date: ;
Mat'l:
Inst's:

of the 50 megohm wirewound resistor in the tank and the voltage selector resistors on the panel. This voltage is compared to the voltage of a 180-volt dry battery. The difference between the signal voltage and the 180-volt battery is applied to one grid of a 5692 double triode tube. The other grid of this tube is grounded. The two triodes form a balanced amplifier. The second stage of the balanced amplifier is another 5692 tube. The unbalance signal from this stage is applied to the grid of the third stage, a 6AG7 sharp cutoff pentode, which is in series with a push-pull rf oscillator. Thus, the B^+ supply for these two tubes is divided between the oscillator tube and the 6AG7. A separate 300-volt supply is used for this purpose. In actual operation the degree of unbalance of the first two stages is adjusted by means of the "balancing" potentiometer in the plate circuit of the first 5692 tube, to give 150 volts drop across the oscillator when there is no potential on the grid of the first tube. So, when the signal voltage exactly equals the reference voltage, the 6AG7 and the oscillator each have 150 volts plate voltage. When the signal voltage changes, the grid of the 6AG7 changes and the drop across this tube changes. This change appears across the oscillator in an opposite sense, and changes the amplitude of the oscillation. The output of the oscillator is taken from the secondary of the rf transformer, is rectified and filtered and applied to the

grid of the 450TH series tube. A change in the signal voltage changes the grid bias on the series regulator tube. This action changes the voltage drop across the series tube to absorb variations in the unregulated high voltage supply over a range of about 5000 volts. The grid of the 450TH is permanently biased by a 90 volt battery to operate over its most sensitive range. The rf transformer has a 14 turn primary and a 20 turn secondary, insulated to withstand 50 KV. In this way the series tube is isolated from the dc amplifier which operates near ground potential. The frequency of oscillation of the rf oscillator is approximately nine megacycles per second.

2.2 Voltage Regulator B: Performance

The voltage delivered by the unregulated high voltage supply is divided between the load and the series tube. A sample of the load voltage is amplified and applied to the series tube in such a way that an increase in load voltage increases the drop across the series tube. The voltage across the load is a function of the input voltage and the load current, or $E_o = E_o(E_i, I_o)$

and

$$\Delta E_o = (\Delta E_o/\Delta E_i)\Delta E_i + (\Delta E_o/\Delta I_o)\Delta I_o \qquad (1)$$

where E_o and I_o are the load voltage and load current respectively, and E_i is the input voltage. It is convenient

to define two parameters, the stabilization ratio $S = \Delta E_i/\Delta E_o$ and the internal resistance of the regulator $R = -\Delta E_o/\Delta I_o$. Then,

$$E_o = (1/S)\Delta E_i - R\Delta I_o \qquad (2)$$

Now $\Delta E_i = \Delta E_o + \Delta E_s$, where ΔE_s is the change in series tube voltage. If f is the sampling fraction of E_o and A the amplification of the feedback loop then $\Delta E_i = fA\Delta E_o$ and

$$S = \Delta E_o(1 + fA)/\Delta E_o = 1 + fA \qquad (3)$$

It is clear that in this regulator, f is a function of the voltage selected, so that the stabilization ratio at the high voltages is less than that at the low voltages. This is not considered a serious handicap in the use of this equipment. The internal resistance can be shown to be equal to r_p/S where r_p is the plate resistance of the series tube[5].

---

[5]Collenge, J. P., Thesis, M.S., Ohio State University(1949).

The stabilization ratio can be determined experimentally from the plot of load voltage vs. input voltage. Figure 9 shows such a plot for a voltage selection of 10 KV. The stabilization ratio is 320. The amplification of the system is 17,000.

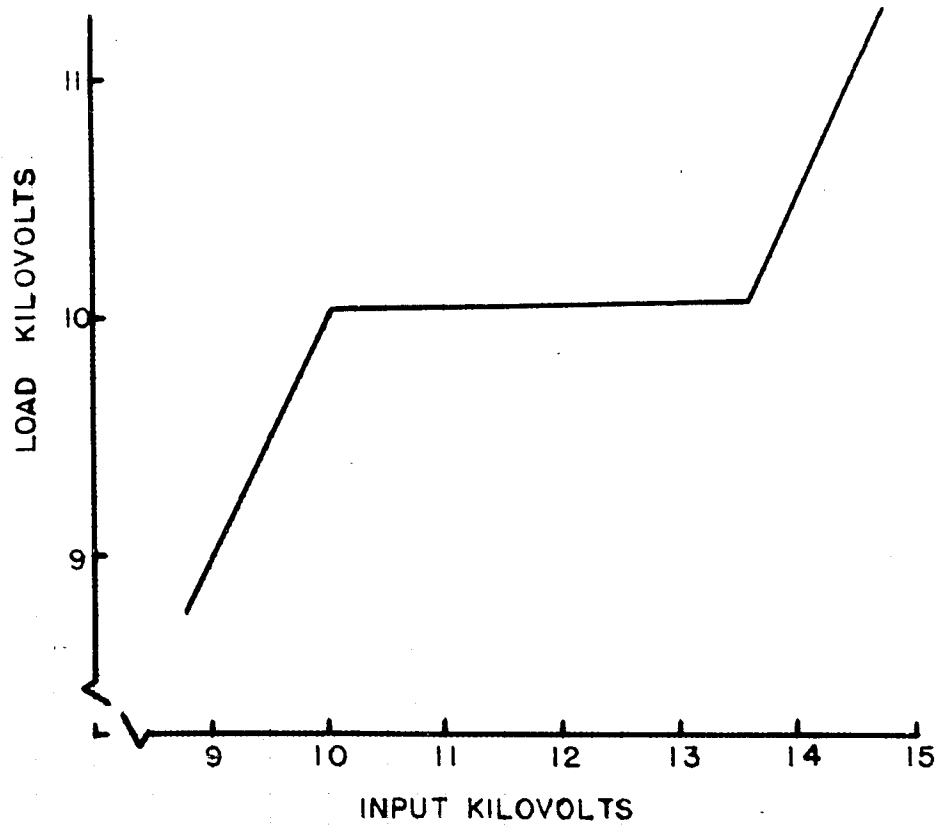

FIGURE 9. LOAD VOLTAGE VS. INPUT VOLTAGE FOR HIGH VOLTAGE POWER SUPPLY.

2.3 Current Regulator A: General

The current regulator is of the series-impedance type described by LeMieux and Beeman[6]. Figure 10 is the circuit diagram and Figure 11 the chassis layout for the current regulator. The anode current from the x-ray tube is passed through a sampling resistor and a low pass filter to provide a signal voltage for the regulator. The reference voltage is the cutoff potential of the first stage of amplification. The filter is inserted because the heating time of the x-ray tube filament is of the order of 0.1 second, and without suitable filtering the system hunts violently. The signal from the first stage is further amplified by the second stage and then applied to the grids of two 6A3 tubes. These tubes are in the secondary of a transformer whose primary is in series with the x-ray filament transformer. When the tubes are conducting, the impedance of the primary is low, and voltage drop across it is small. When the tubes are not conducting, however, the impedance of the transformer is very high and the voltage drop across the primary becomes quite large. The impedance of the transformer is thus a function of the current through the 6A3's, which in turn is a function of the x-ray tube current. A tendency for the x-ray tube current to

---

[6] LeMieux, A. F. and Beeman, W. W., Rev. Sci. Inst., 17, 130 (1944)

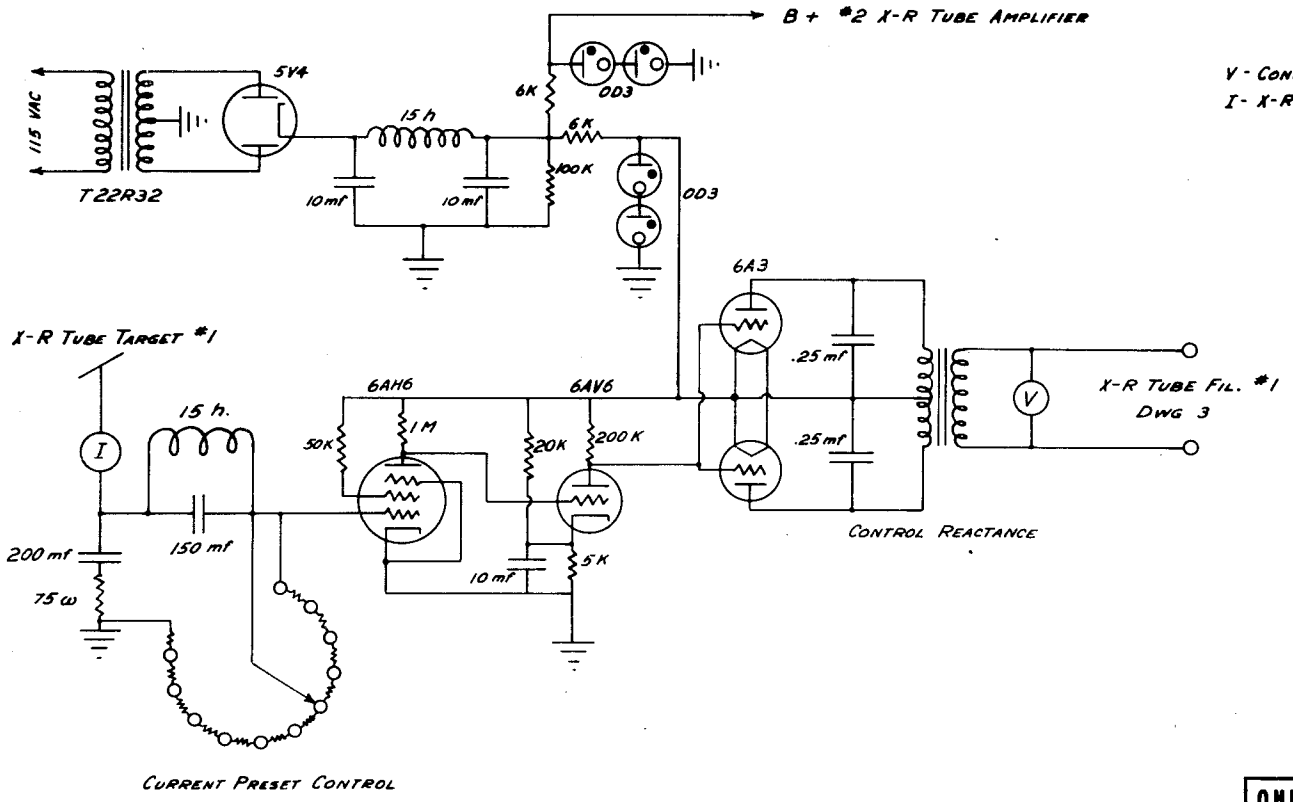

FIGURE 10. CIRCUIT DIAGRAM OF CURRENT REGULATOR.

OHIO STATE UNIVERSITY	
CURRENT REGULATOR AMPLIFIER	
Project No.	; Dwg. No. 4
Scale:	; No. Req.:
Date:	; [redacted]
Mat'l:	
Inst's:	

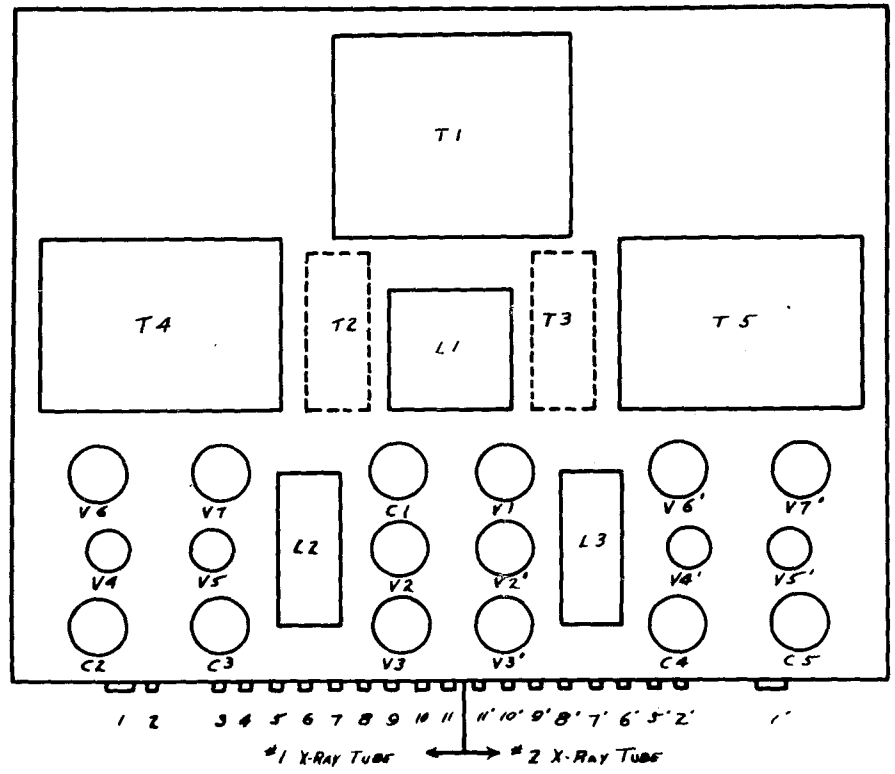

FIGURE 11. CHASSIS LAYOUT OF CURRENT REGULATOR.

T1	Power Transformer
T2, T3	Filament Transformer
T4, T5	Control Impedance
L1	B+ Supply Filter Choke
L2, L3	Input Filter Choke
C1	B+ Supply Filter Condenser
C_2, C_3 C_4, C_5	Input Filter Condenser
V1	5V4
V2, V3	0D3
V4	6AH6
V5	6AY6
V6, V7	6A3
1	Test
2	Ground
3, 4	110 Volts AC
5	Input
6	Milliammeter -
7	Milliammeter +
8, 9	AC Voltmeter
10, 11	Output

OHIO STATE UNIVERSITY

Project No. ; Dwg. No.
Scale: ; No. Req.:
Date: ; [redacted]
Mod'l:
Inst'ls:

rise, decreases the current through the 6A3's, which in turn increases the reactance of the series impedance and decreases the voltage on the primary of the filament transformer.

2.3 Current Regulator B: Performance

A stabilization ratio for the current regulator analogous to the one for the voltage regulator cannot be defined. However, an estimate of the effectiveness of the regulator, called the figure of merit, may be obtained from a comparison of the x-ray tube current as a function of the input voltage with and without the regulator. Figure 12 shows plots of the x-ray tube current against input voltage with and without the regulator. The figure of merit of the regulator is 1000.

The power supply, in general, operated very well. There is some initial drift caused by temperature change of the resistors and the reference battery, but this was not serious. After a warmup period of a few hours, the x-ray intensity remained constant for the duration of the various experiments to one half percent or better. No provisions were made to monitor the intensity with a separate detector.

2.4 Sample Chamber

Figure 13 is a cross-sectional view of the sample chamber, made in three main parts. The outer container

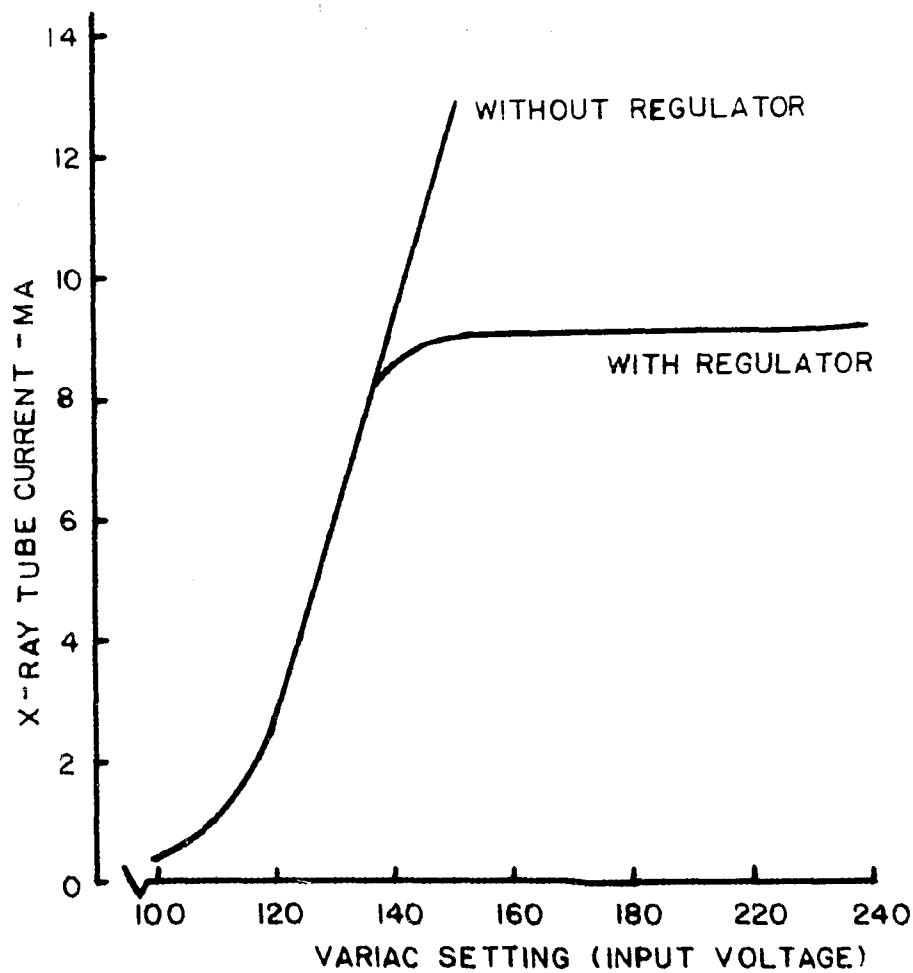

FIGURE 12. X-RAY TUBE CURRENT VS. INPUT VOLTAGE.

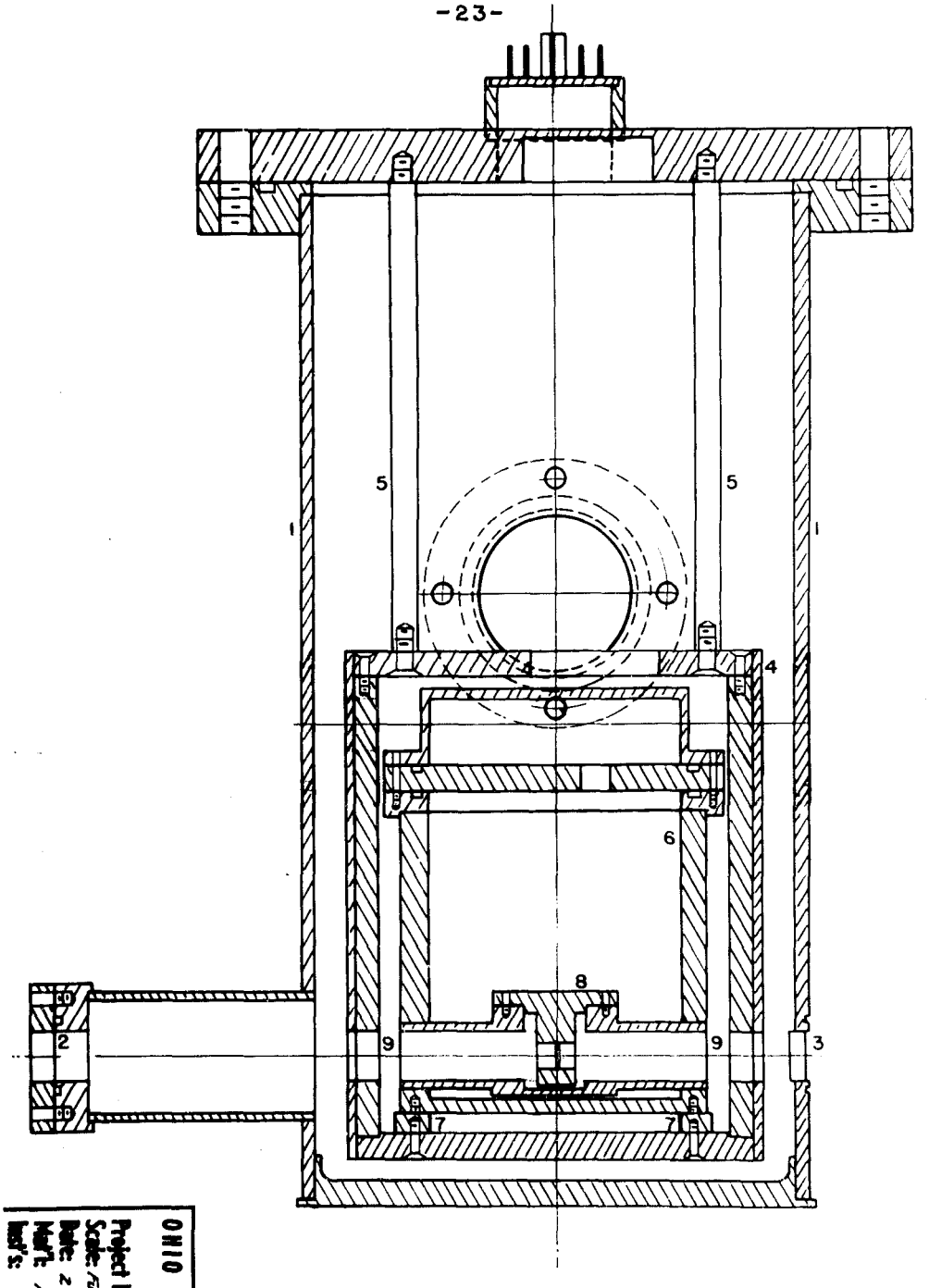

OHIO STATE UNIVERSITY
Assembly
Project No. ; Dwg. No. 12
Scale: Full ; No. Req:
Date: 2-12-53 ;
Mat'l As Specified
Insp'n:

FIGURE 13. SAMPLE CHAMBER.

(1) forms the vacuum jacket and has windows covered with a polyethylene film for passage of the x-rays at (2) and (3). Operating vacuum was of the order of 10^{-5} mm hg. From the top there is suspended the second container (4) by means of three thermally insulating fiber rods (5). This copper jacket was wound with two coils of wire, the first a heating coil of nichrome and the second a resistance thermometer winding of Hytemco wire to be described with the associated circuits later (Section 2.5). The innermost chamber (6) is insulated from (4) by the nylon supports (7). This chamber contains an oil bath to give a large heat capacity and uniform temperature distribution through circulation of the oil. The latter is accomplished by means of an impeller driven through the vacuum seal by a magnetic drive. The stainless steel sample holder (8) is in intimate thermal contact with the container and supports the emulsion sample in the x-ray beam between thin beryllium windows, as described later. The ends of the holes (9) were closed with 0.1 mil aluminum foil to act as radiation shields.

The sample is in the form of a flat disc 0.25 inch in diameter and 0.020 inches thick. Figure 14 is a drawing of the sample holder. The sample is contained between 0.005 inch beryllium windows which are spaced by a stainless steel washer. The windows are sealed by rubber O-ring gaskets.

A copper-constantan thermocouple soldered into place as shown in Figure 14 is used to measure the sample

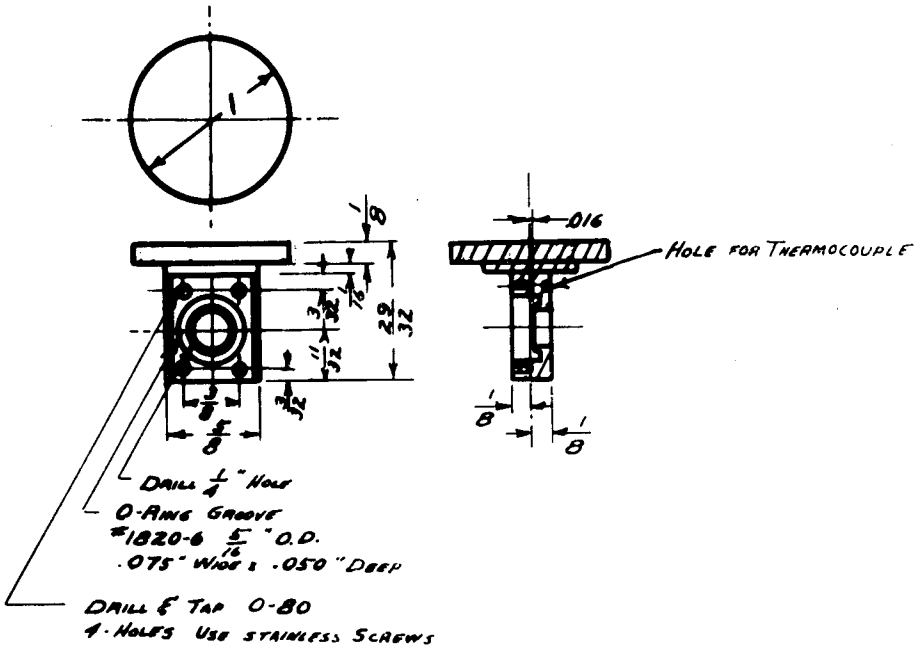

PART 1
MADE OF STAINLESS 304

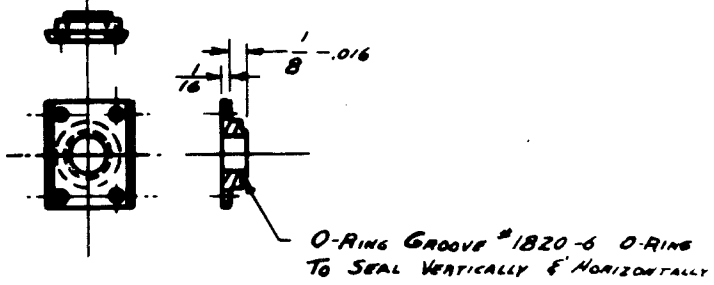

PART 2 TO FIT PART 1
STAINLESS 304

NOTE: ASSEMBLY HAS TWO 0.005" BE WINDOWS AND A 0.020" SAMPLE BETWEEN THE O-RINGS

FIGURE 14. SAMPLE HOLDER.

OHIO STATE UNIVERSITY	
Project No.	; Dwg. No.
Scale:	; No. Req.:
Date:	; [redacted]
Mat'l:	
Inst's:	

temperature. The magnitude of the temperature lag of the sample with respect to the thermocouple was determined in two ways - one by approximate calculation from heat conductivity considerations*, and the other by direct experimental

*Appendix I

evidence†. Both indicate a negligible lag in these experi-

†Section 3.2 C, Fig. 28

ments.

The heater (4) is a copper cylinder closed at both ends. The cylinder has a double set of threads cut into it to hold the heating winding and the resistance thermometer used for temperature control. A tight fitting sleeve fits over the outside of the windings so that both the heater and the thermometer are completely surrounded by the jacket. This design gives very good heat transfer between the windings and the copper jacket.

The entrance and exit ports are 0.5 inch in diameter and arranged for a scattering angle of $2\theta = 29.5^{\circ}$. Thus the range of 2θ values is limited to about 10° on either side of 29.5°. This is ample for the work on sodium, but limits the use of the apparatus with other materials.

All electrical leads enter the vacuum system through an eight-point seal in the top plate of the vacuum jacket. The drive motor for the impeller in the oil bath is also

located on the top plate. It drives the impeller through two vacuum tight walls, one, the outer wall, and the other, the wall between the oil bath and the vacuum. To avoid the troubles of packing type seals, a system using two magnets was devised. One magnet is placed on either side of the plate. The plate having been machined to a thickness of 1/16-inch, a considerable attraction exists between the magnets even at a separation of about 3/32-inches. Two identical units are used to drive through the two vacuum-tight walls. Sufficient power can be transferred in this way to maintain circulation in the oil.

The various openings in the vacuum system are sealed with O-ring gaskets. These gaskets are very reliable and no trouble with leaks has been experienced even though the system has been opened several times in the course of the experiments.

2.5 Temperature Control

The temperature of the heater (4) (Figure 13) is controlled by a bridge-type controller based on a design by Benedict[7]. Figure 15 is the circuit diagram of the

---

[7]Benedict, M., Rev. Sci. Instr., 8, 252(1937).

---

thermostat. The temperature sensitive element is a resistance thermometer of Hytemco* wire. The thermometer

---

*International Nickel Co. special nickel-alloy wire.

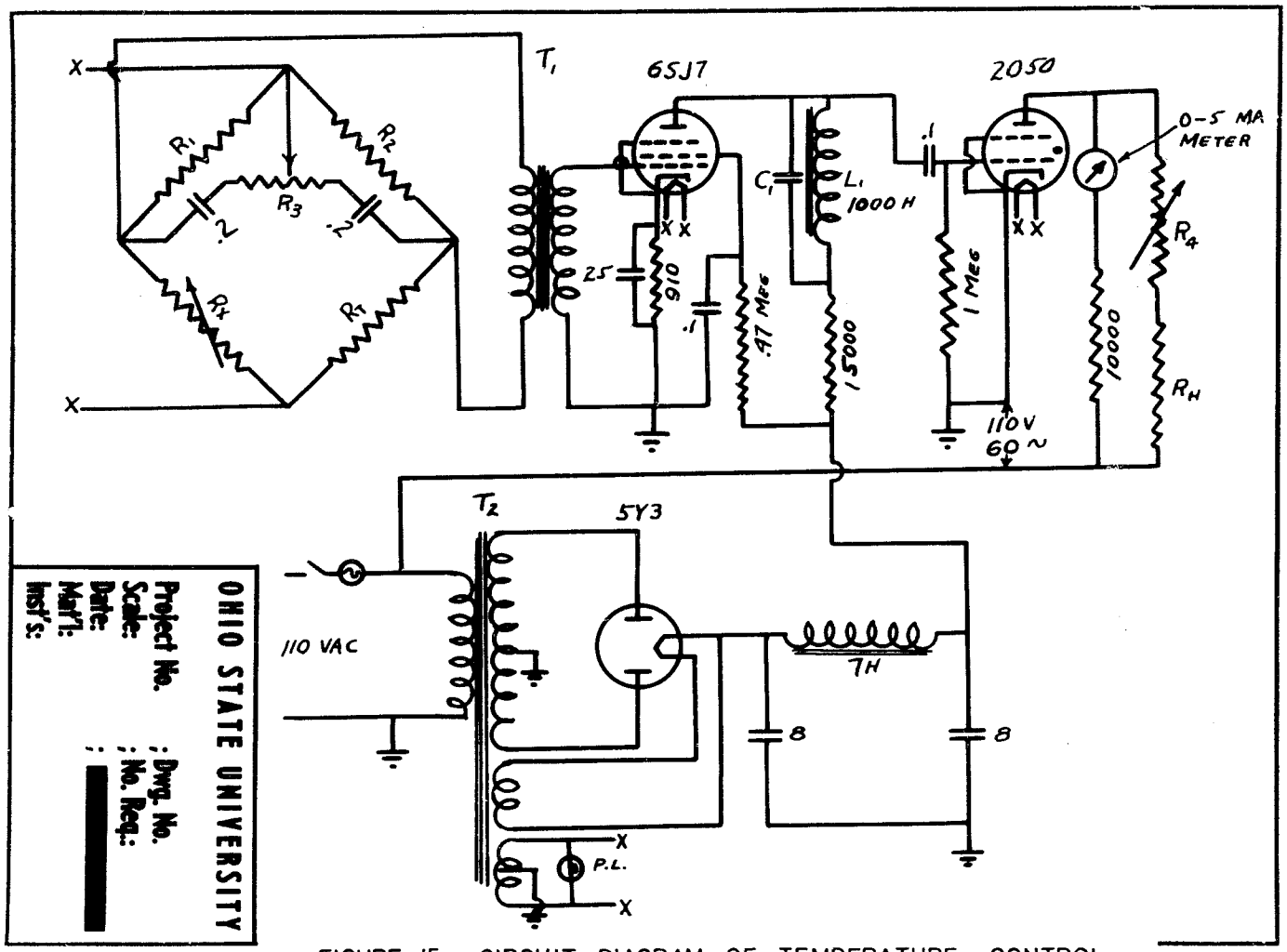

FIGURE 15. CIRCUIT DIAGRAM OF TEMPERATURE CONTROL.

is of 30 gauge, cotton-covered wire, non-inductively wound in grooves in the heater jacket. The temperature is adjusted by means of a ten-turn helipot, R_x, wound with low temperature-coefficient wire.

The power for the bridge is supplied by the filament transformer. The output of the bridge is fed through an impedance matching transformer to a 60-cycle amplifier and then applied to the grid of a thyratron. The thyratron is in series with the heater winding and controls the current in it. The thyratron is operated as a phase controlled valve. When the total signal, bias plus signal from the bridge, lags the plate voltage by 90°, the thyratron passes current during one quarter of the cycle. As the phase of the grid signal changes, the thyratron conducts during a larger or smaller fraction of the cycle. Bias for the thyratron is supplied by the potentiometer R_3 across the output terminals of the bridge. The position of the tap is adjusted to give maximum sensitivity without giving on-off control. When this adjustment is properly made, the current through the thyratron varies smoothly from full-on to full-off as the bridge passes through the balance position. The resistor R_4 in series with the load controls the amount of power dissipated in the heater. It is set so that the regulator operates in its most sensitive range.

The gain of the system is about 3000, and the sensitivity such that a 0.03 percent change in R_T changes the power output by a factor of 2. The thermostat will hold the temperature of the sample chamber constant to within approximately 0.001°C over long periods of time.

2.6 X-Ray Spectrometer

The x-rays are produced by a Machlett A-2 diffraction tube with a copper anode. The tube was normally operated in the range of 25 to 30 kilovolts and five to nine milliamperes. The intensity was adjusted to a convenient value for the particular work being done. The incident beam-defining slits were 0.040 inches wide and about six inches apart. The second slit was located on the oil bath container (6) inside the vacuum system. A 0.060 inch wide slit in front of the x-ray detector completed the collimation system. A nickel filter was used to reduce the intensity of the $K\beta$ line.

The detector was mounted on an arm about seven inches from the sample. The angle of rotation was controlled manually by a micrometer drive. This enabled adjustment of the angle of the counter from 25° to 35° (= 2θ) in a very reproducible manner. The sample was mounted with its plane at an angle of about 75° with the incident x-ray beam.

2.7 Proportional Counter X-Ray Detector

A proportional counter[8] radiation detector was used in the experiments. It was a side-window type similar to those of Dr. R. W. Knowles of the Oak Ridge National Laboratories. The counter had a 5 mil beryllium window, and was filled with 66 cm pressure of xenon gas and 4 cm of methane. All joints were soldered with pure tin to avoid contamination by radioactive lead. Figure 16 shows the details of construction of the counter.

The output of the counter is fed directly into an Atomic Instruments Company type 205-B preamplifier modified slightly to reduce the noise level. Figure 17 shows the preamplifier with the modifications. The high voltage for the counter is supplied by an rf power supply properly filtered to remove interference. This filter is a simple rc filter and is shown in the above mentioned figure. Connections throughout the high voltage circuit were made with RG8U cable and low-noise connectors.

The output of the preamplifier is further amplified by a type 204B* amplifier. The signal is then put into a

---

[8] Korff, S. A., Nucleonics 6, 15(June, 1950).
7, 46(Nov., 1950).
8, 38(Jan., 1951).

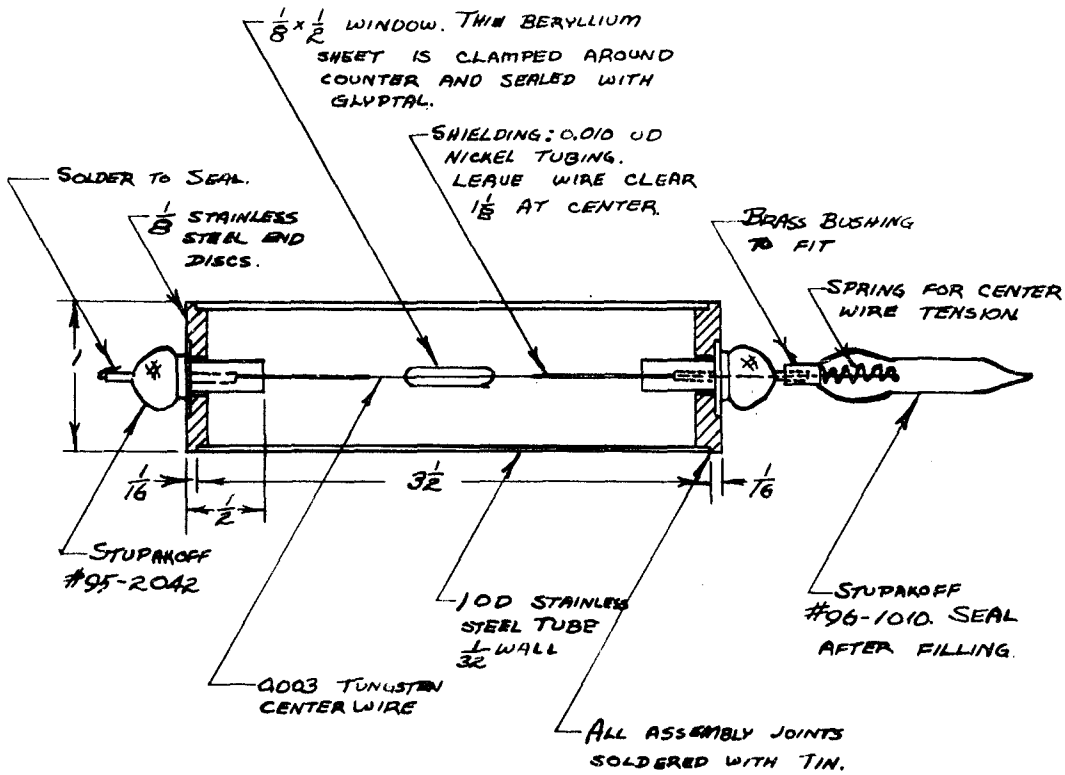

FIGURE 16. PROPORTIONAL COUNTER.

OHIO STATE UNIVERSITY	
Project No.	; Dwg. No.
Scale:	; No. Req.:
Date:	; [redacted]
Mat'l:	
Inst's:	

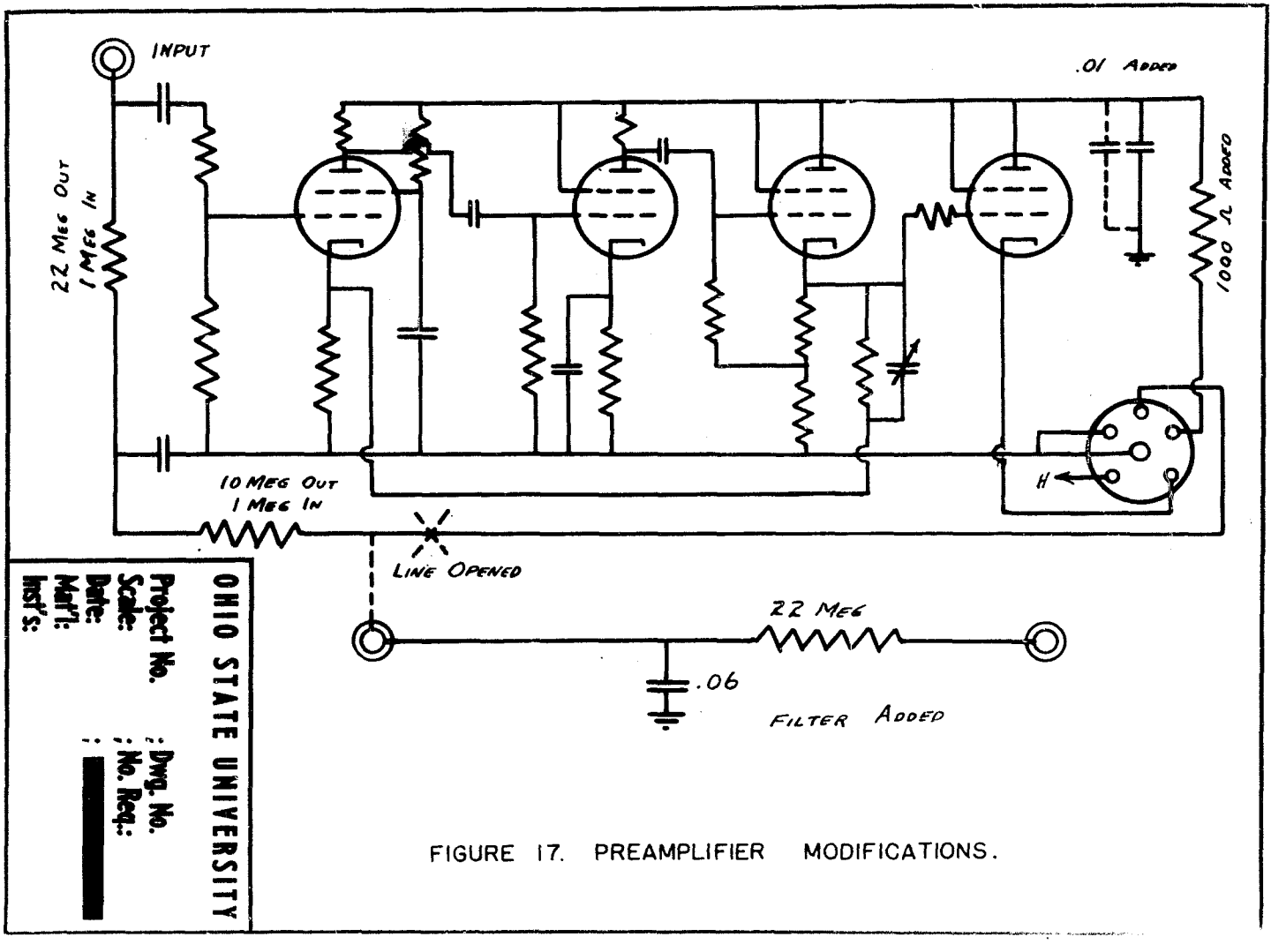

FIGURE 17. PREAMPLIFIER MODIFICATIONS.

*Atomic Instruments Co., Boston, Mass.

pulse-height analyser, designed by Oak Ridge National Laboratories and built in this laboratory, which aids in reducing the general background. The pulses are counted by a scaling circuit*. Figure 18 shows the entire experi-

*Autoscaler by Tracerlab, Inc., Boston, Mass.

mental arrangement.

2.8 The Sample

The first sample used in the experiments was a heavily cold-worked wire of sodium. The wire was formed by passing it through an extrusion press ten times. Following this, the wire was twisted to remove the effects of any preferred orientation produced in the extrusion. The wire was coiled in a small coil and flattened to fit into the sample holder. This sample gave a very good diffraction pattern, but once it melted, the line disappeared and did not return when the sample was solidified. Since this preliminary experiment could not be expected to give a satisfactory picture of the melting or solidification process it was not pursued further. All subsequent work was done with a dispersed sample as described below.

A dispersion of a very small particle size may be obtained in mineral oil if a small amount of linseed oil

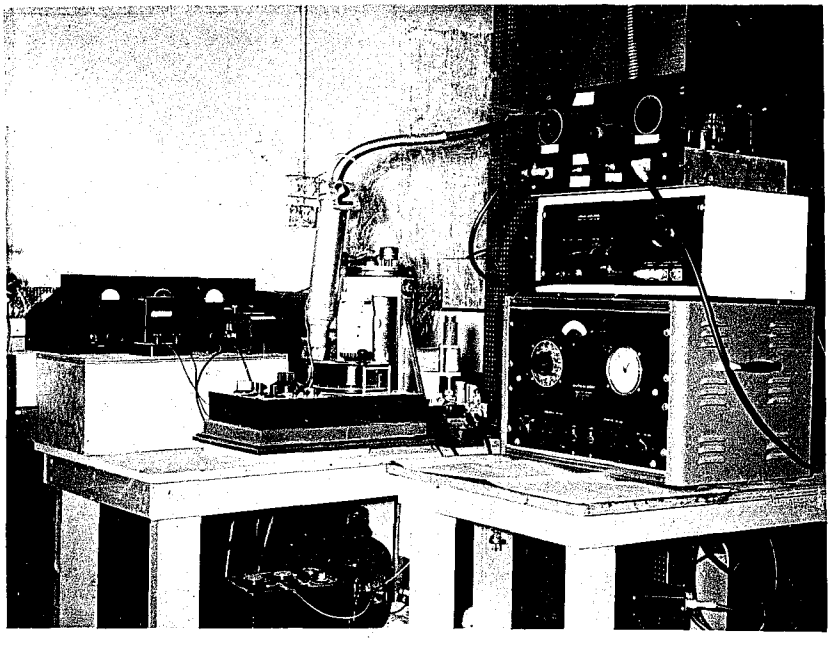

FIGURE 18. EXPERIMENTAL ARRANGEMENT.

is added as a dispersing agent. A mixture of 50 percent mineral oil, 50 percent sodium and about one percent linseed oil was prepared. The sodium was in a single piece and when melted, formed a ball before being subjected to ultrasonic agitation. Thus, any dissolved impurity would be uniformly distributed throughout the sample. The mixture was heated to a temperature of 120° C and subjected to intense ultrasonic agitation. A frequency of 20 kilocycles was used with an input power of approximately 500 watts for a few seconds. Severe cavitation was observed, and the sodium dispersed in very fine particles.

Information on the size distribution of the particles was sought by means of the light microscope. A sample of the emulsion was placed on the stage of an oil immersion microscope with a magnification of 970X. Köhler illumination[9] was used because it affords the best resolution.

---

[9]Shillaber, C. P., Photomicrography, p. 93, Wiley, New York (1949)

Table I shows the results of two fields of view. It was very obvious from the pattern in the microscope eyepiece that the greater number of particles were not being resolved. The minimum resolvable size is of the order of 0.5 microns, so that the table presents only the maximum sizes of particles in the sample.

Table I

Particle Sizes Seen in Microscope Fields

Size (microns)	Number of Particles 1st Field	2nd Field
2.0 - 3.0	2	2
1.5 - 2.0	20	23
1.0 - 1.5	45	40
less than 1.0	75	100

Further evidence of the extremely small particle size is presented by the light violet color. This is the same color reported for sodium vapor in thick layers[10]. The

[10] Mellor's Modern Inorganic Chemistry, p. 552, Longmons, Green and Co., New York(1939).

same dispersed sample was used throughout the entire series of solidification and melting runs and gave very reproducible results. It was estimated that the scattering volume in the x-ray experiments contained about 10^7 particles.

No attempt was made to use spectroscopically pure sodium. The analysis of the sodium used in the preparation of the sample is given in Table II. It is not felt that the percentage of impurities is great enough to affect the results of the experiments except as discussed in the section on solidification.

III DATA AND RESULTS

3.1 Introduction

A series of experiments was planned to investigate the liquid-solid transformation in sodium. Figure 19 shows the 110 line of sodium in the dispersed sample at 95° C (100 percent solid). Figure 20 shows a scan of the same region with the same sample melted. It is to be noted that the latter curve does not represent background only, because

Table II

Analysis of Baker Sodium
Lot No. 5026

Chloride	0.0015%
Nitrogen	0.0005%
Phosphate	0.0003%
Sulfate	0.001 %
Heavy Metals (as Pb)	0.0005%
Iron	0.0005%
Oxide	unknown
Hydroxide	unknown

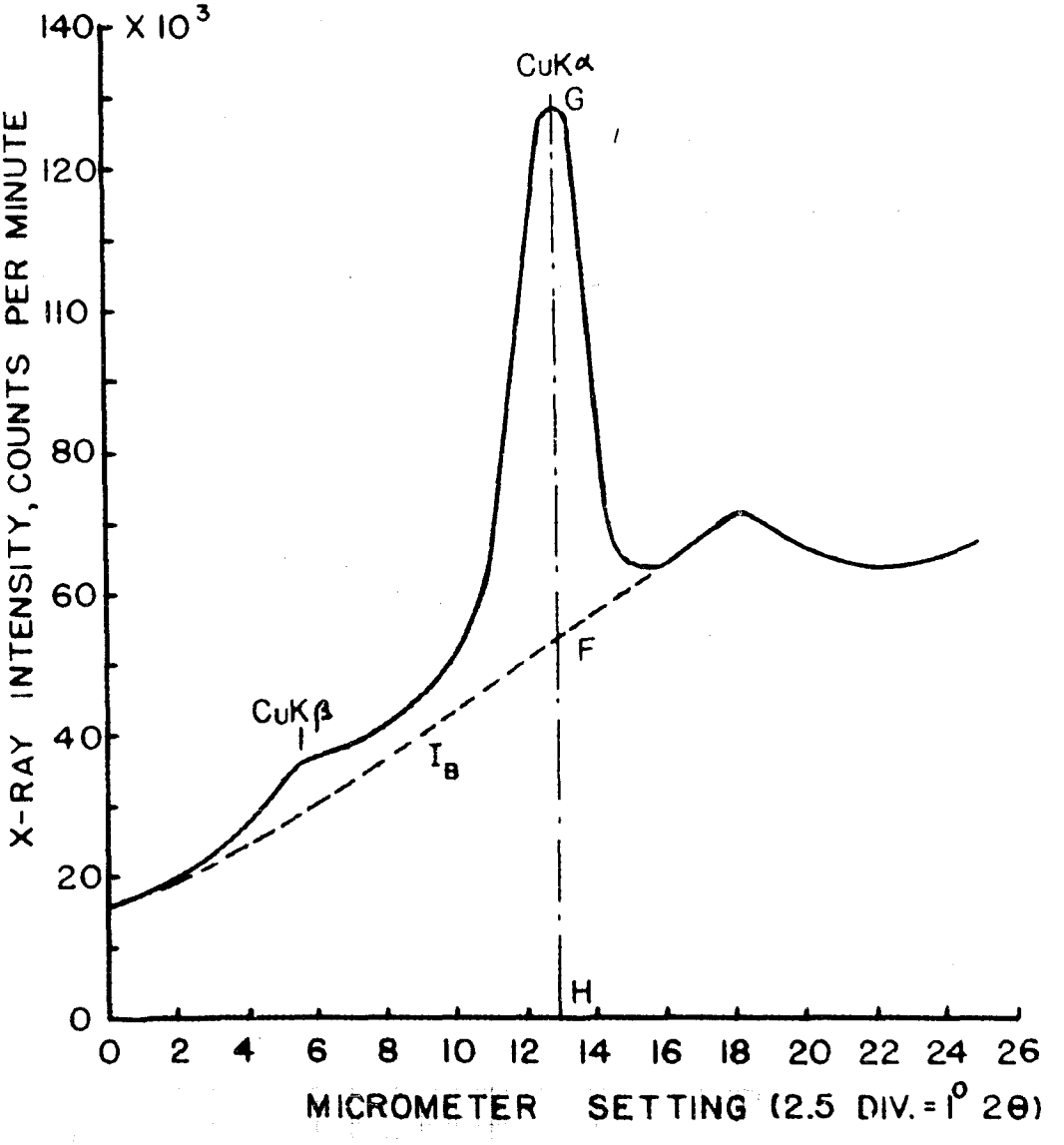

FIGURE 19. 110 DIFFRACTION LINE OF SODIUM DISPERSION.

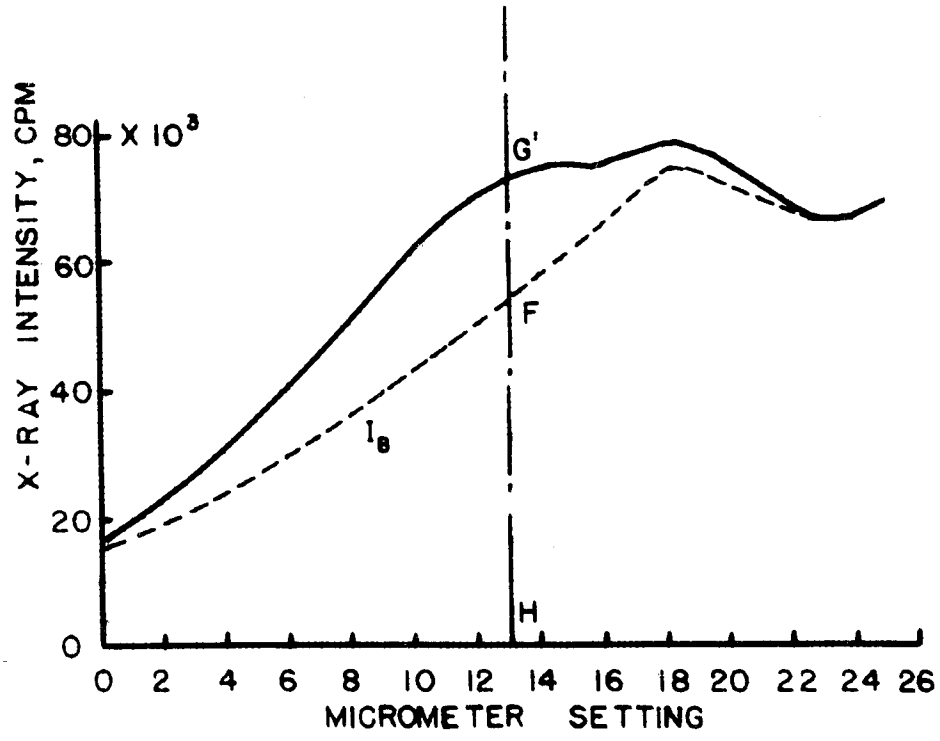

FIGURE 20. LIQUID DIFFRACTION PATTERN OF SODIUM DISPERSION.

the scattering from liquid sodium has a peak in the same region as solid sodium. This peak, however, is very broad. Figure 21 shows the 110 line of the solid (wire) sodium sample and the liquid pattern in the same region. The incoherent and background scattering, obtained after the sample had re-solidified, is also shown for illustrative purposes. One concludes that the background for the dispersed sample is caused partly by scattering from the walls of the sample chamber and partly by scattering from the oil. It is to be noted that the background relative to the intensity for the solid is much larger for the dispersed sample than for the wire sample. There are also diffraction lines from NaOH and Na_2O at 31° and 32° ($= 2\theta$) which partially account for the background. Figure 22 shows the pattern of a 0.013 inch oil sample between beryllium windows. The lines at 25.5 mm and somewhere less than zero are not due to the beryllium, since the first beryllium line is at $2\theta = 46.6^\circ$ but are caused rather by an unidentified impurity in the beryllium. These lines have been previously reported[11] in certain beryllium

---

[11]Structure Reports, Vol. 13, p. 33, OOSTHOEK - UTRECHT(1950).

---

samples.

If it is assumed that the peak intensity is represented by the sum of a background term, a liquid term,

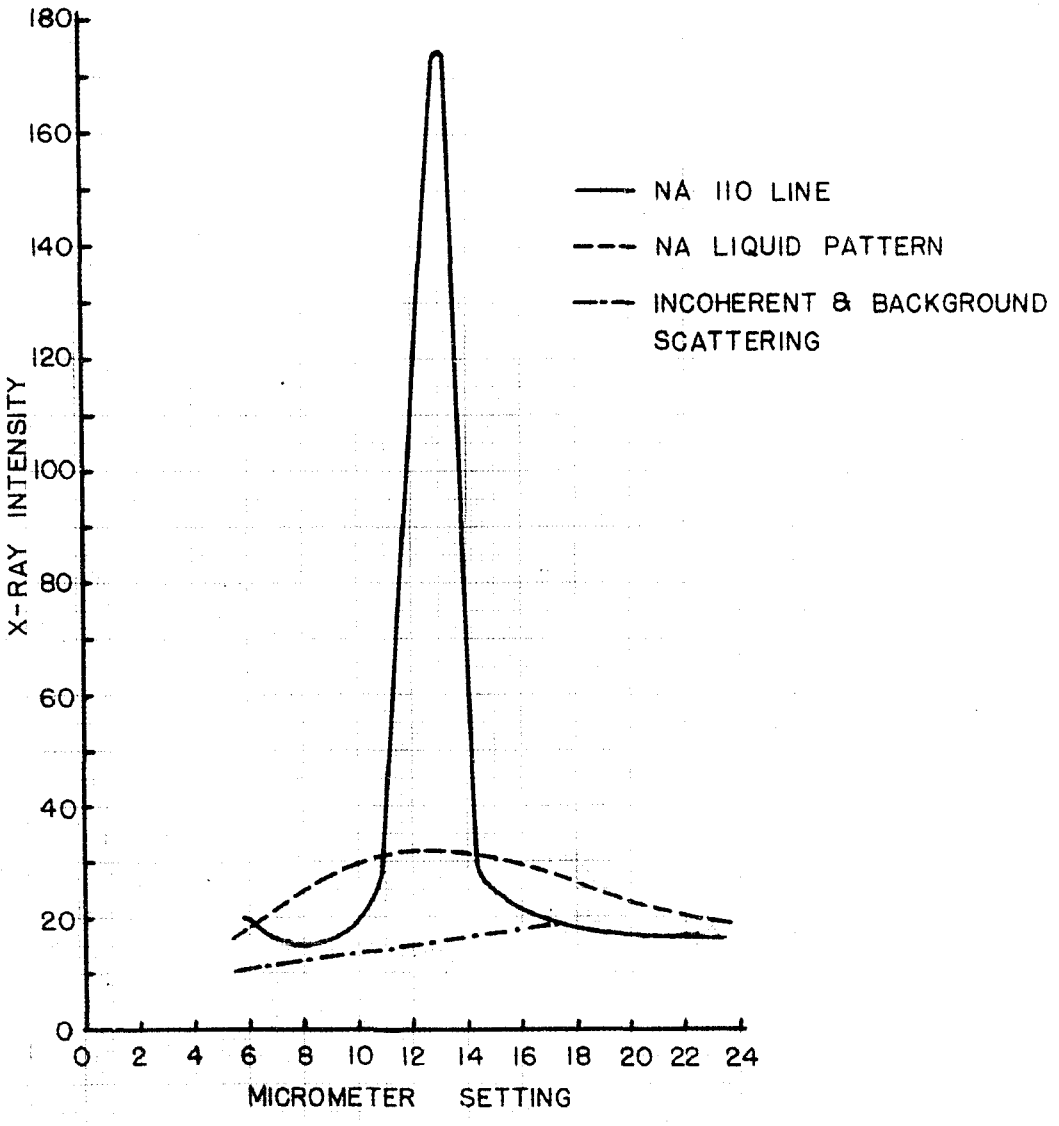

FIGURE 21. DIFFRACTION PATTERNS OF SODIUM WIRE.

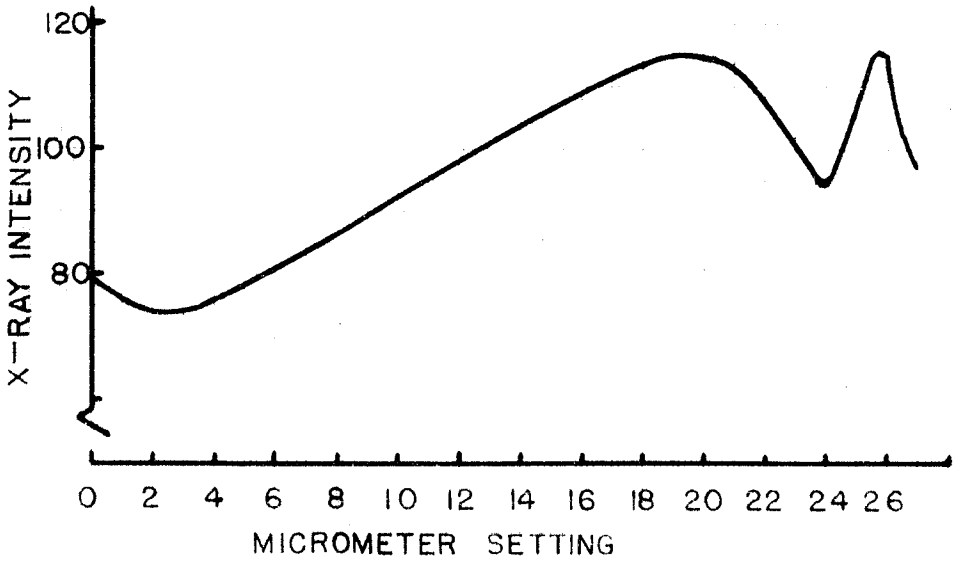

FIGURE 22. DIFFRACTION PATTERN OF OIL BLANK SAMPLE.

and a solid term, then,

$$I = I_B + I_L + I_S \tag{5}$$

Figure 19 is the contour from the sample with the temperature about 2° C under the melting temperature. The intensity at the CuKα peak may be assumed to consist of two parts: (1) the powder diffraction contribution I_S^o represented by FG in the figure and (2) the background contribution I_B given by HF.

Figure 20 is the contour from the sample with the temperature about 1° above the melting point. If it is assumed that the background I_B is unaltered, the liquid contribution I_L^o at the CuKα position will be given by FG.

These, then, fix the counting rates for 100 percent liquid and 100 percent solid and from Equation (5) one can write

$$I = I_B + AI_L^o + BI_S^o \tag{6}$$

where A is the percent liquid, B the percent solid, I_L^o and I_S^o the counting rates as determined above. I as a function of B is plotted in Figure 23. It is linear so that the percent solid sodium in the sample is proportional to the x-ray intensity.

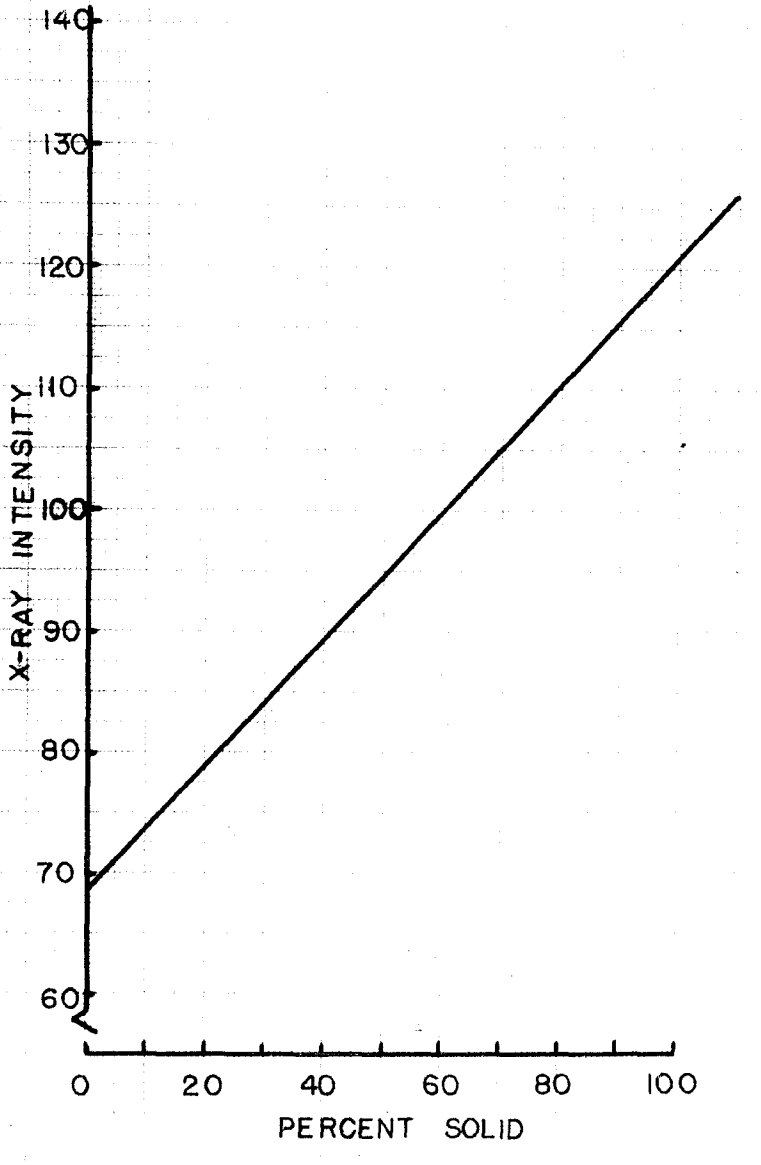

FIGURE 23. X-RAY INTENSITY VS. PERCENT SOLID CONTENT.

3.2 A: Melting

There have been many attempts to derive the conditions for melting theoretically. These attempts are each based on certain criteria for melting, and proceed along classical thermodynamical or statistical mechanical lines. One of the earliest treatments of melting was by Lindemann[12],

[12]Lindemann, F., Physik. Zeit., 11, 609(1910).

who considered the effect of the collision of a vibrating molecule with its neighbor. Later Raschewsky[13] developed

[13]Raschewsky, N. v., Zeit. f. Physik, 40, 214(1927).

a theory of melting based on the instability of a particle under the influence of its neighbors. Under these conditions, melting occurs when the average molecular distance is so great that the elastic force begins to decrease.

Born[14] following an earlier approach by Herzfeld and

[14]Born, M., J. Chem. Phys., 7, 591(1939).

Goeppert Mayer[15], and using the argument that the differ-

[15]Herzfeld, K. and Goeppert Mayer, M., Phys. Rev., 46, 995(1934).

ence between a solid and a liquid is the inability of the liquid to support shearing stresses, investigated the stability of the crystalline lattice under shearing stresses

over a wide range of temperatures. This is a very satisfactory model of melting. Born and his coworkers[16] have

[16]Born, M. et al, Proc. Cambridge Phil. Soc., 36, 160, 173, 454, 466(1940). 37, 34, 177(1941). 38, 61, 67, 82(1942). 39, 101, 104, 113(1943). 40, 151(1944).

further amplified this treatment and have met with some success in treating the general problem of fusion.

Kirkwood and Monroe[17] have presented a unified theory

[17]Kirkwood, J. G. and Monroe, E., J. Chem. Phys., 9, 514 (1941).

of the solid and liquid states with special emphasis on melting. Their treatment has been further amplified and generalized by Mayer[18]. Another interesting approach based

[18]Mayer, J. E., J. Chem. Phys., 15, 187(1947).

on the concept of the order-disorder transition has been presented by Lennard-Jones and Devonshire[19].

[19]Lennard-Jones, E. E. and Devonshire, A. F., Proc. Roy. Soc., (London), 169A, 317(1939).

All of these treatments lead to very complicated mathematical results and many simplifications must be made before they can be applied to specific cases. The effects

of these simplifications are difficult to determine. It is therefore difficult to judge whether the various approaches actually represent the real melting phenomenon.

3.2 B: Properties of Sodium Near its Melting Point

As early as 1924, evidence of pre-melting, or at lease unusual behavior below the melting point, in a crystalline lattice, was noted. Bidwell[20] observed unusual increases in the electrical resistance and the thermoelectric power of sodium and potassium as the temperature increased. There is a decided change in the slope of the plot of these properties vs temperature starting about 100° C below the melting point. There is also a very sharp rise in the curves as the melting point is approached. For sodium this rise starts at about 80° C for the thermoelectric power and at 90° for the resistance. A series of x-ray diffraction pictures showed no change in structure of the samples[21] as this effect progressed.

[20]Bidwell, C. C., Phys. Rev., 23, 357(1924).

[21]Bidwell, C. C., Phys. Rev., 27, 381(1926).

MacDonald[22] repeated the resistance measurements and found a similar rise. He attributes this rise to the

[22]MacDonald, D. K. C., J. Chem. Phys., 21, 177(1953).

formation of vacant lattice sites, so called Frenkel and Schottky defects[23]. At the melting point MacDonald gives

[23]Mott, N. F. and Gurney, R. W., Electronic Processes in Ionic Crystals, p. 28-29, The Clarendon Press, Oxford(1948).

the change in resistance as about 10 percent of R_o, which corresponds to about 0.1 atomic percent vacancies. This is in good agreement with the interpretation of the anomolous rise in specific heat of sodium and potassium as observed by Carpenter and his coworkers[24,25]. They observed an

[24]Carpenter, L. G., Harle, T. F. and Steward, C. J., Nature, 141, 1015(1938).

[25]Carpenter, L. G. and Steward, C. J., Phil. Mag., 27, 551 (1939).

anomalous rise in the specific heat starting about 100° C below the melting point, and interpreting this as due to the formation of Frenkel and Schottky defects, found vacancy concentrations of the order of 0.3 atomic percent[26].

[26]Carpenter, L. G., J. Chem. Phys., 21, 2244(1953).

This concentration is below detection by x-rays, and hence the x-ray diffraction intensity is not expected to show any anomalies because of the formation of vacant lattice sites.

Dawton[27] has investigated the intensities of x-ray

[27]Dawton, R. H. V. M., Proc. Phys. Soc., London, 49, 249 (1937).

reflections from single crystals of sodium in the temperature range 120 to 370° K. He found that there was considerable hysteresis in the intensity of the reflections from the low order planes as the temperature was raised and lowered. The effect was very erratic and depended on the particular crystal used as well as upon its thermal history. Reproducible results were generally obtained only after the crystal had been submerged in liquid air before the measurements were made. The effects were interpreted as being due to imperfections and changes in the mosaic structure of the single crystal. After submersion in liquid air, the crystals were supposed to have a more perfect mosaic structure, at least as far as the x-ray reflections are concerned.

3.2 C: Data and Results of Melting Studies

Figure 24 shows the diffracted intensity as a function of temperature up to the melting point of the well-annealed dispersed sample. At the melting point, the intensity drops sharply to the intensity of the liquid scattering pattern. There is some structure to the drop as will be discussed later.

The effect of thermal agitation of the atoms of a crystal on the intensity of the x-ray diffraction lines has been studied in detail by Debye[28] and later by Laue[29],

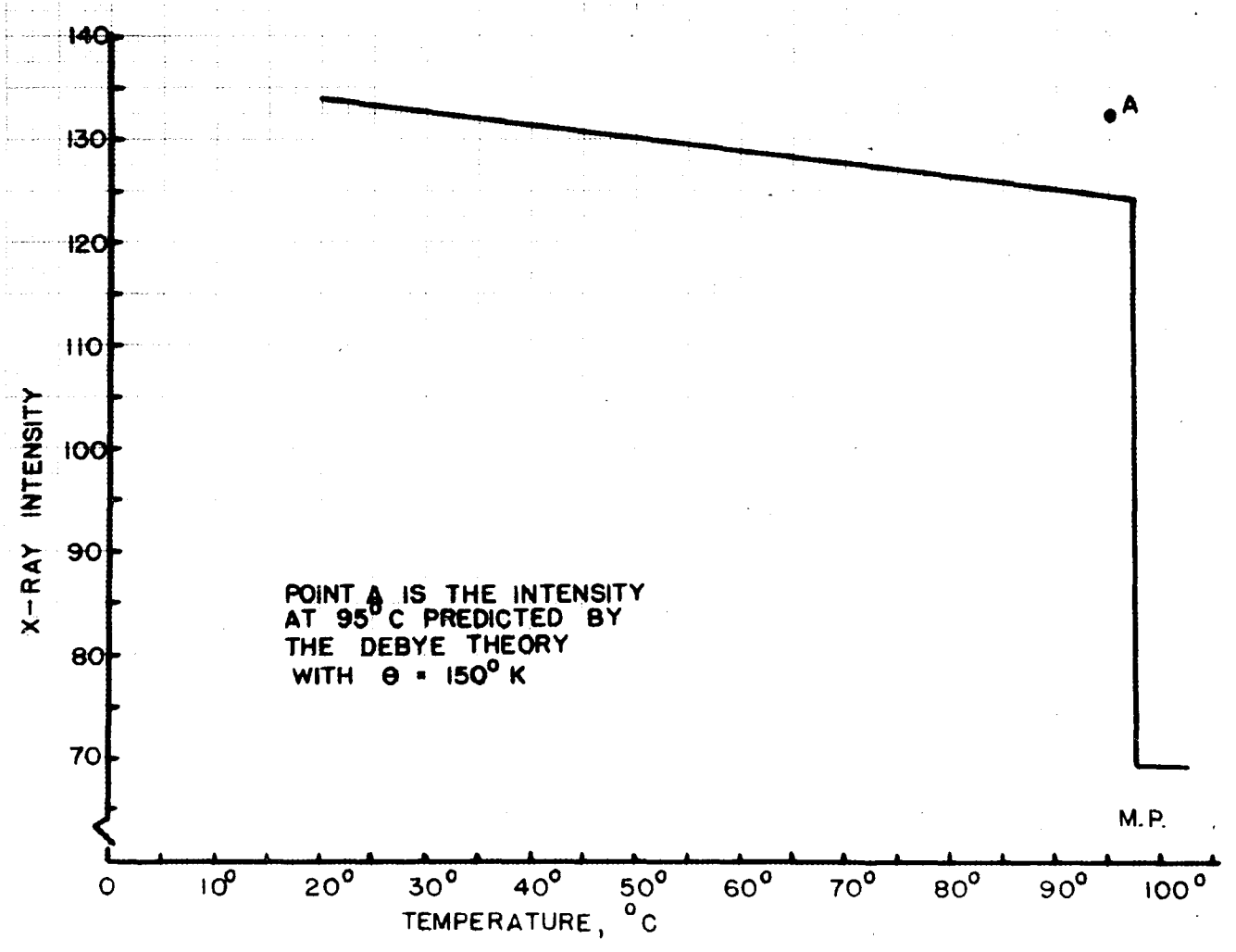

FIGURE 24. DIFFRACTED INTENSITY VS. TEMPERATURE.

[28]Debye, P., Ann. d. Physik, 43, 49(1913).

[29]Laue, M. v., Ann. d. Physik, 81, 877(1926).

Darwin[30], Schroedinger[31], Faxen[32], Brillouin[33], Waller[34],

[30]Darwin, C. G., Phil. Mag., 6-27, 675(1914).

[31]Schroedinger, E., Physik. Zeit., 15, 79(1914).

[32]Faxen, H., Ann. d. Physik, 17, 615(1918).
Zeit. f. Physik, 17, 266(1923).

[33]Brillouin, L., Ann. d. Phys., 17, 88(1922).

[34]Waller, I., Zeit. f. Physik, 17, 398(1923).
51, 213(1928).

and Zener and Jauncey[35]. The net result is that the lines

[35]Zener, C. and Jauncey, G. E. M., Phys. Rev., 49, 17(1936).

are not broadened but the intensity is decreased by a factor exp(-2M), where M is equal to B $\sin^2\theta/\lambda^2$, in which

$$B = [3h^2/mk\Theta][\phi(x)/x + 1/4], \qquad (7)$$

m is the mass of the atom, h is Planck's constant, k is Boltzmann's constant and $x = \Theta/T$, where Θ is the so-called Debye characteristic temperature of the crystal. The term $\phi(x)$ is a Debye function given by

$$\phi(x) = (1/x)\int_0^x d\xi/[\exp(\xi) - 1]. \qquad (8)$$

Values of this function are conveniently tabulated in the International Tables for the Determination of Crystal Structures[36].

[36] Gebrüder Borntraeger, Berlin(1935).

There is, however, some difficulty in determining the value of θ. This quantity was originally defined from the Debye theory of specific heats[37], and from this point of

[37] Debye, P., Ann. Physik, 39, 789(1912).

view θ for sodium is about 150° K[38]. The International

[38] Seitz, F., The Modern Theory of Solids, p. 110, McGraw-Hill, New York(1940).

Tables for Determination of Crystal Structures gives the value of θ to be 202°. Still another value of θ is given by Compton and Allison[39], 172°. Such discrepancies are not

[39] Compton, A. H. and Allison, S. K., X-Rays in Theory and Experiment, p. 438, Van Nostrand(1935).

unusual since the Debye temperature is quite dependent on the particular temperature chosen for the experiment as well as upon the method of calculation, i.e. whether the data used comes from specific heat curves, from the elastic constants or from x-ray scattering measurements. The value of θ from x-ray scattering measurements is considerably

lower than that calculated from other measurements[40]. The

[40] Alexopolus, K. and Euthymion, P., Phil. Mag., 45, 1132 (1954).

data in Figure 24 indicate that the intensity falls off much more rapidly in the neighborhood of the melting point than is predicted by the Debye theory. This effect was also noted by James and Waller[41] for NaCl.

[41] James, R. W. and Waller, I., Proc. Roy. Soc., (London), 117A, 214(1927).

In the region near the melting point of sodium, the temperature was raised very slowly and some unusual effects were noticed in the first two melting runs. Figure 25 shows the details of the first melting run. The intensity just prior to the actual melting is rather erratic. This may be the result of the annealing of the particles since it is probable that quite high strains were induced in the sample during the dispersion operation. Following this melting, the temperature was raised 0.25° above the melting point, held for 10 minutes and then lowered to room temperature.

Figure 26 shows the details of the second melting of the sample. The temperature here was raised more slowly than in the first run. The irregularities in intensity are still very much apparent. It may be that the strains persisted to a certain degree even though the sample had

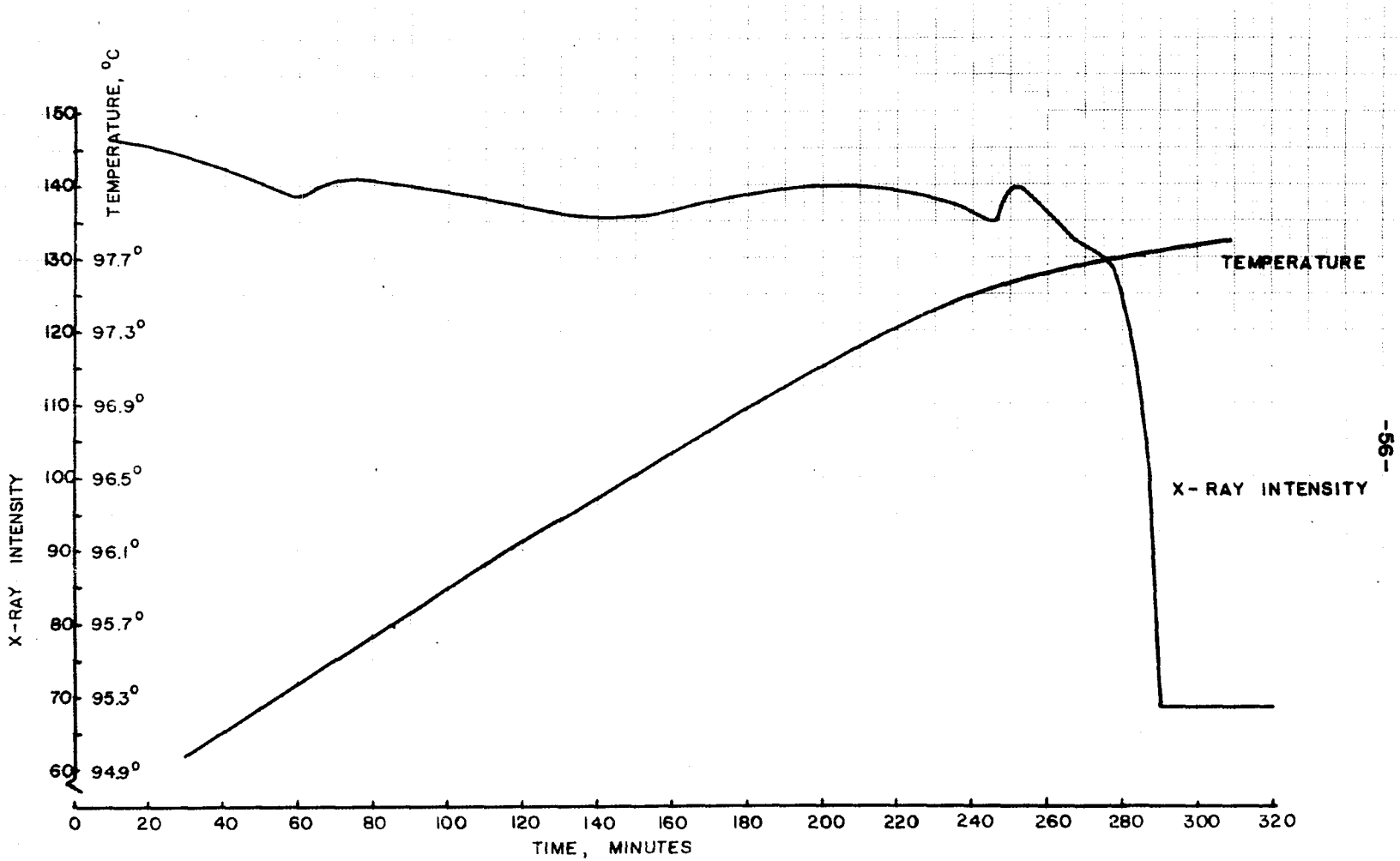

FIGURE 25. DIFFRACTED INTENSITY VS. TIME NEAR THE MELTING POINT. FIRST MELTING.

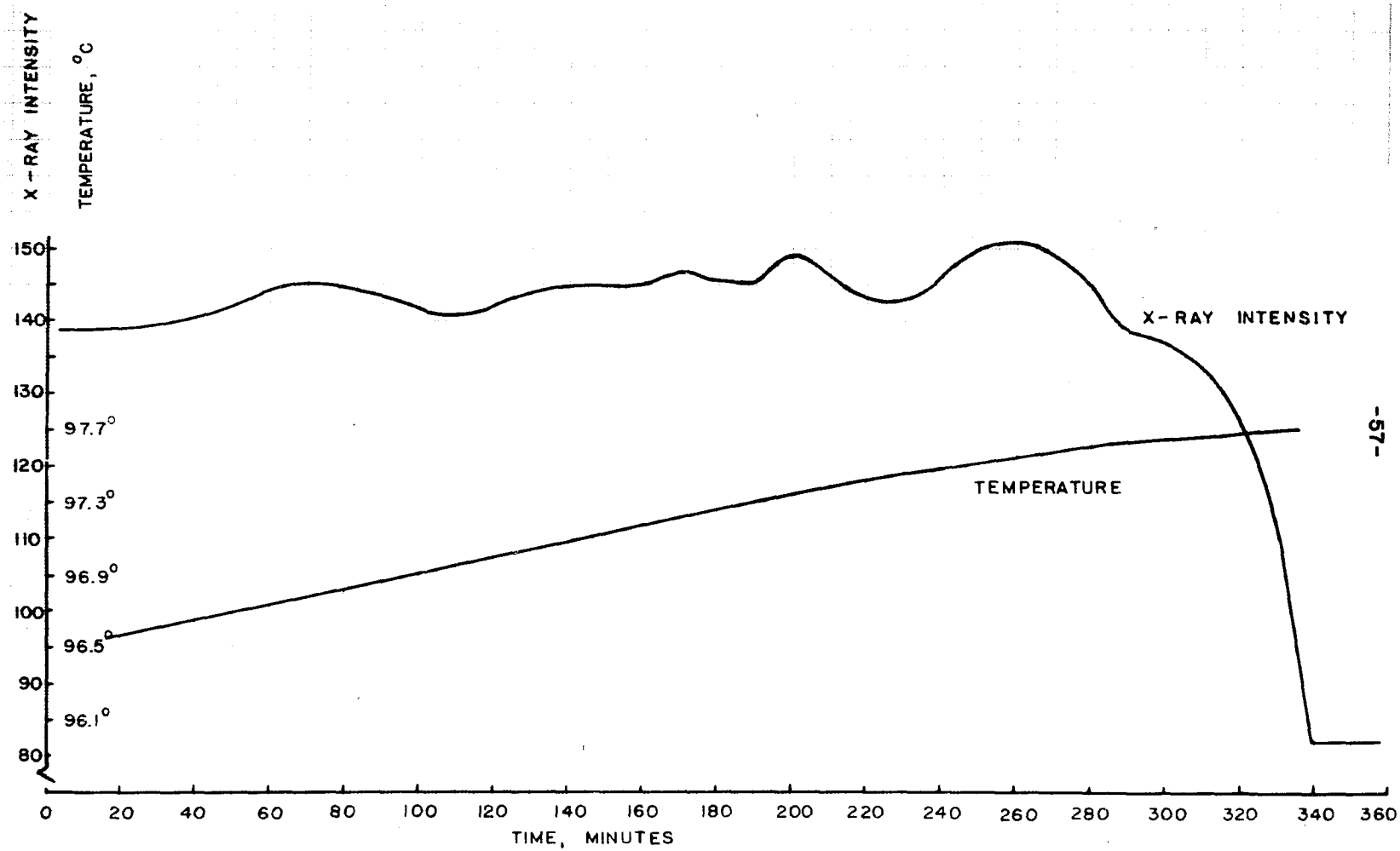

FIGURE 26. DIFFRACTED INTENSITY VS. TIME NEAR THE MELTING POINT. SECOND MELTING.

been melted. Guinier[42] has reported experiments which

[42]Guinier, A., European Scientific Notes, 6, 295(1952).

reveal that metals which are melted and then solidified often have the same crystal orientation after solidification as they had before they were melted. Whether this implies that strains can persist in a metal even though it has been melted and cooled is not known.

After the second melting, the temperature was raised 1.35° above the melting point and held there for 12 hours. The sample was then slowly cooled. Figure 27 shows the type of curve observed for the third and all subsequent meltings. The experimental points are shown for this curve as being representative of the results in general. There are no premelting irregularities of the nature previously noted. Subsequent attempts to reproduce these irregularities by cooling the sample fast from the molten state were not successful and all future curves were very smooth in the region below the melting point.

Wilchinsky[43], in a theoretical and experimental study

[43]Wilchinsky, Z. W., Acta. Cryst., 4, 1(1951).

of the diffraction of x-rays by crystalline powders of various sizes, found that under carefully controlled conditions, the diffracted intensity increased with decreasing

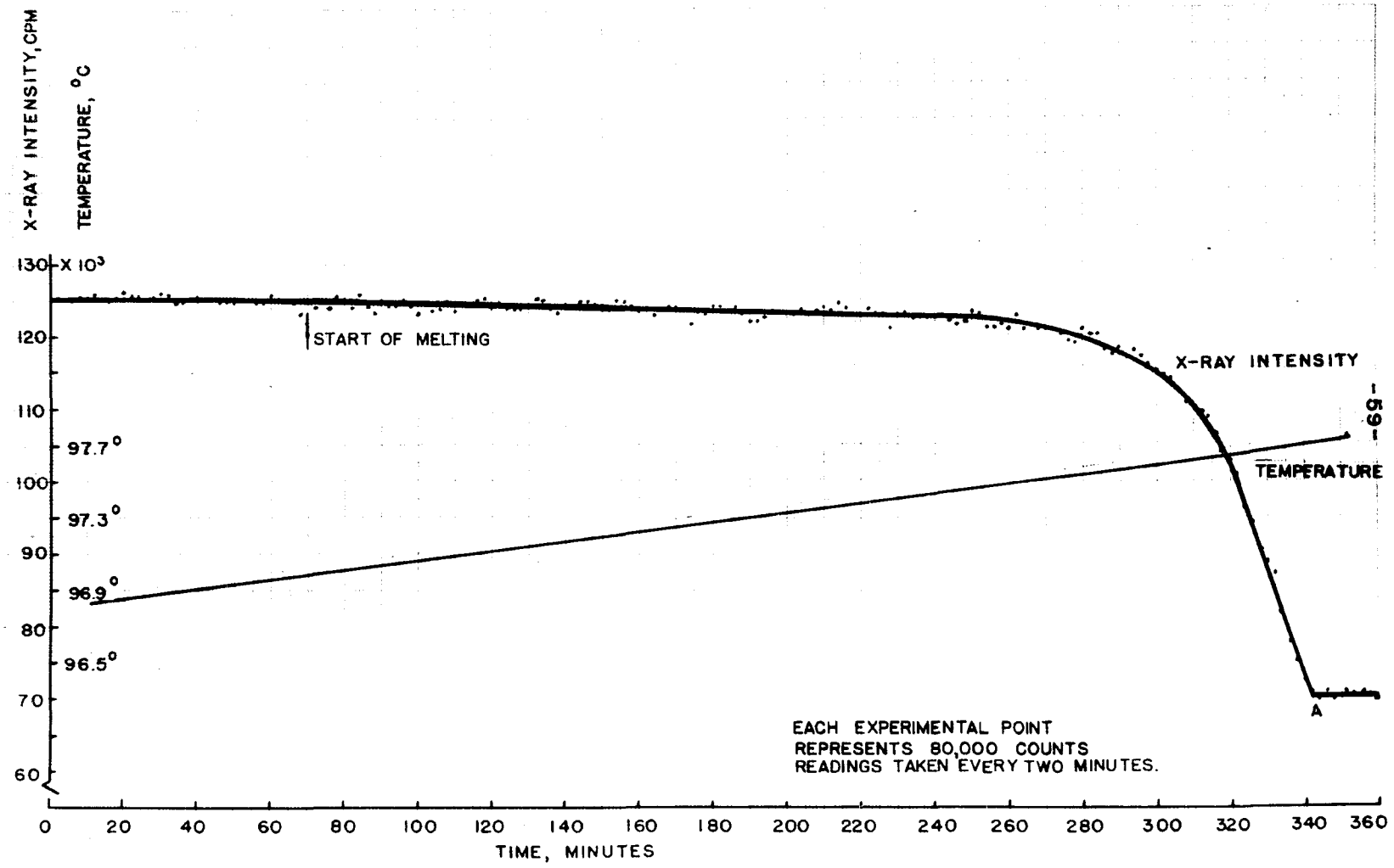

FIGURE 27. DIFFRACTED INTENSITY VS. TIME NEAR THE MELTING POINT. THIRD MELTING.

particle size in the range 10^{-3} to 10^{-5} cm. This is the range just above that where line broadening due to small particle size becomes appreciable. The data in Figures 25 and 26 might then be interpreted as a breaking up of the crystals into smaller ones as the melting point is approached. This approach has been suggested by Kossel[44].

---

[44]Kossel, W., Die Molekularen Vorgänge beim Kristallwachstum, Leipzig(1928).

It is believed that the anomalies in the intensity observed in Figures 24 and 25 were real, but that the data in the later runs are more reliable and more characteristic of the melting process.

As discussed previously (Section 2.4), it is of considerable interest to know whether the sample thermocouple reading is an accurate indication of the sample temperature. Figure 28 was taken as a test. Heating of the outer chamber ((4) in Figure 13) was reduced at point A in Figure 28 to such an extent that the inner chamber no longer continued to receive heat. This reduction in the outer chamber temperature was estimated to be about 2° C. As shown, the x-ray intensity immediately became constant, and remained so until heating was resumed about an hour later, when melting again proceeded. The experiment was repeated at point B, but the reduction in temperature of the outer chamber was only about 1° C. This probably accounts for

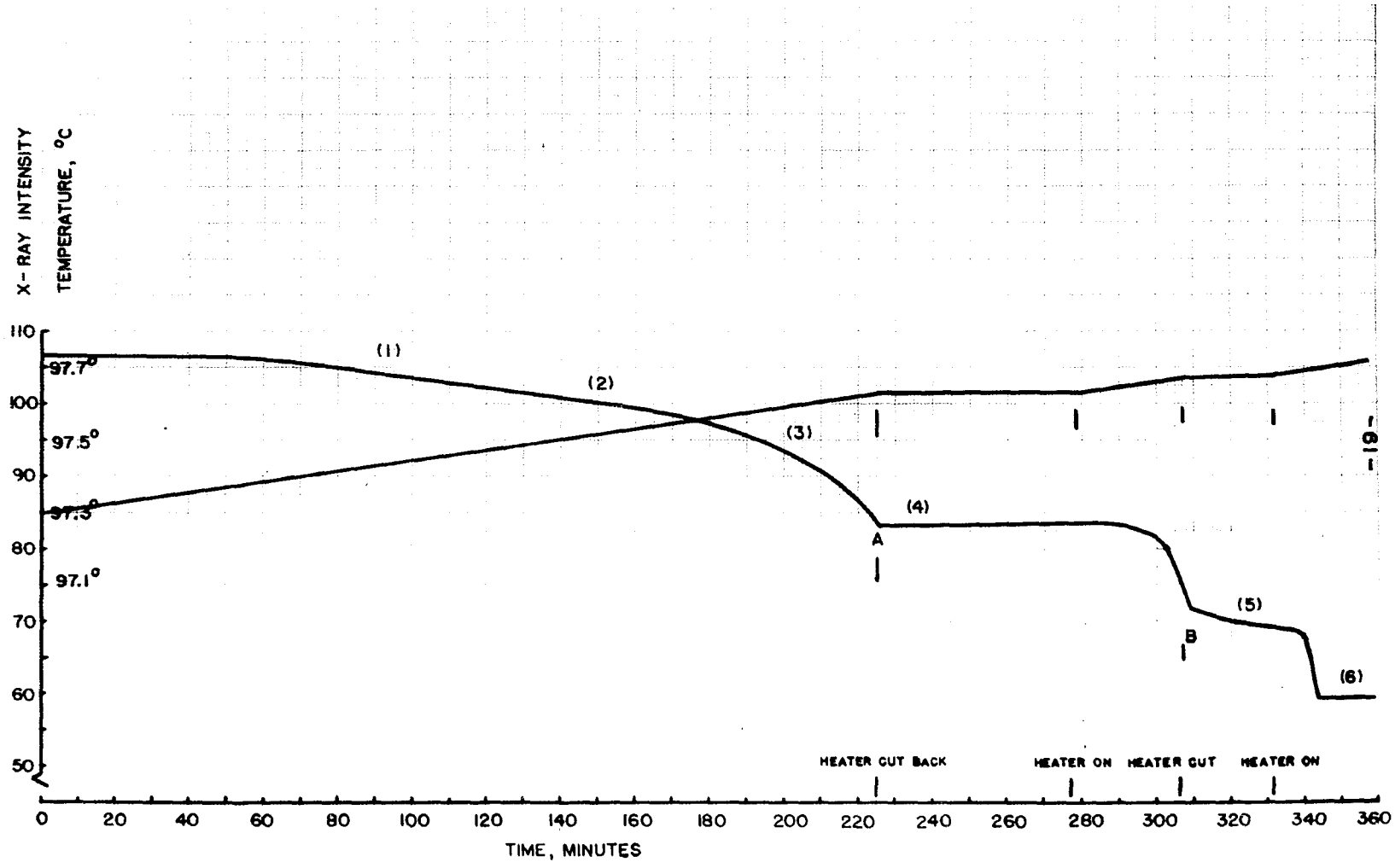

FIGURE 28. DATA FOR INTERRUPTED MELTING RUN.

the fact that the slope is not zero, though the steepness of the melting curve in this region might likewise be significant. The line was scanned at points (1), (2), (3), (4), (5), (6) and the results are shown in Figure 28A. There is no detectable change in width of the line as the melting progresses.

Returning now to Figure 27, there is a decided change in the slope of the curve considerably in advance of the sharp break. This is at a temperature about 0.65° below the melting point. That this represents actual melting of the sample has been established by allowing the intensity to drop in amounts equal to 10 and 30 percent liquid content of the sample, and then lowering the temperature until the sample was 100 percent solid. The solidification curve was typical of the solidification curves of the 100 percent melted sample. The curve for the 30 percent partial melting is shown in Figure 28B. It was particularly noticeable in these solidification curves that the maximum undercooling attained was approximately equal to the maximum undercooling with the completely melted sample. It appears that the melting of the sample at temperatures under the melting point of the bulk of the sample is a particle size effect.

Pavlov[45] was the first to study the effect of particle

---

[45]Pavlov, J., J. Russ. Phys. Chem. Soc., XL, 1022(1908).

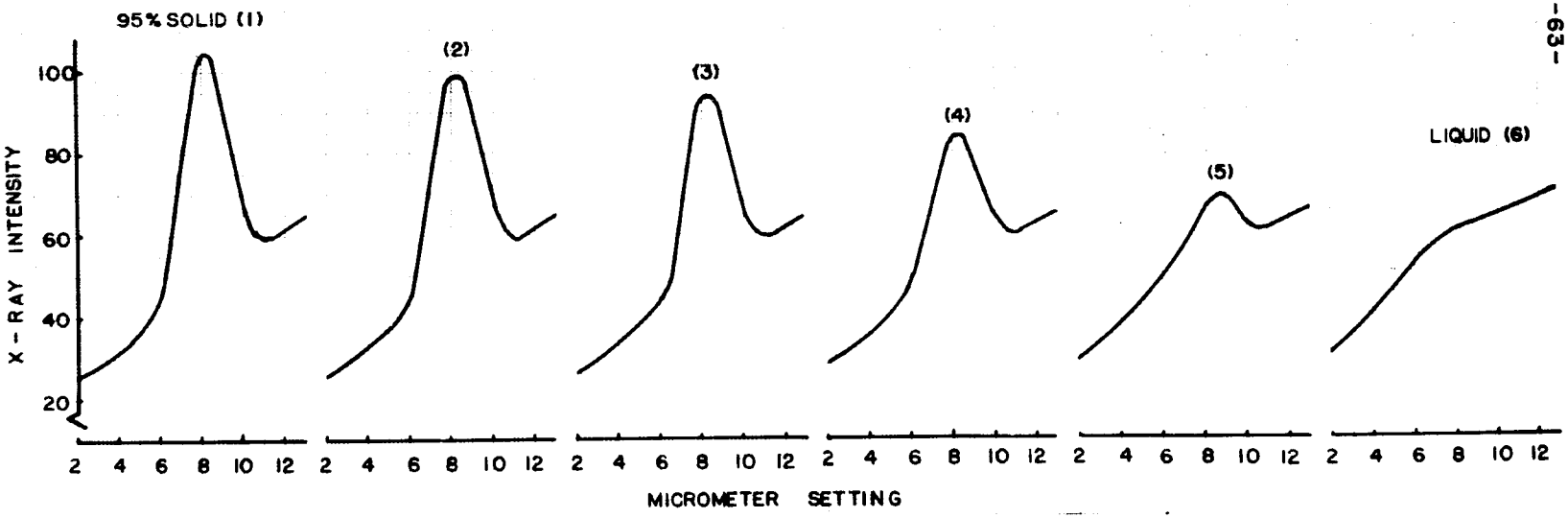

FIGURE 28A. 110 LINE OF SODIUM AS MELTING PROGRESSES.

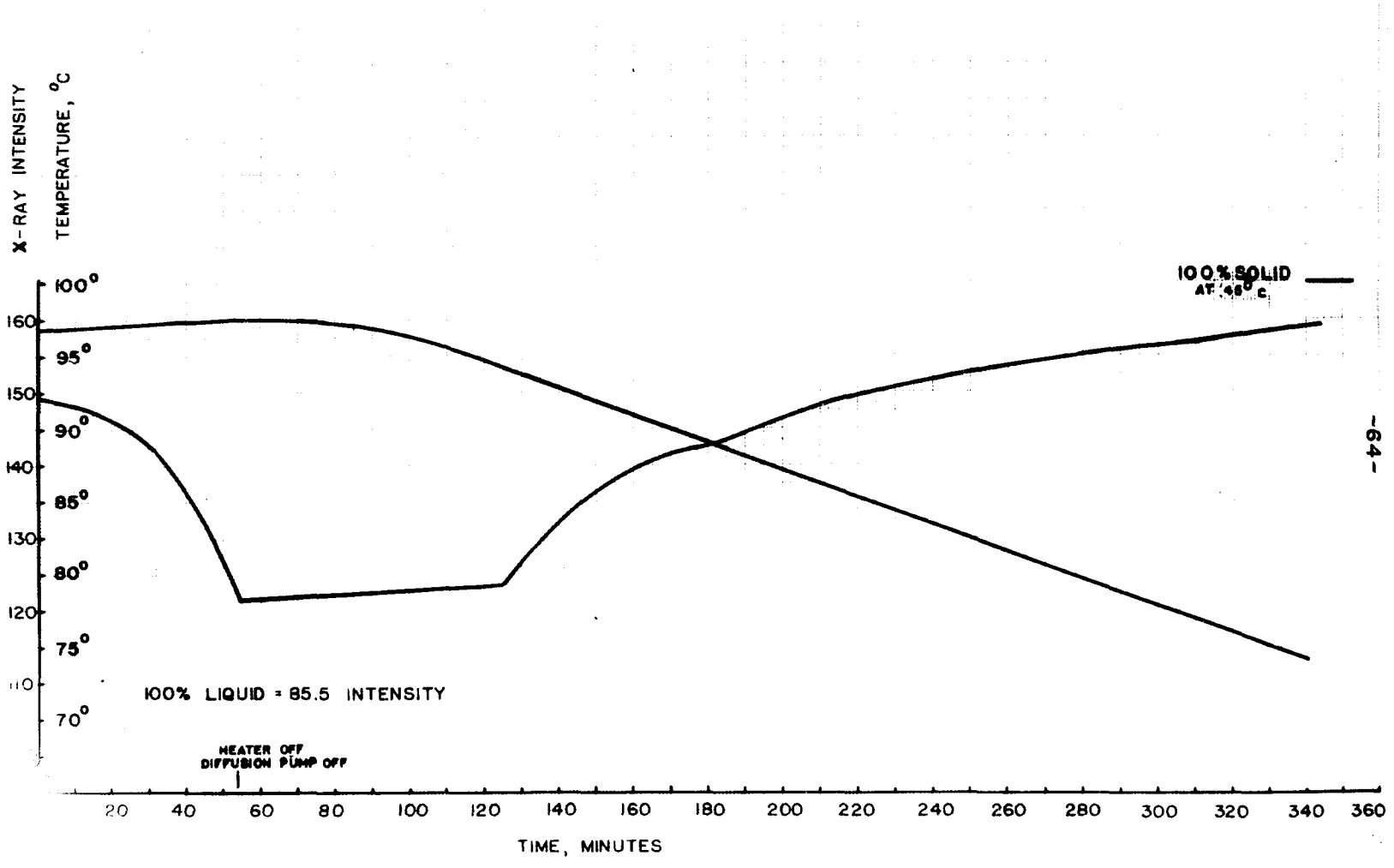

FIGURE 28 B. PARTIAL MELTING AND RESOLIDIFICATION (30% LIQUID).

size on the melting temperature. He came to the conclusion that the smaller the particle size the lower the melting point. From a thermodynamical point of view, and assuming the principle of continuity can be applied to crystals in equilibrium with their melt, the following relationship can be derived[46],

[46] Rie, E., Zeit. f. Phys. Chem., 104, 354(1923).

$$\Delta T/T_o = 2\sigma/rQd \qquad (9)$$

where σ is the surface free energy of the liquid vs the solid, ΔT is the lowering of the melting point, r the radius of the droplet, Q the latent heat of crystallization, d the density of the solid phase, and T_o the melting temperature of a bulk sample. The value of σ in this expression has been criticised by Harbury[47], who states that σ is not

[47] Harbury, L., J. Phys. and Colloid Chem., 50, 190(1946).

merely the surface free energy of the material but must include many other factors, largely of unknown character and importance. According to Harbury, the effect should be noticeable only in the range of particle size 10 to 100 $\mathring{A}$, but Rie[46] indicated the effect may be noticeable for values of r approximately equal to 10^{-5} cm.

Hinshelwood and Hartley[48] in a series of experiments

[48] Hinshelwood, C. N. and Hartley, H., Phil. Mag., 6-43, 78(1922).

on the equilibrium between small crystallites and their melt found that ΔT varied as $1/r$ and that the effect was appreciable for particles of r of the order of 10^{-5} cm.

Figure 27 may be analysed on the basis of the melting of the smaller particles at temperatures below the melting point of the bulk. Figure 29 shows the percent solid as a function of temperature below the melting point where, now, the "melting point" is assumed to be the temperature for complete melting (point A, Figure 27). If the assumption is made that 90 percent of the volume of the sample consists of particles with a radius greater than 5×10^{-6} cm*, then Equation (9) may be used to find the

*see Appendix III

cumulative volume as a function of particle size. Ten percent of the sample had melted at $\Delta T = 0.15^{\circ}$ C. From Equation (9), $\sigma = 1.3$ ergs per cm^2. Figure 30 shows a plot of the cumulative sample volume as a function of the particle radius. The slope of this curve gives the particle size distribution in the sample, shown in Figure 30A. This curve is to be compared to a similar curve plotted from the solidification studies.

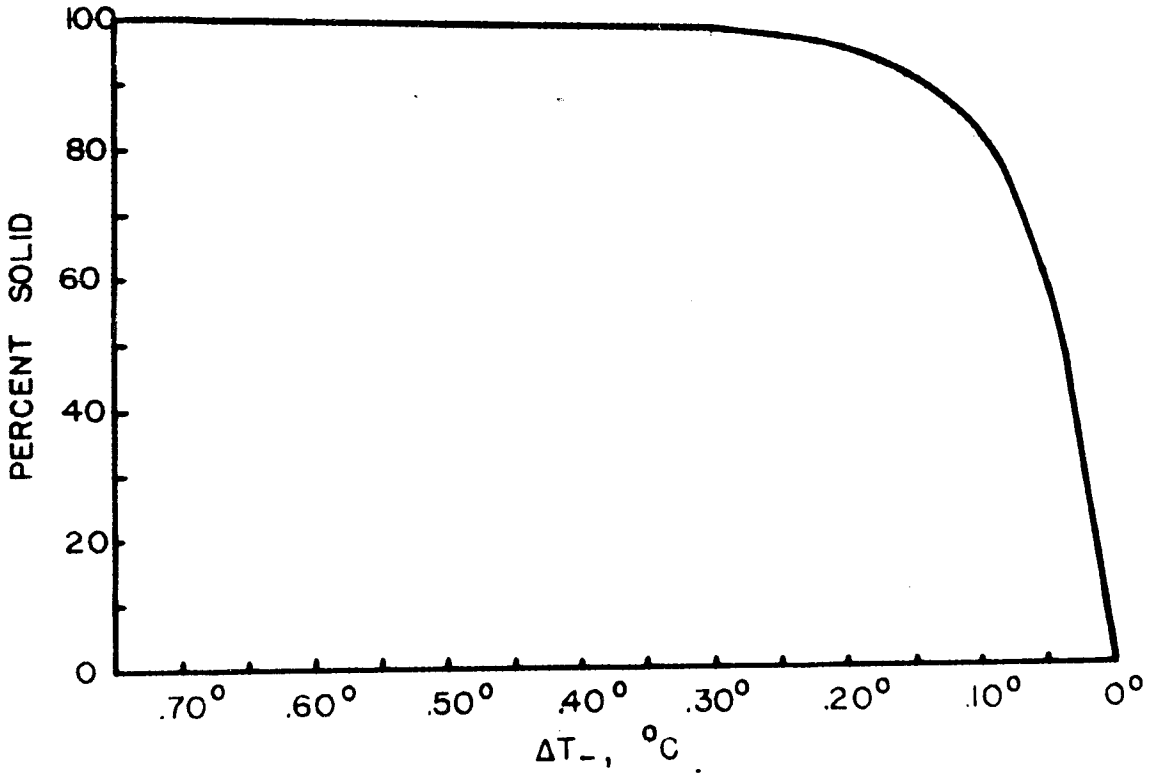

FIGURE 29. PERCENT SOLID VS. TEMPERATURE UNDER THE MELTING POINT.

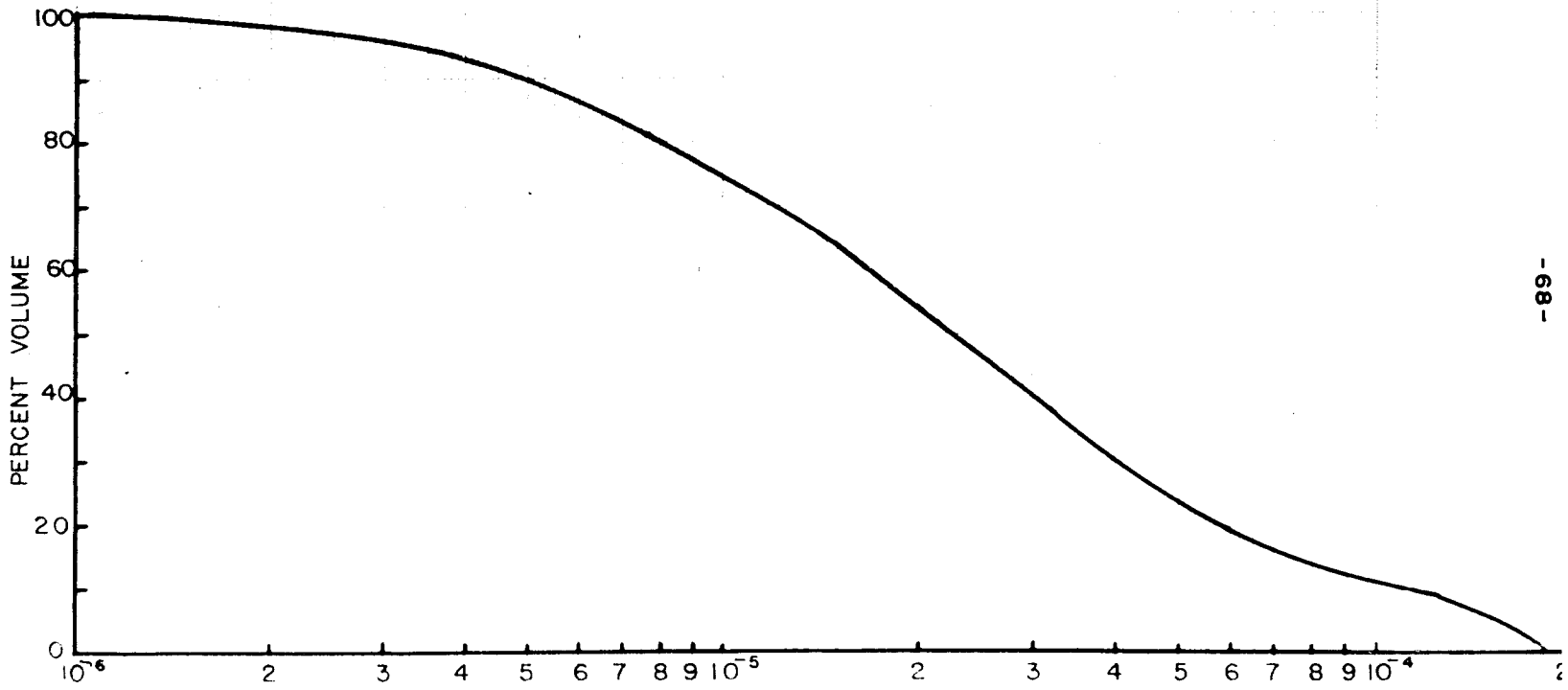

FIGURE 30. CUMULATIVE PERCENT VOLUME VS PARTICLE SIZE FROM MELTING CURVE.

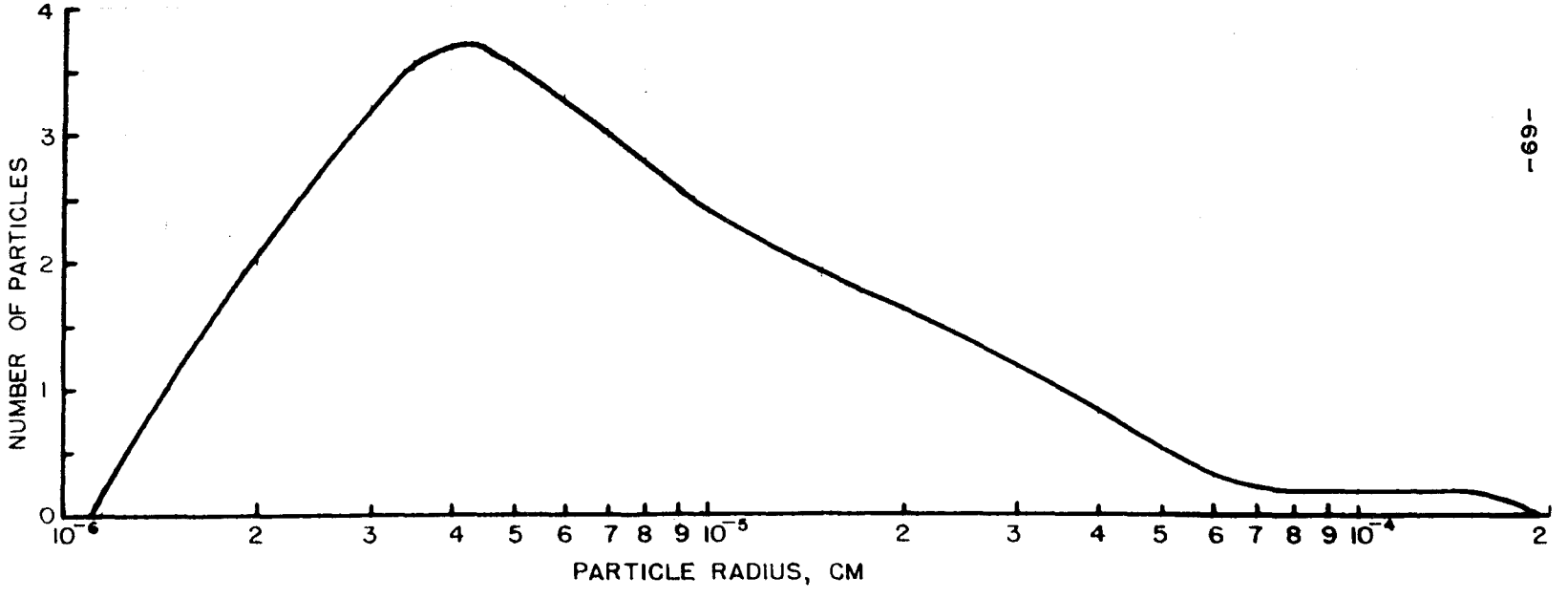

FIGURE 30A. PARTICLE SIZE DISTRIBUTION FROM THE MELTING CURVE.

There was some question as to the location melting point because of the linear portion of the curve in Figure 27. If the sample melted isothermally, the intensity would be expected to drop linearly for the time required to melt the sample. A calculation* was made of

*see Appendix II.

the amount of heat necessary to completely melt the sample, and of the amount of heat available from the oil bath, if the oil bath temperature is 0.01° C above the melting point of the sample. This calculation showed that 0.23 calories are necessary to melt the sample completely and that 1.6 calories are available from the oil bath. So, if the melting is isothermal, there is ample heat available to continue the melting at the points A and B in Figure 28. However, the melting stops when heat is no longer put into the oil bath chamber, so it is to be concluded that the observed shape of the melting curve represents a particle size effect and that the "bulk" melting point is at a temperature no lower than point A in Figure 27.

3.3 A: Solidification

The inability of thermodynamic theories to explain many observed processes in phase transformations has led to the theory of nucleation and growth. The first theories

were developed to explain the nucleation of the liquid phase in super-saturated vapor. Volmer and Weber[49] were

[49] Volmer, M. and Weber, A., Zeit. f. Phys. Chem., 119, 227 (1925).

the first to propose a reasonable model. They proposed that dense clusters of molecules appeared in the vapor by thermal fluctuations. These clusters, (called embryos) under certain conditions, could grow to a size large enough to become nuclei for the new phase. Becker and Döring[50]

[50] Becker, R. and Döring, W., Ann. d. Phys., 5-24, 719(1935).

improved this theory by considering the possibility that embryos and nuclei can shrink as well as grow. The theory in the form presented by them is the basis for applications of nucleation and growth theory to other transformations. A review of the theory is useful at this point.

In gases, fluctuations of density are predicted by statistical theories. These fluctuations result in unusual scattering of light near the critical point. The results of light scattering experiments in both liquids and gases, are excellently described by the theories of Smoluchowski[51]

[51] Smoluchowski, M., Ann. d. Physik, 25, 205(1908).

and Einstein[52]. The average value of the density fluctuations

[52]Einstein, A., Ann. d. Physik, 33, 1275(1910).

turns out to be inversely proportional to the square root of the number of molecules in the region considered.

Even in view of these fluctuations, it seems unreasonable that a sufficient number of molecules to form a stable nucleus would come into contact simultaneously. The assumption is therefore made[53], that embryos are born,

[53]Volmer, M. and Weber, A., Zeit. f. Phys. Chem., 119, 227 (1925).

grow to nuclei, or disappear by a sequence of bimolecular reactions, thus,

$$\begin{aligned} \alpha + \alpha &\rightleftharpoons \beta_2 \\ \beta_2 + \alpha &\rightleftharpoons \beta_3 \\ &\cdot \\ &\cdot \\ \beta_{i-1} + \alpha &\rightleftharpoons \beta_i \end{aligned} \qquad (10)$$

where α represents an atom or molecule of the phase α and β_i an embryo of the phase β containing i atoms or molecules.

Another basic assumption of the theory of Volmer and Weber and Becker and Döring is that the free energy of the embryos can be calculated by assuming them to be small droplets of the liquid phase, and that the surface energy per cm^2 of the embryo is equal to that for a flat surface

of the liquid. The free energy of a system of small drops of liquid β dispersed in a gas α is

$$G = n_\alpha g_\alpha + n_\beta g_\beta + 4\pi r^2 \sigma, \qquad (11)$$

where n_α and n_β are the numbers of molecules of α and β and g_α and g_β the free energies per particle of phases α and β respectively, r is the radius of the drop and σ the surface free energy of the liquid with respect to the vapor. For $r = 0$, $G_0 = (n_\alpha + n_\beta)g_\alpha$, and

$$\Delta G = G - G_0 = (4\pi r^3/3v_\beta)(g_\beta - g_\alpha) + 4\pi r^2\sigma, \qquad (12)$$

which has a maximum when $r = r_c$, found by setting

$$\partial \Delta G/\partial r = (12\pi r^2/3v_\beta)(g_\beta - g_\alpha) + 8\pi r\sigma = 0.$$

Then

$$g_\alpha - g_\beta = 2\sigma v_\beta/r_c \qquad (13)$$

or

$$r_c = 2\sigma/\Delta G_v, \qquad (14)$$

where ΔG_v is the change in free energy per unit volume in the transition $\alpha \rightarrow \beta$.

Equation (12) becomes,

$$\Delta G = 4\pi\sigma(r^2 - 2r^3/3r_c), \qquad (15)$$

where r_c is the critical radius for equilibrium. The equilibrium is unstable because of the nature of the energy curve.

It is sometimes convenient to write ΔG in terms of the number of atoms or molecules i in an embryo of radius r. Thus,

$$\Delta G_i = Ai^{2/3} + Bi. \tag{16}$$

The maximum value of ΔG is

$$\Delta G^* = (1/3)(4\pi\sigma r_c^2) = 16\pi\sigma^3/3(\Delta G_v)^2. \tag{17}$$

Figure 31 shows a plot of Equation (15). Curve 1 is

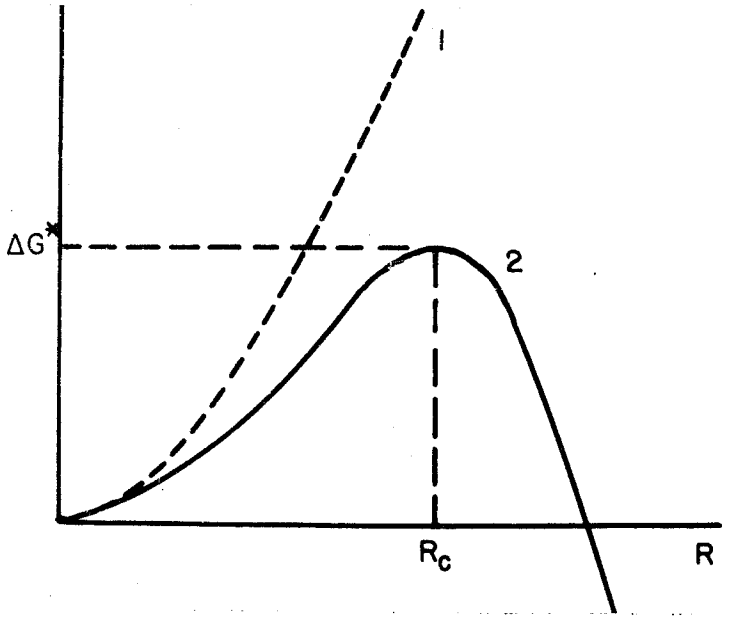

Figure 31. Energy of formation of an embryo as a function of its size, in a stable phase (1) and unstable phase (2).

a plot of the first term and represents the energy as continually increasing with no maximum and therefore no possibility of the embryo becoming a stable nucleus capable of starting a transformation. Curve 2 is a plot of the complete equation. From the curve it is observed that embryos smaller than r_c will, in general, evaporate, so that the critical size can be reached only by the kinetic process of statistical fluctuations that is allowed in view of the statistical nature of the second law of thermodynamics. Embryos of a size r_c are called nuclei. They have an equal chance of growing or evaporating, but once they start to grow they rapidly progress to stable particles of the new phase.

The equilibrium number of embryos, containing i molecules each, may be found by minimizing the free energy of the system with respect to the number of embryos. The free energy change upon introducing n_i embryos is

$$\Delta G = n_i \Delta G_i - T\Delta S_{n_i} \tag{18}$$

where ΔS_{n_i} is the entropy of mixing n_i embryos with the remaining particles. If the number of embryos of all sizes is very much smaller than the number of untransformed atoms, the entropy of mixing reduces to

$$\Delta S_{n_i} = kn_i(1 - \ln(n_i/n)). \tag{19}$$

Then,

$$\partial \Delta G/\partial n_i = \Delta G_i + kT\ln(n_i/n). \qquad (20)$$

Setting this equal to zero and solving for n_i,

$$n_i = N \exp(-\Delta G_i/kT) \qquad (21)$$

where N is the number of atoms per cm^3 in the system. Now if $\Delta G_i = \Delta G^*$ then $n_i = n^*$ and the number of nuclei in the system will be

$$n^* = N \exp(-\Delta G^*/kT). \qquad (22)$$

The basic problem in nucleation theory is the calculation of the rate of nucleation of a new phase. In the theory of Volmer and Weber, the nuclei were assumed only to grow, and not to evaporate, hence the rate of stable nucleation is equal to the number of unstable nuclei multiplied by the number of molecules per second striking the surface of the nucleus. From the kinetic theory of gases[54]

---

[54] Loeb, L., Kinetic Theory of Gases, p. 105, McGraw-Hill, New York(1934).

---

the number of molecules striking a unit surface in unit time is

$$\eta = p/\sqrt{2\pi MkT}, \qquad (23)$$

where p is the pressure and M the molecular weight. Thus,

the rate of nucleation will be

$$I = (4\pi N r_c^2 p/\sqrt{2\pi MkT})\exp(-4\pi\sigma r_c^2/3kT) \qquad (24)$$

and the rate of condensation into the phase β will be

$$R = I\, i_c, \qquad (25)$$

where i_c is the number of atoms in the stable nucleus. Equation (24) is the formula derived by Volmer and Weber.

Becker and Döring[55] took into account the fact that

---

[55]The derivation is rather complex and is given in detail in Ann. d. Physik, 5-24, 719(1935).

---

embryos have a chance of evaporating as well as growing. If S_i is the surface area of an embryo containing i molecules, P' the probability of growing and P_i'' that of evaporation per unit area per unit time these authors find

$$I = (P'S_i/i_c)\sqrt{A/3\pi}\, \exp(-4\pi\sigma r_c^2/3kT). \qquad (26)$$

Equation (26) differs from Equation (24) only in the coefficient, the two exponents are identical. Actually the exponential term completely dominates the expression and the effect of the other differences is not detectable when comparing with experiment. However, the treatment of Becker and Döring does avoid some of the thermodynamic uncertainties of earlier theories.

Attempts[56,57] have been made to improve the expression

[56]Kirkwood, J. G. and Buff, F. P., J. Chem. Phys., 18, 991 (1950).

[57]Reiss, H. J., J. Chem. Phys., 20, 1216(1952).

for the free energy of the embryos, especially the surface energy term. In an extremely small droplet, 10 to 100 molecular diameters, there is no definite surface, but rather a transition zone 2 to 5 molecular diameters in thickness[58,59]. These theories lead to substantially

[58]Tolman, R. D., J. Chem. Phys., 17, 333(1949).

[59]Kirkwood, J. G. and Buff, F. P., J. Chem. Phys., 17, 338 (1949).

different values of ΔG^*.

The previous development has been based on the assumption that nucleation takes place solely by thermal nucleation. That is to say, it is spontaneous and occurs by thermal fluctuations alone. This is termed homogeneous nucleation.

It has been observed that particular samples used in nucleation experiments have given widely different results. The results are very sensitive to the purity of the sample and to the thermal history. It therefore appears that most transformations are nucleated by foreign objects or influences on the system. Such nucleation is called heterogeneous nucleation. Recognizing this, Volmer[60] expanded his

[60]Volmer, M., Zeit. f. Elektrochem., 35, 555(1929).

earlier theory to include the effect of a finite contact angle between a liquid embryo and a plane foreign surface. This resulted in an expression for $\Delta G_s^* = \Delta G_o^* f(\theta)$, where ΔG_o^* is the free energy for homogeneous nucleation as in Equation (17) and $f(\theta)$ a function of the contact angle. This results in an expression for the rate of nucleation,

$$I = K \exp(-\Delta G_s^*/kT) \qquad (27)$$

where K is an undetermined coefficient.

One would assume that the free energy for heterogeneous nucleation will be less than that for homogeneous nucleation, so that if enough sites for heterogeneous nucleation exist, the entire reaction will proceed by this process. However, if insufficient sites exist, the reaction will not go to completion and the rate of nucleation will be a function of time. This possibility was recognized, and a formal theory developed to describe it by Avrami[61]. The nucleation rate as a function of time

[61]Avrami, J., J. Chem. Phys., 7, 1103(1939).

is shown in Figure 32. The initial buildup of the nucleation in vapor-liquid systems is very rapid, though not

instantaneous as predicted by the theory of Becker and Döring. Theories of the dependence of the rate of nucleation on time have been proposed by Zeldovich[62] and more

[62]Zeldovich, J. B., Acta Physiochim., USSR, 18, 1(1943).

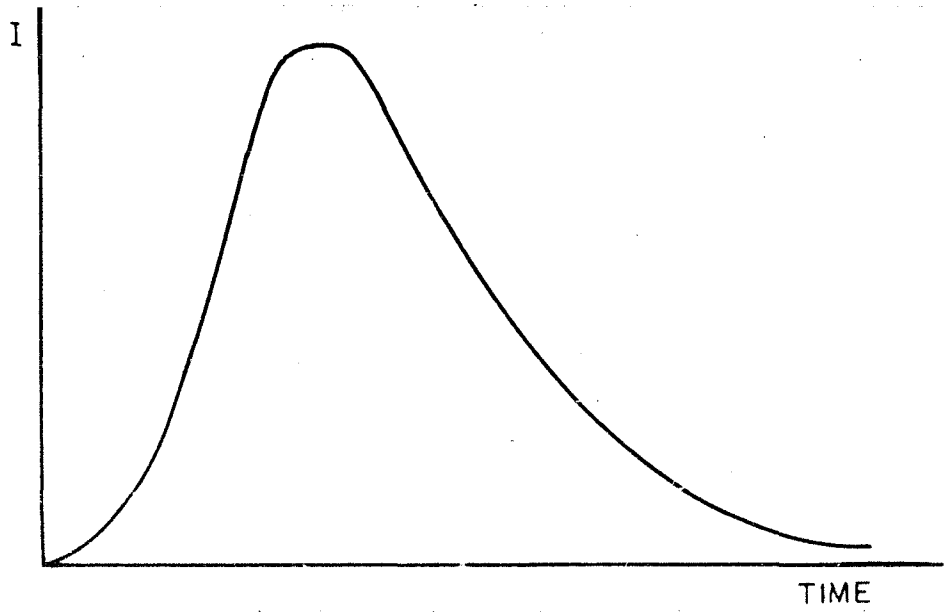

Figure 32. Rate of heterogeneous nucleation vs time for a limited number of nucleation sites.

recently by Kantrowitz[63] and Probstein[64], but they have been

[63]Kantrowitz, A., J. Chem. Phys., 19, 1097(1951).

[64]Probstein, R. F., J. Chem. Phys., 19, 619(1951).

only qualitatively effective in explaining experimental results of nucleation in very rapid expansions. The general expression for the curve has the form,

$$I_t = N_o f \exp(-ft + i_c^2/4n_c\eta t), \qquad (28)$$

where N_o is the number of nucleation sites, f is the nucleation frequency per site, and n_c the number of surface atoms in the nucleus. η is usually large, so that the second term is small, except for very rapid changes in temperature or pressure.

As far as the general agreement between theory and experiment is concerned, it may be said that the theory as presented by Becker and Döring gives excellent agreement with the experimental results of Volmer and Flood[65] on

---

[65]Volmer, M. and Flood, H. Z., Zeit. f. Phys. Chem., 170A, 273(1934).

---

the nucleation of water from supersaturated vapor. Agreement of the other theories discussed above is not as satisfactory.

The success of the Becker and Döring theory in the case of vapor-liquid transitions, has encouraged the use of similar assumptions in extending the theory to homogeneous nucleation in liquid-solid and solid-solid transitions.

Becker[66] was the first to extend the theory to the

---

[66]Becker, R., Ann. d. Physik, 32, 128(1938).

---

liquid-solid transformation. It was assumed that the free

energy for formation of embryos in a condensed system is of identical form as that for formation of embryos in gaseous systems. However, in condensed systems the kinetic theory expression for the rate of bombardment of the nucleus by atoms or molecules of the parent phase can no longer be used. The movement of an atom across an interface must be expressed in terms of an activation energy, say ΔG_A. Hence Becker's expression has the form,

$$I = C \exp(-(\Delta G^* + \Delta G_A)/kT) \qquad (29)$$

where C is an undetermined coefficient.

More recently Turnbull and Fisher[67] using the same basic assumptions as Becker and Döring, applied absolute reaction rate theory[68] to the problem. This theory predicts that the net transfer of atoms across an interface is,

$$\nu = (kT/h) \exp(-\Delta G_A/kT). \qquad (30)$$

Substituting (30) for η in Equation (23), and making reasonable assumptions concerning the size of the nucleus and the magnitude of the energies involved, they were able

[67] Turnbull, D., and Fisher, J. C., J. Chem. Phys., 17, 71(1949).

[68] Glasstone, S., Laidler, K. J. and Eyring, H., The Theory of Rate Processes, McGraw-Hill, New York(1941).

to arrive at a quantitative expression for the rate of nucleation. Thus,

$$I = n^*(a\sigma/9\pi kT)^{\frac{1}{2}}n(kT/h)\ \exp(-(\Delta G^* + \Delta G_A)/kT), \qquad (31)$$

where a is determined by the geometrical shape of the nucleus, n^* is the number of atoms in the surface of a nucleus of critical size, and n the number of atoms per unit volume of the parent phase. For spherical nuclei,

$$(a\sigma/9\pi kT)^{\frac{1}{2}} = (\sigma/kT)^{\frac{1}{2}}(2v/9\pi)^{1/3}, \qquad (32)$$

where v is the volume per atom in the parent phase.

Following the treatment for transient nucleation, I_t may be written

$$I_t = I\ \exp(-ft + i^{*2}/4n^*\nu t). \qquad (33)$$

Since in condensed systems ν can be very small, this may be an important factor in nucleation in condensed systems even at ordinary rates of change of temperature.

In general, the theory is applied to experiment by the adjustment or calculation of ΔG^*, for, in fact, except over a small range of temperature, this is the controlling factor. The theory has been applied with moderate success by Turnbull, Holloman, Fisher and Vonnegut at the General Electric Research Laboratories and by LaMer and Pound elsewhere, to the problem of crystallization from an

undercooled melt. Excellent review articles have been written on the subject[69,70,71,72].

---

[69]Holloman, J. H. and Turnbull, D., Progress in Metal Physics, 4, 333(1953).

[70]LaMer, V. K., Ind. Eng. Chem., 44, 1269(1952).

[71]Pound, G. M., Ind. Eng. Chem., 44, 1278(1952).

[72]Turnbull, D. and Vonnegut, B., Ind. Eng. Chem., 44, 1292 (1952).

The above theory has been advanced to explain homogeneous nucleation. However, there is ample evidence that most liquid-solid transformations are nucleated by heterogeneities on the walls of the container holding the sample. Following a study of the effect of catalysts on the surface of the sample container, Turnbull and Vonnegut[73] derived

---

[73]Turnbull, D. and Vonnegut, B., Ind. Eng. Chem., 44, 1292 (1952).

---

an expression for the nucleation frequency per unit area of catalyst surface. Their expression had the same exponential term as Volmer's Equation (27), but a different coefficient. The rate of nucleation as derived by them is,

$$I = n_s kT/h \exp(-\Delta G^* f(\theta)/kT) \qquad (34)$$

where n_s is the number of atoms in contact with the catalytic surface. The heterogeneities may take the form of microcavities in which crystals of the solid phase may persist

somewhat above the melting point of the bulk sample. Such a process might be reflected in a thermal history effect such that $(\Delta T_-)_m$ is proportional to ΔT_+, where $(\Delta T_-)_m$ is the maximum undercooling and ΔT_+ is the amount of heating over the normal melting point. Turnbull[74] has calculated

[74] Turnbull, D., J. Chem. Phys., 18, 198(1950).

the free energy of formation of an embryo in cylindrical and conical cavities, which in part, explains the effect of thermal history on ΔT_-.

Another especially interesting set of experiments, and an extension of the theory for the case of nucleation of the solid phase in a liquid melt catalysed by surface films, has been made by Turnbull[75,76]. He measured the

[75] Turnbull, D., J. Appl. Phys., 21, 1022(1950).

[76] Turnbull, D. and Vonnegut, B., Ind. Eng. Chem., 44, 1292 (1952).

maximum supercooling of liquid mercury droplets which were coated with various surface films. These, as well as experiments with aluminum[77,78] and other metals[79] have

[77] Eborall, M. D., J. Inst. Metals, 76, 321(1949).

[78] Chibula, A., J. Inst. Metals, 80, 1(1951).

[79] Reynolds, J. A. and Tottle, C. R., J. Inst. Metals, 80 93(1951).

resulted in a theory of nucleation catalysis based upon the crystallographic similarity of the catalyst and material involved. The treatment is in part based on the concepts put forward by Frank and Van der Merwe[80] to explain the

[80] Frank, F. C. and Van der Merwe, J. H., Proc. Roy. Soc., (London), 198A, 216(1949).

formation of oriented monolayers on crystalline substrates. The basic postulate of the theory proposed by Turnbull and Vonnegut[76] is that the interfacial energy between the nucleus and the catalyic surface element is a minimum when the nucleus forms coherently with the catalyst. Using this and the dislocation model of interphase boundaries of Van der Merwe[81] and Brooks[82] for determining the interfacial

[81] Van der Merwe, J. H., Proc. Phys., 63A, 616(1950).

[82] Brooks, H., Metal Interfaces, Am. Soc. Metals, Cleveland (1952).

energy, they have derived an expression for the critical free energy for heterogeneous nucleation of the form

$$\Delta G^* = 4\pi\sigma_{LS}^3(2 + m)(1 - m^2)/3(\Delta G_v + c\epsilon^2)^2, \qquad (35)$$

where $m = \cos\theta = (\sigma_{CL} - \gamma - \alpha(\delta - \epsilon))/\sigma_{LS}$, γ is the non-structural component of σ_{SC} and $\alpha(\delta - \epsilon)$ is the structural component of σ_{SC}, α is a constant, δ the disregistry between the nucleus and the film, and ϵ the strain in the nucleus.

The disregistry is defined as $\Delta a/a_o$, with a_o equal to the lattice constant, and Δa the difference in the lattice constants of the nucleus and the film.

If a reasonable value of nucleation is 1 per cm^3 per second, then Equation (27) gives $\Delta G_s^* \approx 60kT$. Setting Equation (35) equal to this and making some other plausible assumptions it is found that for large δ,

$$\Delta G_v \propto \delta$$

and

$$\Delta G_s^* \propto 1/\delta. \tag{36}$$

Thus, the potency of a nucleation catalyst is inversely proportional to the disregistry between the crystal structure of the nucleus and the crystal structure of the catalyst.

The theory is greatly simplified and the various quantities involved in the expression for the free energy are largely unmeasured or unmeasurable, and, as such, represent, to a certain extent, arbitrary constants. However, the theory explains, at least qualitatively, many of the observed features of heterogeneous nucleation, catalysed by known substances.

Nucleation theory has also been qualitatively applied to many problems in solid-solid transformation, however, as yet no quantitative theory has been developed. The reason for this is a lack of quantitative experimental

data and the great complexity of the problem. Some recent reviews have been made by Smoluchowski[83,84] and others[85].

---

[83] Smoluchowski, R., Phase Transformations in Solids, p. 149, Wiley, New York (1951).

[84] Smoluchowski, R., Ind. Eng. Chem., 44, 1321(1952).

[85] Fisher, J. C., Holloman, J. H. and Leschen, J. G., Ind. Eng. Chem., 44, 1324(1952).

The sample used in the experiments to be described later was in the form of small spheres. It is therefore worthwhile to note the effect of sample volume on the rate of nucleation. From Equation (31) for homogeneous nucleation, the rate of nucleation in a sample of volume v will be

$$I_v = Iv. \tag{37}$$

If the nucleation is catalysed by a surface film or other surface defect, then

$$I_v = I_s a_s. \tag{38}$$

Considering the kinetics of solidification of a sample of small spheres having a range of diameters, the following relations may be derived[86]. Let v_D be the volume and a_D the surface area of a droplet of diameter D, and V_D the volume of all the droplets with diameters lying between D and D + dD that remain liquid at time t. A function y(t) may be defined,

$$y(t) = (1/V)\int_0^D V_D dD, \tag{39}$$

where V is the total volume of the solid sample. At t = 0,

$$y(0) = (1/V^o)\int_0^D V_D dD, \tag{40}$$

where V^o is the volume of the liquid sample. If the volume rate of solidification is assumed to follow the radioactive decay law then,

$$-dV_D/dt = k_D V_D, \tag{41}$$

where k_D is the rate of nucleation of a drop of diameter D. The total rate of solidification is

$$-dV_D/dt = \int_0^\infty k_D V_D dD. \tag{42}$$

Integrating,

$$V_D = V_D^o \exp(-k_D t), \tag{43}$$

and,

$$V = \int_0^\infty V_D^o(\exp(-k_D t))dD. \tag{43a}$$

From above, for homogeneous nucleation,

$$k_D = Iv_D$$

and

$$V = \int_0^\infty V_D^o(\exp(-Iv_D t)dD. \qquad (44)$$

For nucleation catalysed by a surface condition,

$$V = \int_0^\infty V_D^o \exp(-I_s a_D t)dD. \qquad (45)$$

Experimentally, $y(0) = f(D)$ and $V = f(t)$ are measurable, at various constant temperatures. Comparing the experimental data with Equations (44) and (45) above, it is possible to determine if the solidification is dependent upon the volume, or the surface area of the sample.

3.3 B: Data and Results of the Solidification Studies

The first experiment involved decreasing the temperature and observing the intensity of the line, and the temperature, as a function of the time. Figure 33 is a plot of the data of a typical solidification run. The temperature was normally lowered by first turning off the diffusion pump and allowing it to cool completely, then cutting off the power to the heater. The pressure in the system rose to a few microns and the oil bath cooled by radiation and convection. The rate of cooling was quite reproducible. A faster rate of cooling could be obtained

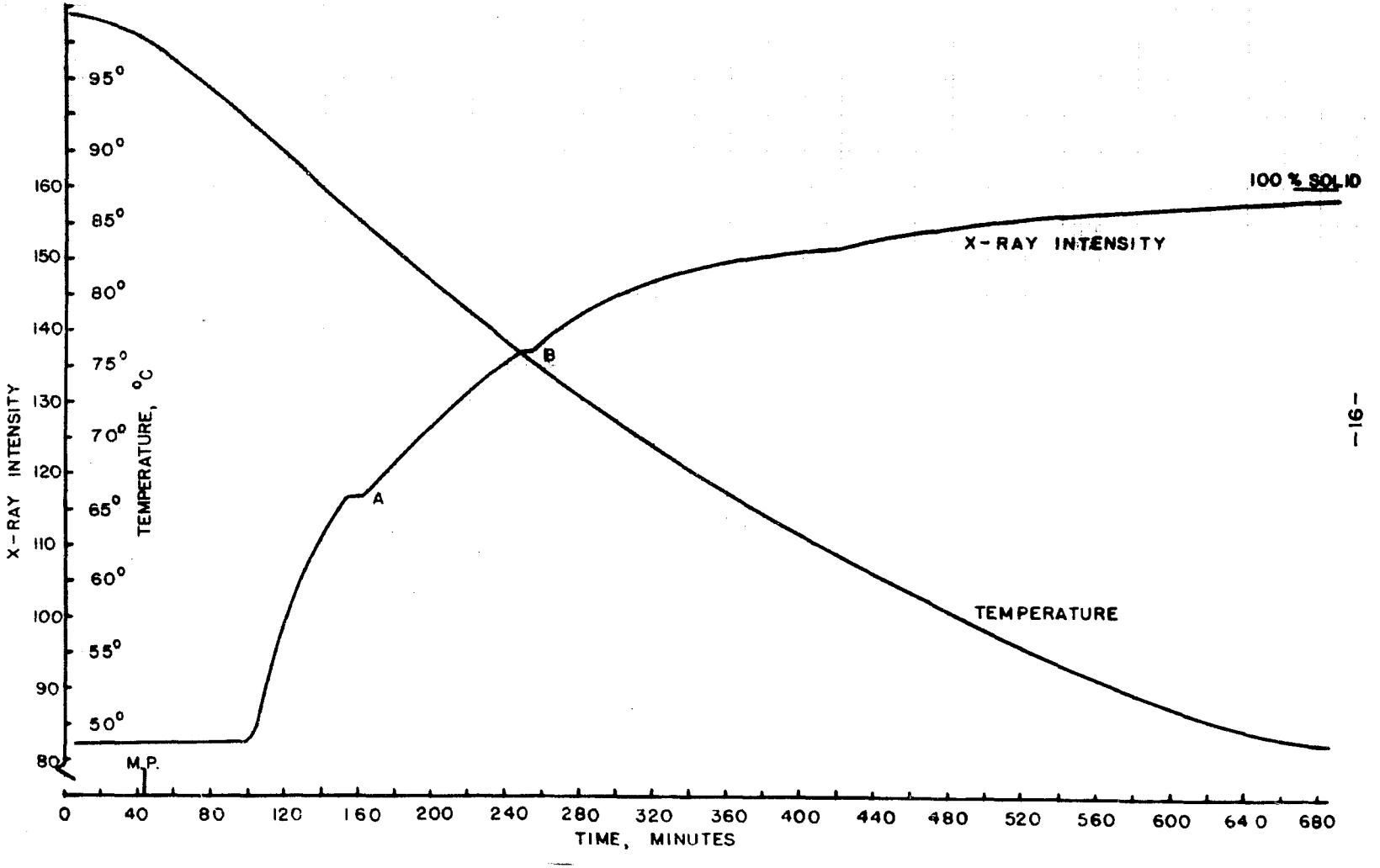

FIGURE 33. X-RAY INTENSITY VS. TIME FOR SOLIDIFICATION OF THE SAMPLE

by bringing the pressure up to atmospheric before turning off the heater, and a slower rate, by leaving the diffusion pump on while cooling. The temperature normally dropped at a rate of approximately five degrees per hour during the initial stages and three degrees per hour, during the latter stages of the experiment.

Several features of the curve are noteworthy. First, there is decided undercooling before any appreciable solidification takes place. This temperature is usually repeatable, but is dependent on the rate at which the temperature is lowered. Slower rates of cooling result in greater undercooling up to a point, then have no further effect. The most reproducible data were taken with rates of cooling of five degrees per hour or less. Faster rates of cooling resulted in a lesser amount of undercooling. The minimum undercooling observed was 1.1°. The exact dependence of the undercooling as a function of the rate of cooling has not been determined. With the slow rate of cooling, the temperature at which solidification starts is repeatable and equal to $92.3^{\circ} \pm 0.2^{\circ}$ C. Data over a considerable period of time is given in Table III.

The amount of undercooling gives a clue to the general nature of the nucleation process, that is, whether it is homogeneous (thermal fluctuations) or heterogeneous (non-thermal cause). In an extensive study of the supercooling

Table III

Summary of Undercooling Data

Date	Maximum Temp., T_m	Time at T_m, Hours	ΔT_+	ΔT_-	Cooling Time, Min.
11-19-54*	97.92° C	0.2	0.25°	1.1°	30
11-24-54	98.95	16	1.25	5.4	60
11-30-54	104.7	64	7.00	5.4	90
12- 9-54	98.40	27	0.70	5.6	300
1- 8-55	97.98	1	0.28	3.2	30
1- 9-55	97.98	1	0.28	3.3	30
1-14-55	98.90	38	1.20	3.0	30
1-20-55	99.50	25	1.60	2.1	20
1-21-55	97.94	1	0.24	2.2	25
1-28-55	97.85	1	0.15	3.2	40
2- 9-55	99.50	12	1.80	1.4	5
3-25-55	97.70	--	----	3.3	60

ΔT_+ = Temperature over the Melting Point.
ΔT_- = Undercooling.
Cooling time = Time from M.P. to start of solidification.
*First Melting.

of liquid metal droplets, Turnbull and Ceck[87] found that

[87]Turnbull, D. and Ceck, R. E., J. Appl. Phys., 21, 804 (1950).

for most metals tested, $(\Delta T_-)_m$, the maximum undercooling was of the order of 0.18 T_o, where T_o is the absolute melting temperature. Their study was carried out using visual observation of small droplets of the metal on a vacuum stage of a microscope. The droplets were first melted and then cooled slowly until a large number solidified. It was observed that a great majority of the droplets froze in a narrow temperature range about $(\Delta T_-)_m$, when care was taken to use moderately pure materials and to exclude surface films. Metals studied included tin, bismuth, lead, antimony, aluminum, silver, gold, copper, manganese, nickel, cobalt, iron and palladium. On this basis and assuming that this undercooling represents the maximum possible because of the onset of homogeneous nucleation, sodium in the form of small droplets should undercool about 60° before appreciable solidification takes place. In the present experiments such is not the case, and therefore one is led to the conclusion that the nucleation is heterogeneous.

Further evidence of the heterogeneous nature of the nucleation process studied, stems from the work of Turnbull and Vonnegut[88] on nucleation catalysts. Following a series

[88]Turnbull, D. and Vonnegut, B., Ind. Eng. Chem., 44, 1292 (1952).

of experiments on the effects of various substances on the maximum undercooling of ice[89] in which silver iodide was

[89]Vonnegut, B., J. Appl. Phys., 18, 593(1947).

found to be the most effective in lowering (ΔT_-), they proposed the theory outlined in Section 3.3 A. Further experiments by Turnbull[90] on mercury droplets coated with

[90]Turnbull, D., J. Chem. Phys., 20, 411(1952).

various compounds of mercury including mercury sulfide, mercury acetate, mercury iodide, mercury stearate and mercury laurate, indicated a wide range of potency of catalysts. For example, for an unknown substance called HgX, ΔT_- was three degrees, while for mercury laurate, ΔT_- was 77°. Unfortunately, the crystal structure of most of the substances used in both Vonnegut's and Turnbull's work was not known. However, silver iodide, used in the ice experiments, very closely resembles ice in its crystal structure.

In the preparation of the dispersed sodium sample a limited amount of air was introduced into the oil by the ultrasonic agitation. Since sodium is very reactive, it is probable that the sodium immediately took up the oxygen

and water vapor in the air to form Na_2O, Na_2O_2 and NaOH. In the event of an excess of oxygen, the reaction would continue with the production of Na_2O_2 which is stable in dry air[91]. In the presence of water vapor the reaction

[91] see for example, Mellor's Modern Inorganic Chemistry, Longmon's, Green and Co., New York(1939).

would continue to form sodium hydroxide. Other impurities are present only to the extent of one part in 25,000, and therefore would not seem to be important. The structure of sodium is body-centered cubic with a_o = 4.282 Å. The structure of Na_2O was determined by Hüttig and Bradkarb[92]

[92] Hüttig and Bradkarb, Zeit. f. Anorg. Chem., 161, 256(1927).

and listed by Wyckoff[93]. This oxide has a fluorite arrange-

[93] Wyckoff, R. W. G., Crystal Structures, Interscience, New York(1951).

ment with an oxygen atom at the center of a cube formed by eight sodium atoms. Each sodium atom has about it a tetrahedron of oxygen atoms. The arrangement is very nearly body-centered cubic with a_o equal to 5.55 Å. There are four molecules per unit cell. The melting point is 800° C.

The structure of Na_2O_2 is also listed by Wyckoff. Its melting point is 460° C. It has a tetragonal symmetry

with $a_o = 6.65$ Å, and $c_o = 9.91$ Å, with eight molecules per unit cell. Each sodium atom has eight equidistant neighbors at the centers of the surrounding cubes and six others slightly farther away. This gives a split coordination of 14, which is not very different from the 12-fold coordination of the hexagonal close packed and cubic arrangements. The sodium atoms are located at 000 and $\frac{1}{2}\frac{1}{2}\frac{1}{2}$. Thus, on the basis that impurities with crystal structures very similar to the solid phase of sodium make good catalysts, both Na_2O and Na_2O_2 should be good catalysts.

Sodium hydroxide also has an interesting structure. It has what might be called a thallous iodide structure with orthorhombic symmetry. The orthorhombic structure is stable in the temperature range used in the experiments, but breaks down at higher temperatures. Its melting point is 319° C. The unit cell is elongated with $a_o = c_o = 3.40$ Å and $b_o = 11.32$ Å. There are four molecules per unit cell. The Na-Na interatomic distance in the layers is 3.40 Å, and between layers in the structure is 3.99 Å. Thus, this compound, too, should make a potent catalyst for the solidification of sodium.

The presence of the oxides and the hydroxide in quantities sufficient to nucleate the transition should be detectable with x-ray diffraction techniques. Figure 34 shows the x-ray diffraction pattern of the sample taken with a Debye-Scherrer camera of radius such that 1 mm on

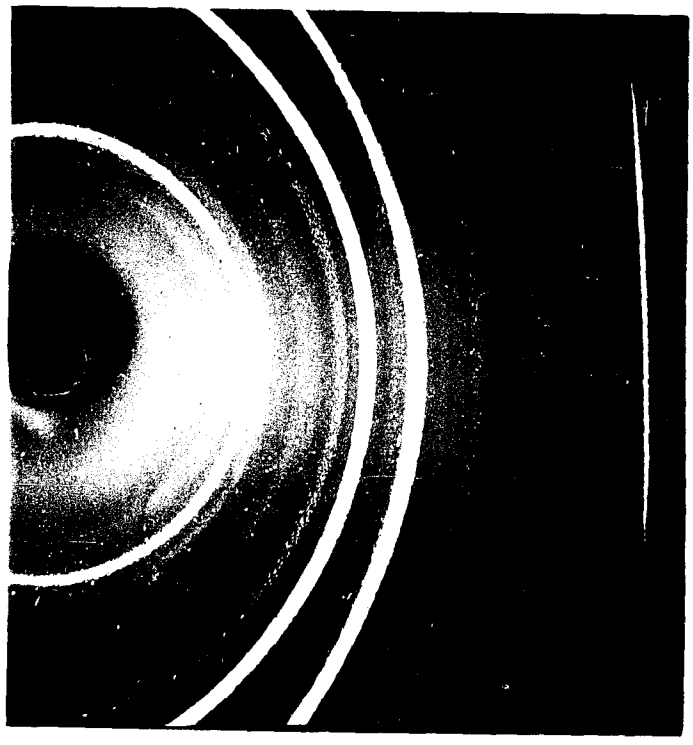

FIGURE 34. X-RAY DIFFRACTION PATTERN OF THE SAMPLE.

the film corresponds to 2θ equal to 1°. Table IV lists the diffraction lines seen as well as their identification. All lines are accounted for, and all the lines of Na_2O and NaOH expected in the range of 2θ to 85° are present. Thus in addition to the sodium, sodium monoxide and sodium hydroxide are present.

The diffraction lines of sodium appear as very narrow streaks on the film. The streaks are actually doublets which resolve the Cu $K\alpha_1$ and Cu $K\alpha_2$ lines. The very narrow diffraction widths appear to be due to the fact that the diffracting particles are very perfect tiny single crystals of sodium. The various intensities of the streaks result from the various particle sizes present, but no attempt has been made to measure the intensities of the streaks for the purpose of estimating the particle size distribution.

The presence of Na_2O and NaOH is therefore well established, so that it may be concluded that heterogeneous nucleation catalysed by one or both of these compounds is the mechanism by which the sample solidifies. It is not known with certainty which of these compounds would be the better catalyst. From the interatomic spacings listed earlier, it would appear that NaOH would be the most potent catalyst because the disregistry between it and sodium is less than that between Na_2O and sodium. In

Table IV

Complete Powder Diffraction Pattern of the Sodium Sample

Line Number	2θ	Identification
1	25.5°	Impurity in Be
2	27.5	Na_2O
3	29.5	Na (110)
4	31.5	NaOH and Na_2O
5	37.0	Impurity in Be
6	38.5	NaOH
7	42.2	Na (200)
8	44.5	NaOH
9	46.5	Be and Na_2O
10	47.5	NaOH
11	50.0	Be
12	52.0	Na (211)
13	52.5	Be
14	53.8	NaOH
15	56.0	NaOH
16	58.0	Na_2O
17	61.0	Na (220)
18	63.0	NaOH
19	68.0	Na_2O
20	69.0	Na (310)
21	71.0	Be
22	74.5	Na_2O
23	84.5	Be

fact if the effect of the disregistry is as predicted by Turnbull and Vonnegut, then NaOH should be about four and a half times as active as Na_2O, so that the effective catalyst is NaOH. This however assumes that NaOH is present in sufficient quantity on each droplet to nucleate the solid phase. From the manner of preparation of the sample there is no reason to believe that the NaOH and Na_2O will be distributed in any preferred way over the droplets. The amount of each on the droplets should be proportional only to the total number of surface atoms. The critical size of the nucleus is of the order of 100 molecules for water[94] and of the same order of magnitude for potassium chloride[95]. Since a cube of 125 molecules has only five molecules on a side, a catalyst of five molecules should be sufficient to nucleate the transition. It is therefore reasonable to assume that there are enough NaOH molecules on each droplet to form at least one small crystal and nucleate the droplet. Hence, the entire transition can be ascribed to heterogeneous nucleation by the NaOH.

---

[94]Rodebush, N. H., Ind. Eng. Chem., 44, 1289(1952).

---

[95]Preckshot, G. W. and Brown, G. G., Ind. Eng. Chem., 44, 1314(1952).

A second feature of Figure 33 is the fact that solidification takes place over a very wide range of temperature - about 50°. Turnbull in this work on mercury droplets[96]

[96] Turnbull, D., J. Chem. Phys., 20, 411(1952).

reported a range of 2° to 4°, with undercooling ranging from 3° to 77°. The temperature was lowered at a rate of about 1° per minute. The droplet size was 10 to 50 microns, and the isothermal solidification was observed to follow the theory for heterogeneous nucleation outlined previously.

A series of experiments by Pound and LaMer[97] on the

[97] Pound, G. M. and LaMer, V. K., J. Chem. Phys., 74, 2323 (1952).

solidification kinetics of liquid tin revealed further complications. They used droplets ranging in size from 2.5 to 5 microns coated with tin oxide, and observed a range of solidification greater than 10° at a supercooling of 120°. It was noted also in this series that, at a given temperature, the isothermal rate of solidification was very dependent on droplet size. According to nucleation theory, if nucleation is catalysed by surface coatings the isothermal rate of nucleation should vary as the square of the droplet radius. If the nucleation is catalysed by volume inclusions, the rate should be proportional to the cube of the radius. The experimental variation[97] was much

greater than either of these functions. Their experiments were conducted with samples having particle size ranges from 2.5 to 5 microns, from 5 to 7 microns, from 6 to 10 microns and from 9 to 13 microns. A further difference between the results of Turnbull and Pound and LaMer is that where Turnbull's data were explained by a single value of ΔG_s^*, no such assumption could be made in the latter instance. In order to explain their data, Pound and LaMer first postulated a method of nucleation in which the nucleus in the liquid formed around a spherical foreign core (the catalyst). This resulted in a temperature independent free energy, of value somewhat less than the free energy for homogeneous nucleation. To explain the shape of the isothermal solidification curves, they postulated a Poisson distribution of impurities among the tin droplets according to the volume, and to the surface area of the droplets. This established that the rate of nucleation was proportional to the surface area and not the volume of the droplets. It was further necessary to postulate the existence of more than one catalyzing agency, in order to explain the isothermal solidification curves. Both Turnbull and Pound and LaMer used a dilatometric method to determine the percent of the sample which had solidified.

In order to obtain more information about the kinetics of solidification of sodium droplets, the isothermal solidification curves at several temperatures were taken by the author. For the first run, the sample was brought quickly to a temperature of 96.6° C from several degrees above the melting point. Two percent of the sample solidified while the temperature was dropping, but no further solidification took place in 72 hours. The sample was then taken to a temperature 2° over the melting point and "quenched" to a temperature of 94.0° C. It was actually a slow quench, taking about eight minutes. The results of this run are plotted in Figure 35. After about 16 hours the transformation ceased, and no further solidification took place in the next 32 hours. The sample was 56 percent solidified. The temperature was quickly dropped to 89.1° C and after about 10 minutes, no further solidification took place. The total time at this temperature was again 48 hours and the sample 81 percent solidified. The temperature was again dropped, this time to 85.1° C. After this temperature was reached, there was no change in the solid content for 48 hours. The sample was 90 percent solidified. The sample then was completely solidified. It is noted that for each temperature, the transformation eventually ceased. Comparing data with those of Turnbull and Pound and LaMer, it is to be noted that the range of solidification found by

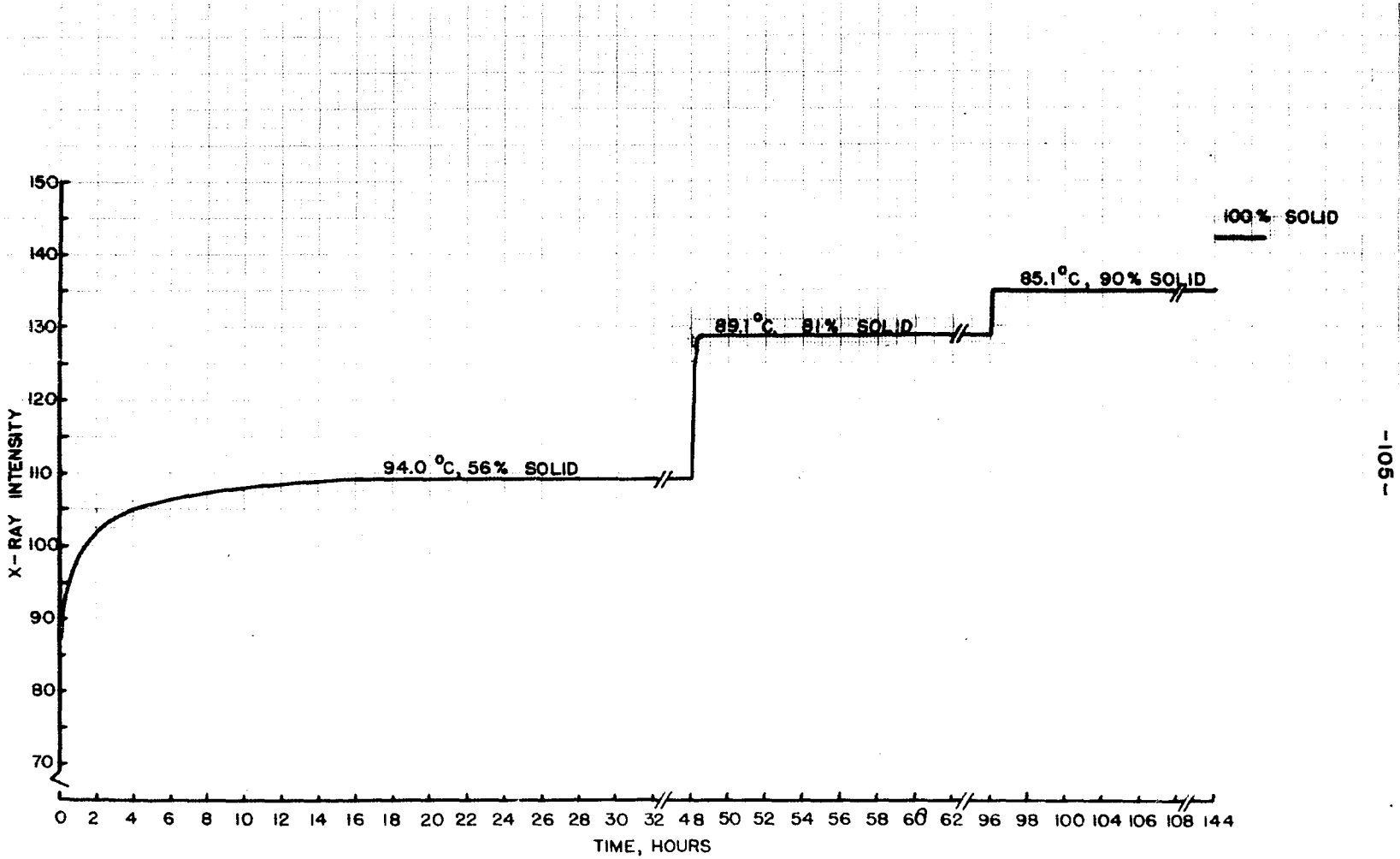

FIGURE 35. ISOTHERMAL SOLIDIFICATION AT 94.0°, 89.1°, AND 85.1°.

Pound and LaMer was about 10° for particle sizes 2.5 to 5 microns, and the range of solidification found by this author was about 50° for particle sizes less than 2 microns. Thus, it seems to be that the wide range of solidification observed here is due to the small particle size of the sample.

From the standpoint of nucleation theory, it is considered that at a given temperature, there is a certain distribution of embryos, characterized by an average size and distribution of sizes. Basic nucleation theory predicts that only over a very narrow range of temperatures (3 to 5° C) will the rate of nucleation be measurable. Above the maximum temperature it will be too slow, and below the minimum temperature it will be too fast to be measured. Two alternatives suggest themselves to explain the very broad range of temperatures over which the transformation observed here takes place. One of these may be that the distribution of embryo sizes is very broad and flat and essentially temperature independent. Then, as the temperature is lowered, only a limited number of embryos become nuclei for the transformation. It is difficult to imagine this mechanism, since one of the basic postulates of nucleation theory is that embryos are formed by the addition of molecules which move into favorable position by thermal fluctuations. It is therefore almost imperative

that the number of molecules, hence the size, of the embryo be temperature dependent.

The other alternative is to assume that the critical size of the embryo is in some way dependent on the temperature. This dependence may be implicit or explicit. An example of implicit dependence would be a dependence of the critical size of the embryo on the volume of the particle. In this case successively smaller particles would solidify as the temperature is lowered. A somewhat similar situation would be that of several catalysts present in limited amounts with various potencies. Part of the sample would be solidified at a certain temperature by the action of the most potent catalyst. The temperature would then have to be lowered so that the less potent catalysts may become effective.

The method of sample preparation of Turnbull, of Pound and LaMer, and of the author of the experiments described here insured an excess of the coating material so that all particles can be presumed to be thoroughly covered. It therefore seems likely that the wide range of solidification and the non-isothermal character of the transition is a particle size effect.

In view of the unusual occurrences noted above, it seemed worthwhile to examine some of the other characteristics of the transformation. The path of the transformation

between the second and third runs and between the third and fourth runs previously described had been recorded. Figure 36 shows the percent solid as a function of time while the temperature was being lowered from 94.0° to 89.1°, after being held at 94.0° for 48 hours. There is a marked lag in the transformation as the temperature is lowered. The same behavior was observed when the temperature was lowered from 89.1° to 85.1°, after being held at 89.1° for 48 hours. This effect might be called "stabilization" of the system, a term which has been found useful in other cases[98].

---

[98] Cohen, M., Phase Transformations in Solids, Chapt. 17, Wiley, New York(1951).

It is of some interest to consider the points A and B in Figure 33. The leveling-off of intensity was observed in all the solidification runs. These, however, are very small effects and, if real, would bear more careful scrutiny than given in this work. They might be correlated with effects of particle size distribution, stabilization or the action of the various catalyzers.

A further experiment was planned in an attempt to observe reversibility in the transformation. Table V shows the procedure for this run which lasted several days. Figure 37 shows the x-ray intensity as a function of temperature for this experiment. The stabilization noted in

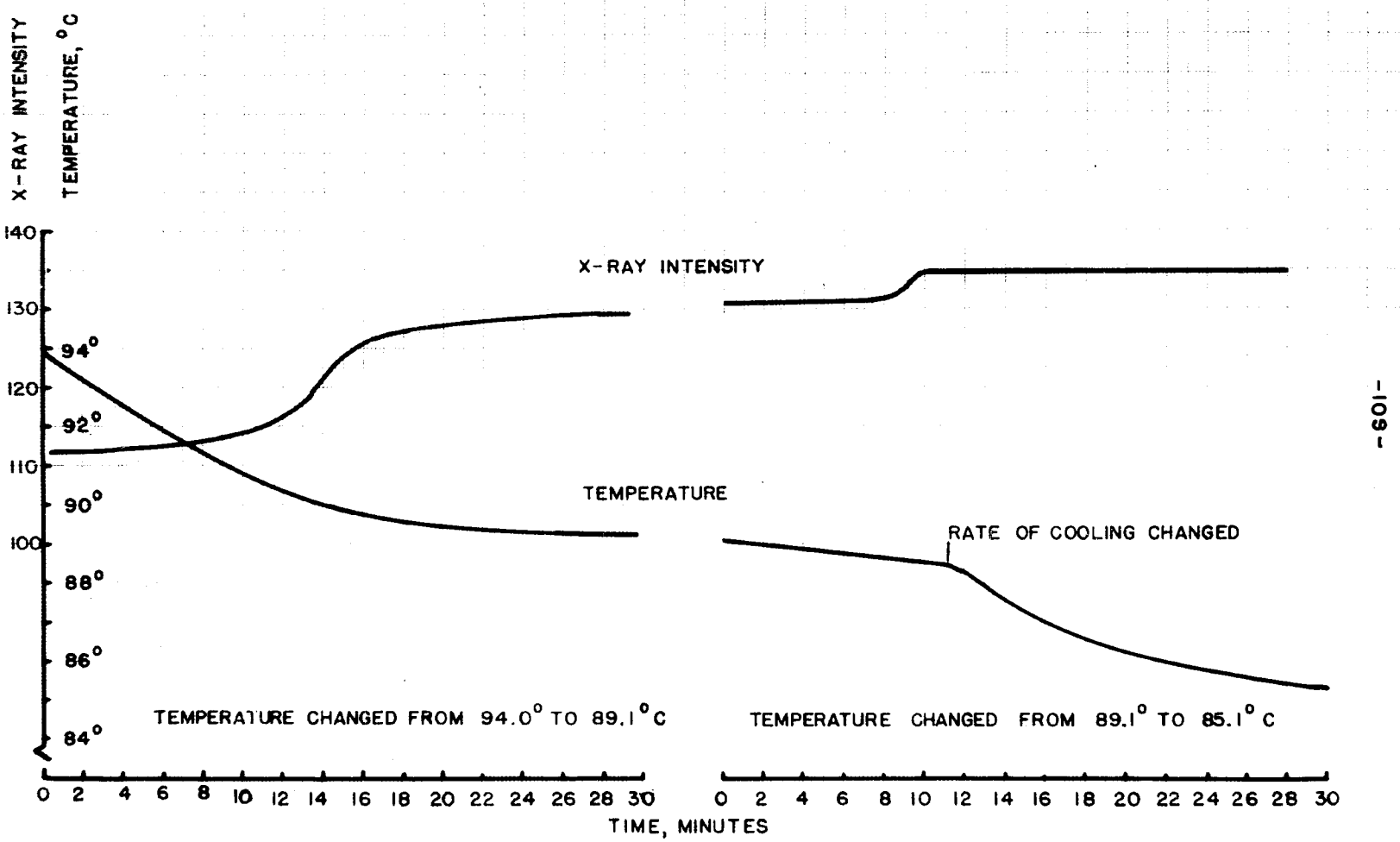

FIGURE 36. STABILIZATION EFFECT.

Table V

Procedure for Run Showing Reversal of the Transformation

Step	Remarks
1.	Sample Melted.
2.	Temperature lowered to 86.3° C in six hours and held for nine hours. Point A on Curve.
3.	Temperature lowered to 75.4° in two hours and to 75.2° in the next five hours. Point B.
4.	Temperature raised to 76.7° in one hour and held two and one-half hours. Point C.
5.	Temperature raised to 78.5° in three hours. Point D.
6.	Temperature raised to 79.7° in three hours and held for 27 hours. Point E.
7.	Temperature raised to 83.0° and held for 74 hours. Point F.
8.	Temperature lowered to 74.3° over a period of 24 hours. Point H. There was no change in the x-ray intensity until Point G was reached.
9.	Heater off, sample cooled to room temperature.

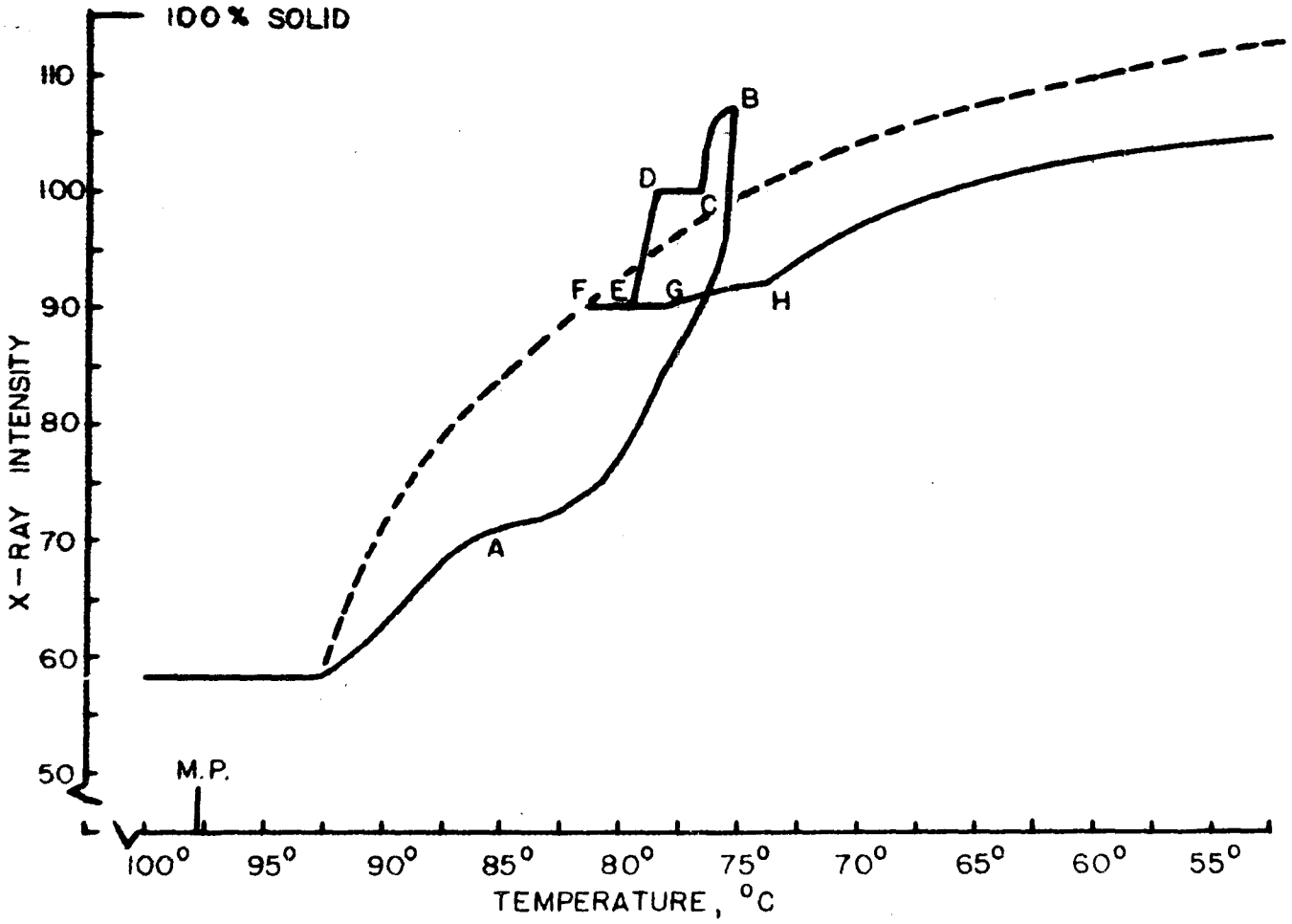

FIGURE 37. REVERSIBILITY OF THE TRANSFORMATION.

earlier experiments is seen here at point A. The dashed curve shows the data of Figure 33 plotted as a function of temperature. There is positive evidence of a reversal in the transformation, though it is with considerable hysteresis and apparently with a maximum amount of reversibility. The rate of change of temperature doubtless effects the form of this curve.

Following this experiment a series of runs was made to check the above. The temperature was lowered until a certain x-ray counting-rate was reached and then raised slowly until the sample remelted.

For the first "loop", the temperature was lowered to 90.8° C. Thirteen percent of the sample solidified and remained solid until the melting point was reached. For the second loop, the temperature was lowered to 80.5° C. Thirty-one percent of the sample solidified, and as the temperature rose, another 4 percent of the sample solidified, and remained solid until the sample melted again. The temperature was reduced to 75.0° C for the third loop, and 57 percent of the sample solidified. As the temperature rose, another 4 percent of the sample solidified and remained solid until the melting point was reached. Thus, in these three cases, no reversibility was observed. In the fourth case, however, reversibility was observed. For this loop, the temperature was lowered to 72.0 C and

77 percent of the sample solidified. As the temperature rose, however, 16 percent of the sample "remelted". The remaining 61 percent remained solid until the melting temperature was reached. Figures 37A and 37B show the data for the third and fourth loops.

Loops three and four were repeated as a check. The temperature was lowered to 84.9° C and 60 percent of the sample solidified. No further solidification took place as the temperature was raised to the melting point. For the next loop, the temperature was lowered to 74.0° C and 80 percent of the sample solidified. When the temperature was raised, eight percent of the sample remelted.

The reversal appears to have a critical point below which it does not occur, and below which it cannot be forced when approaching from above. This was borne out by the seventh loop. In this case, the temperature was first lowered to 77.5° C and 80 percent of the sample solidified. The temperature was then raised to 93.7° C and held for 145 hours. The solid content decreased to about 70 percent and after about 65 hours began to rise again. In the next 80 hours the solid content rose to 84 percent. Figure 38 shows the data for this experiment. Thus the transformation is not reversible over the entire range of temperature and solid content. The critical point appears to be between 60 and 70 percent. The highest temperature

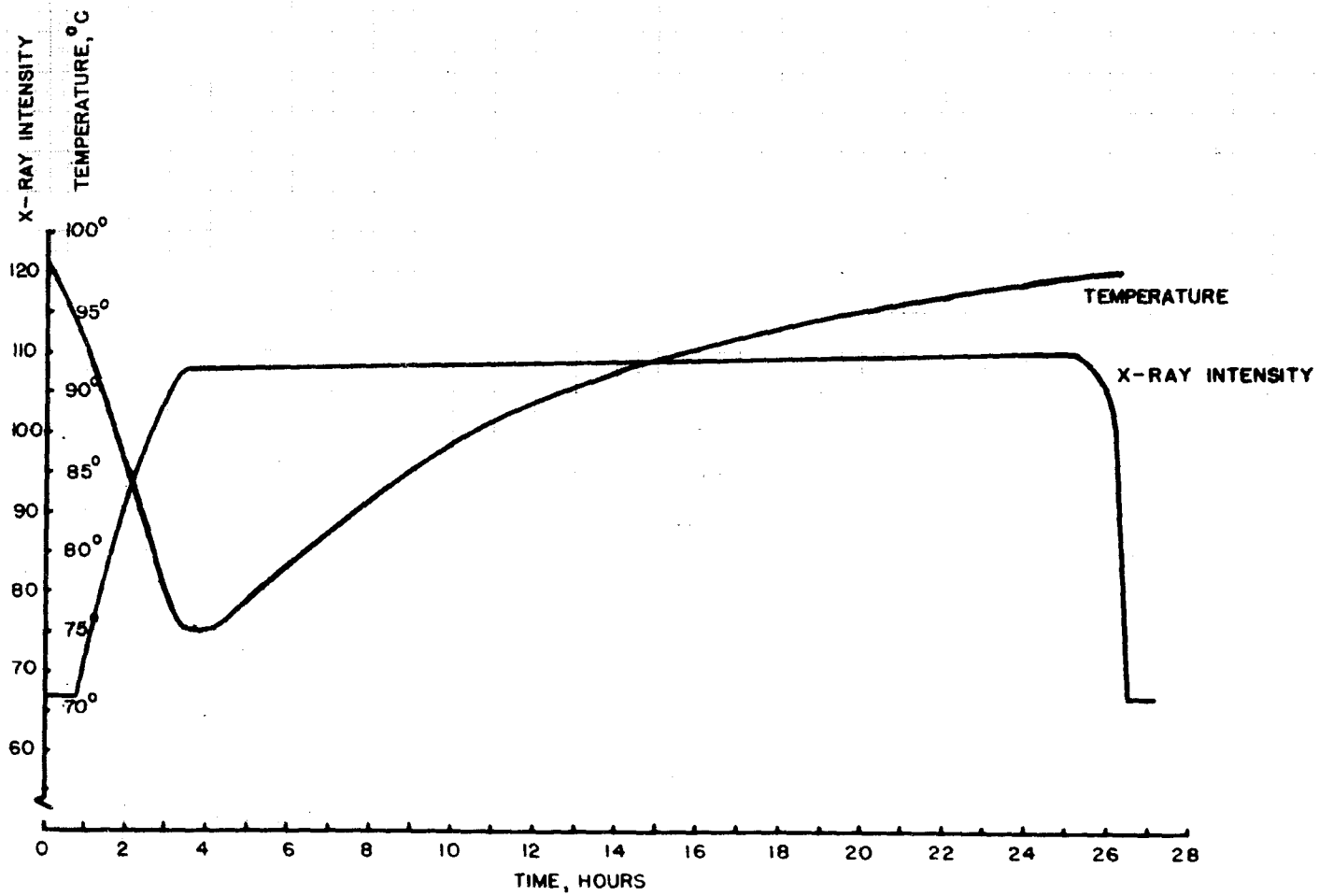

FIGURE 37A. THIRD LOOP. SHOWING NO REVERSIBILITY.

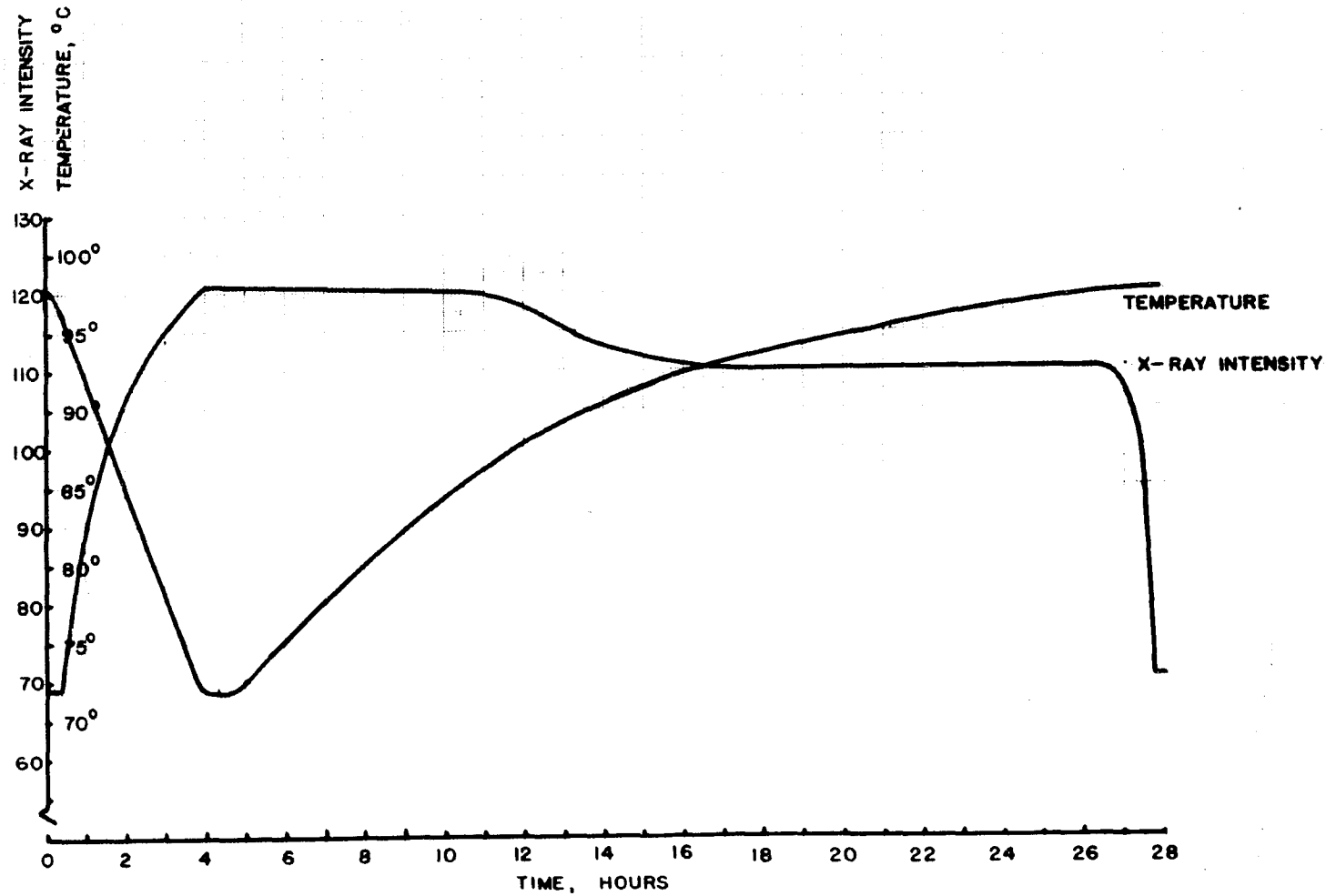

FIGURE 37 B. FOURTH LOOP, SHOWING REVERSIBILITY.

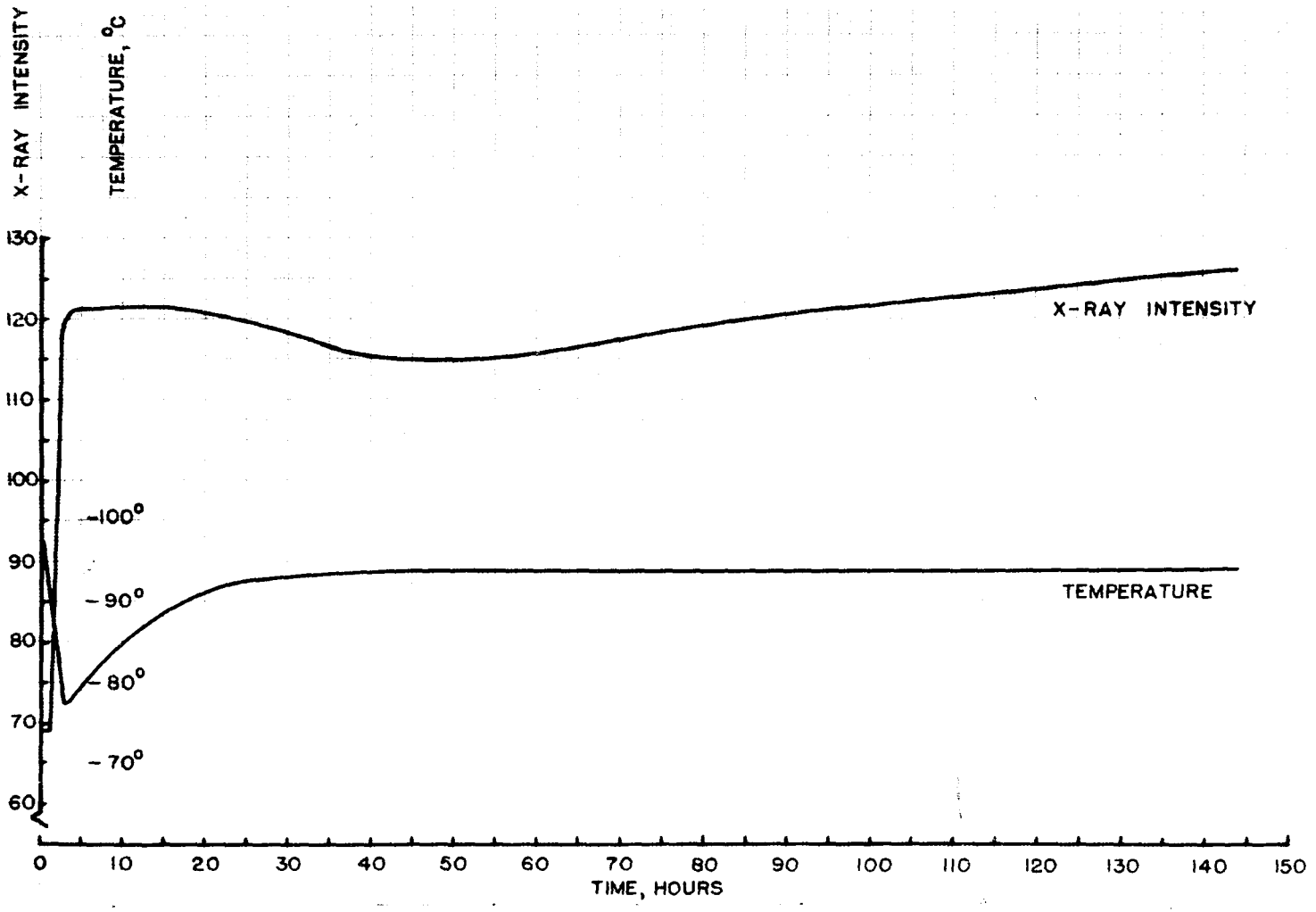

FIGURE 38. REVERSIBILITY AND ISOTHERMAL CHARACTER OF THE TRANSITION AS TEMPERATURE IS LOWERED AND THEN RAISED TO A CONSTANT VALUE.

at which reversibility takes place is obscure and depends on the temperature at which solidification starts.

The seventh loop also showed that in the region of reversibility if the temperature is raised and held at a higher point, the transformation eventually proceeds isothermally at a slow rate. This series completed the experiments on the liquid-solid transformation of the sodium sample.

IV A MECHANISM FOR HETEROGENEOUS NUCLEATION OF VERY SMALL SODIUM DROPLETS

The experimental evidence presented above indicates that the expression previously given (Equation (17)) for the free energy of activation of the nucleation process must be modified for the case of very small droplets. The activation energy for the nucleation process is the difference between the free energy of the bulk liquid and the free energy of the liquid plus the nucleus. In the previous derivation of this term, the free energy of the liquid was taken as $n_\alpha f_\alpha$ where n_α is the number of liquid atoms and f_α the free energy per atom in the liquid state. In the case of very small particles, it is necessary to consider the effect of the surface energy on the energy of the liquid. The change in free energy in the process of forming small droplets from the bulk liquid can be derived as follows. For a spherical drop of radius R, the volume

is $(4/3)\pi R^3$. If n is the number of atoms in the drop and v the atomic volume then,

$$nv = (4/3)\pi R^3, \tag{46}$$

and

$$dn = (4\pi R^2/v)dR,$$

but $4\pi R^2 = s$, the surface area, and

$$ds = 8\pi R dR. \tag{47}$$

If F is the free energy in the drop, and F_o the free energy in a large body of the liquid, the change in free energy in a transfer of dn molecules from the bulk liquid to the droplet, is,

$$\begin{aligned} dF &= (F - F^o)dn, \\ &= \sigma ds, \end{aligned} \tag{48}$$

the change in surface energy. Substituting ds from Equation (47) into this equation results in,

$$(F - F^o) = 2\sigma M/\rho AR = 2S/R \tag{49}$$

where M is the atomic weight, ρ, the density, A, Avogadro's number, and $(F - F^o)$ is the excess free energy per atom in the droplet over the free energy in the bulk liquid. S is defined by Equation (49).

The free energy of the liquid in the droplet and the embryos for the new phase, assuming spherical embryos, can be written

$$G = n_\alpha g_\alpha + n_\alpha 2S/R + n_\beta g_\beta + 4\pi r^2 \sigma' \qquad (50)$$

where r is the radius of the embryo and σ' the interfacial energy between the embryo and the liquid. For r = 0;

$$G_o = (n_\alpha + n_\beta) g_\alpha + (n_\alpha + n_\beta) 2S/R.$$

Then,

$$\Delta G = n_\beta (g_\beta - g_\alpha) - n_\beta 2S/R + 4\pi r^2 \sigma'. \qquad (51)$$

This has a maximum value with respect to r, found in the usual way.

$$\partial \Delta G/\partial r = 12\pi r^2/3v_\beta (g_\beta - g_\alpha) - 12\pi r^2/3v_\beta (2S/R) + 8\pi r\sigma' = 0$$

Solving for r_c, the value of r for maximum ΔG,

$$r_c = 2\sigma'/(\Delta G_V - A/R) \qquad (52)$$

where $A = 2S/v_\beta$. The maximum value of ΔG is

$$\Delta G^* = (16\pi/3)[\sigma'^3/(\Delta G_V - A/R)^2] \qquad (53)$$

as compared to the simple case (Equation (17)).

$$\Delta G^* = (16\pi/3)[\sigma'^3/(\Delta G_V)^2].$$

The kinetics of solidification can now be described. As the temperature is lowered, no solidification takes place until a temperature is reached at which the rate of nucleation

$$I = K \exp(-\Delta G^*/kT) \qquad (27)$$

is appreciable. ΔG^* then has a certain value dependent on R. Solidification will continue isothermally along the path predicted by Avrami for the case of a limited number of nucleation sites for each value of R until all the droplets of a certain size or larger have solidified. The transformation then stops. The value of this "critical" radius is found from Equation (52),

$$R_o = A/\Delta G_v. \qquad (54)$$

If the temperature is lowered further, the transformation continues as the smaller droplets solidify. If at any time the temperature is held constant the transformation stops after a period of isothermal nucleation, which becomes shorter as the temperature decreases.

Equation (53) then contains three parameters σ', A and ΔG_v which must be assumed, calculated, or determined from the experimental data. The value of G_v can be estimated to an accuracy sufficient for the present purposes. It is necessary to consider ΔG_v as a function of temperature

since in this experiment, ΔT_- extended over a considerable range. It is believed that the available data are not sufficiently accurate to justify a more precise free energy function than

$$\Delta G_v = \lambda \Delta T / T_o. \tag{55}$$

where λ is the heat of fusion per cm^3 and $\Delta T = T - T_o$. For a supercooling of 3.7^o for sodium, $\Delta G_v = 1.26 \times 10^7$ ergs per cm^3, and for $\Delta T_- = 12.6^o$, $\Delta G_v = 4.78 \times 10^7$. The values of σ' and S should now be calculable from the data in this paper.

The kinetic coefficient for heterogeneous nucleation, as derived by Turnbull, has been given previously as

$$K = (n_s kT/h)\exp(-\Delta F_A/kT), \tag{56}$$

where n_s is the number of surface atoms of the droplets per cm^3 of sample, k, T and h have their usual meaning and ΔF_A is the activation energy for diffusion. The term $\exp(-\Delta F_A/kT)$ is usually assumed to be about unity. For sodium droplets with radius of 0.5 microns, $K \approx 10^{31}$. An error of a factor of 10 in this coefficient introduces an error of only a few percent in the value of ΔG^* (Equation (27)).

If it is assumed that a measureable value of I is 100 per second per cm^3 and that the largest particles

freeze first, then at T = 367° K, Equation (27) becomes, for R = 5 x 10^{-5} cm,

$$100 = 10^{31} \exp[-16\pi\sigma'^3/3kT(1.26 \times 10^7 - 2A \times 10^4)^2]$$

and

$$\sigma'^3 = (207/16\pi)k367(12.6 \times 10^7 - 2A \times 10^4)^2. \qquad (57)$$

The temperature at which 90 percent of the sample was solidified, was 358° K. If 90 percent of the sample is assumed to consist of particles with r greater than 0.05 microns,

$$\sigma'^3 = (207/16\pi)k358(4.8 \times 10^7 - 2A \times 10^5)^2. \qquad (58)$$

Solving Equations (57) and (58), σ' = 2.5 ergs per cm^2 and A = 195 ergs per cm^2.

The value of ΔG^* for a constant temperature as a function of R can now be calculated from Equation (53). Figure 39 shows a plot of this variation. The slope of the line at the lower temperature is very steep, so that as the temperature is lowered the transformation becomes more nearly non-isothermal. This agrees with the results of the isothermal solidification runs.

The value of R_o, the critical radius for nucleation at a given temperature, is given by Equation (54). The value of ΔG_v is given by Equation (55). From these

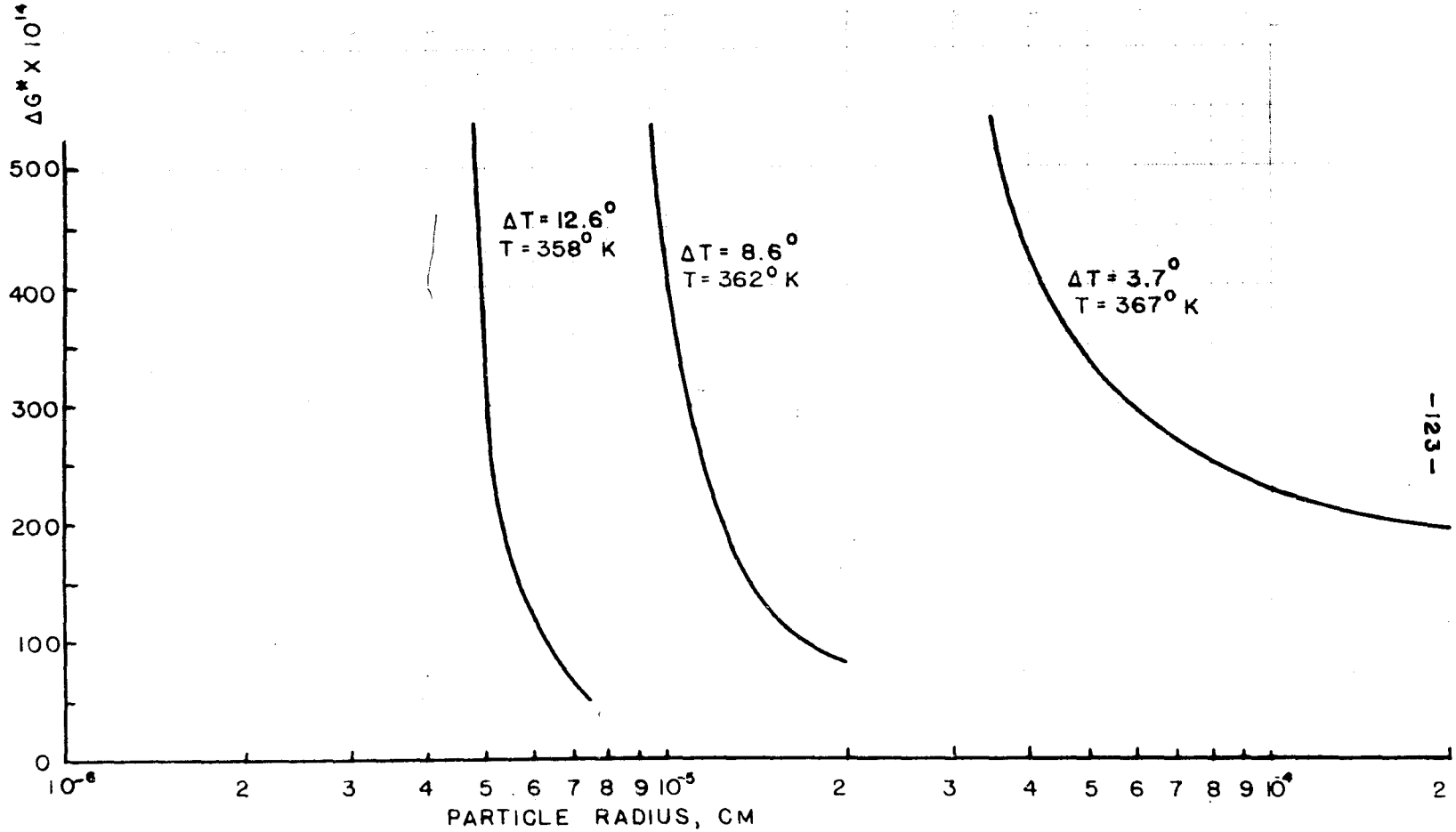

FIGURE 39. ΔG^* AS A FUNCTION OF R.

quantities the value of R_o as a function of temperature can be determined. Figure 40 shows the value of R_o as a function of temperature. Figure 41 shows the rate of nucleation as a function of R at 367°, 362° and 358° K as determined with the aid of Equations (27) and (53). From these curves, and an assumed value of I = 100 per cm^3 per sec, one gets, at T = 367° K, $R_o = 5 \times 10^{-5}$ at T = 362°, $R_o = 1 \times 10^{-5}$, and at T = 358° K, $R_o = 0.49 \times 10^{-5}$. The assumed value for I is roughly consistent with the minimum observable percentage of new solidification of two percent in the reasonable time of 48 hours.

From the data of the isothermal solidification runs (Figure 35) the following particle size distribution can be determined. Ninety percent of the volume of the sample is made up of droplets with a radius greater than 0.49×10^{-5} cm, 81 percent of droplets with greater than 1×10^{-5} cm radius, 56 percent of droplets with radius greater than 5×10^{-5} cm, and not more than two percent of the volume comes from droplets with a radius of 1.7×10^{-4} cm or greater.

Figure 42 shows the cumulative percent volume as a function of the droplet radius R. The particle size distribution obtained from the slope of this curve is shown in Figure 43. This curve is to be compared with Figure 30A, as obtained from the melting experiments on the same sample.

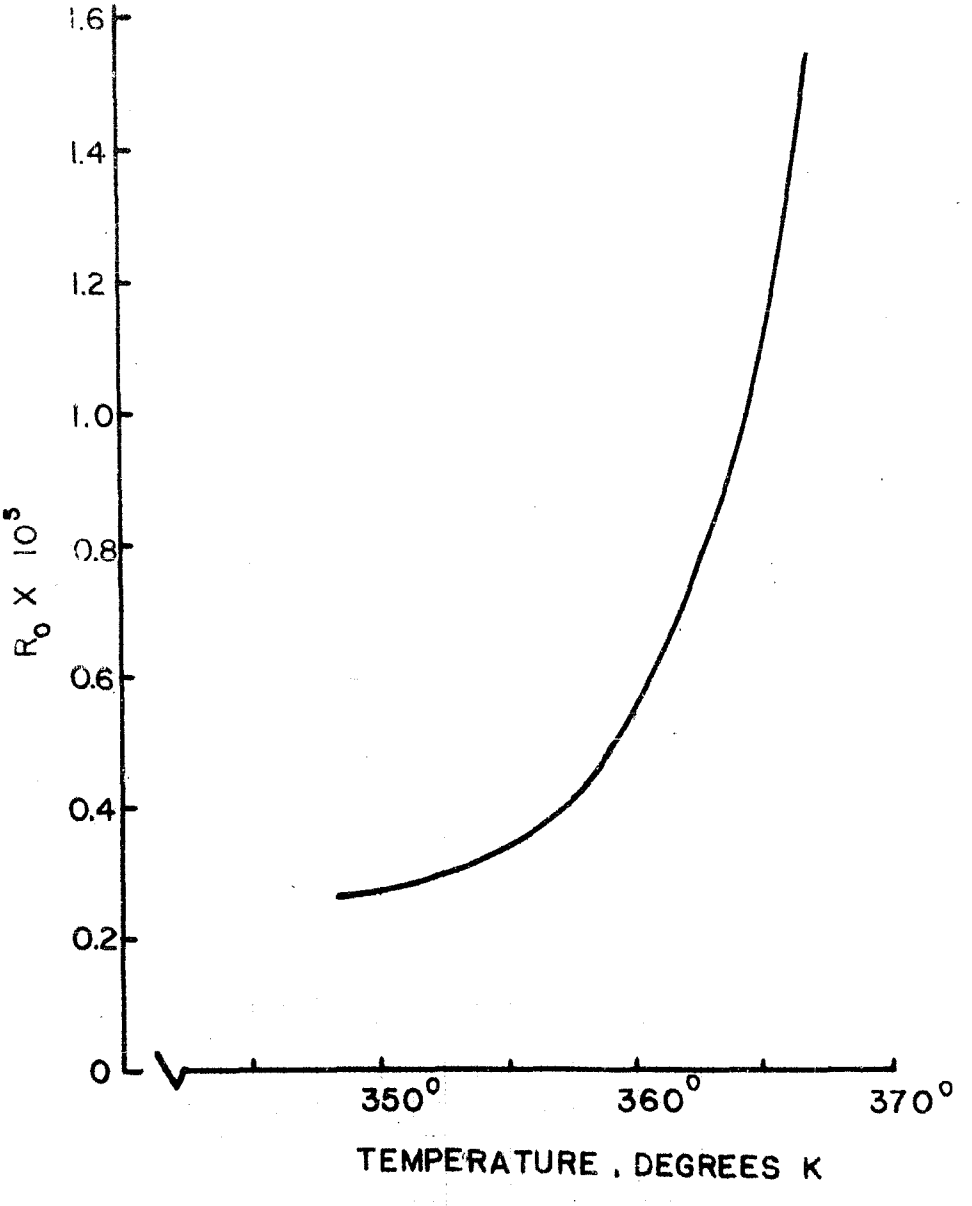

FIGURE 40. R_o AS A FUNCTION OF TEMPERATURE.

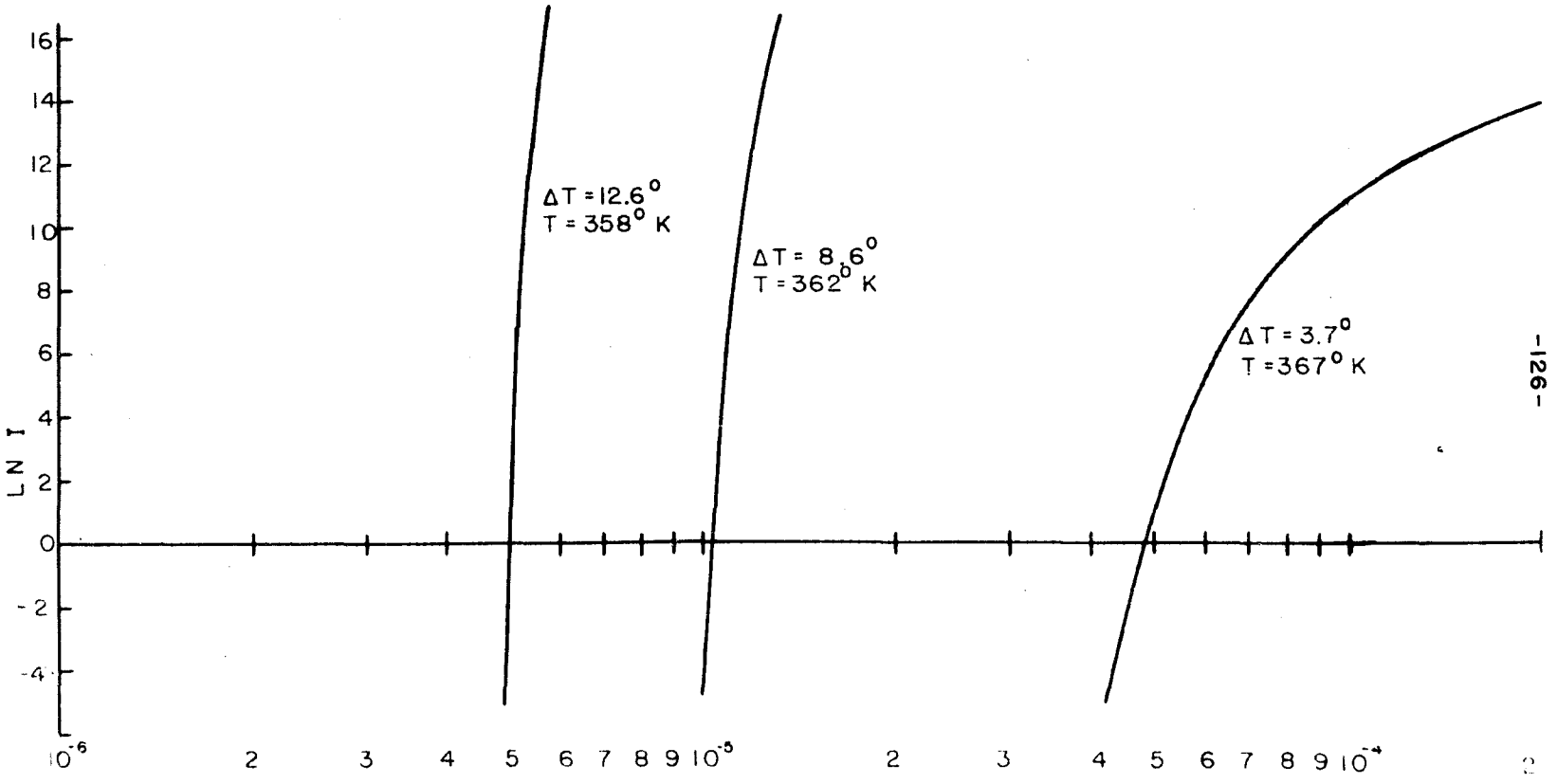

FIGURE 41. LN I AS A FUNCTION OF R.

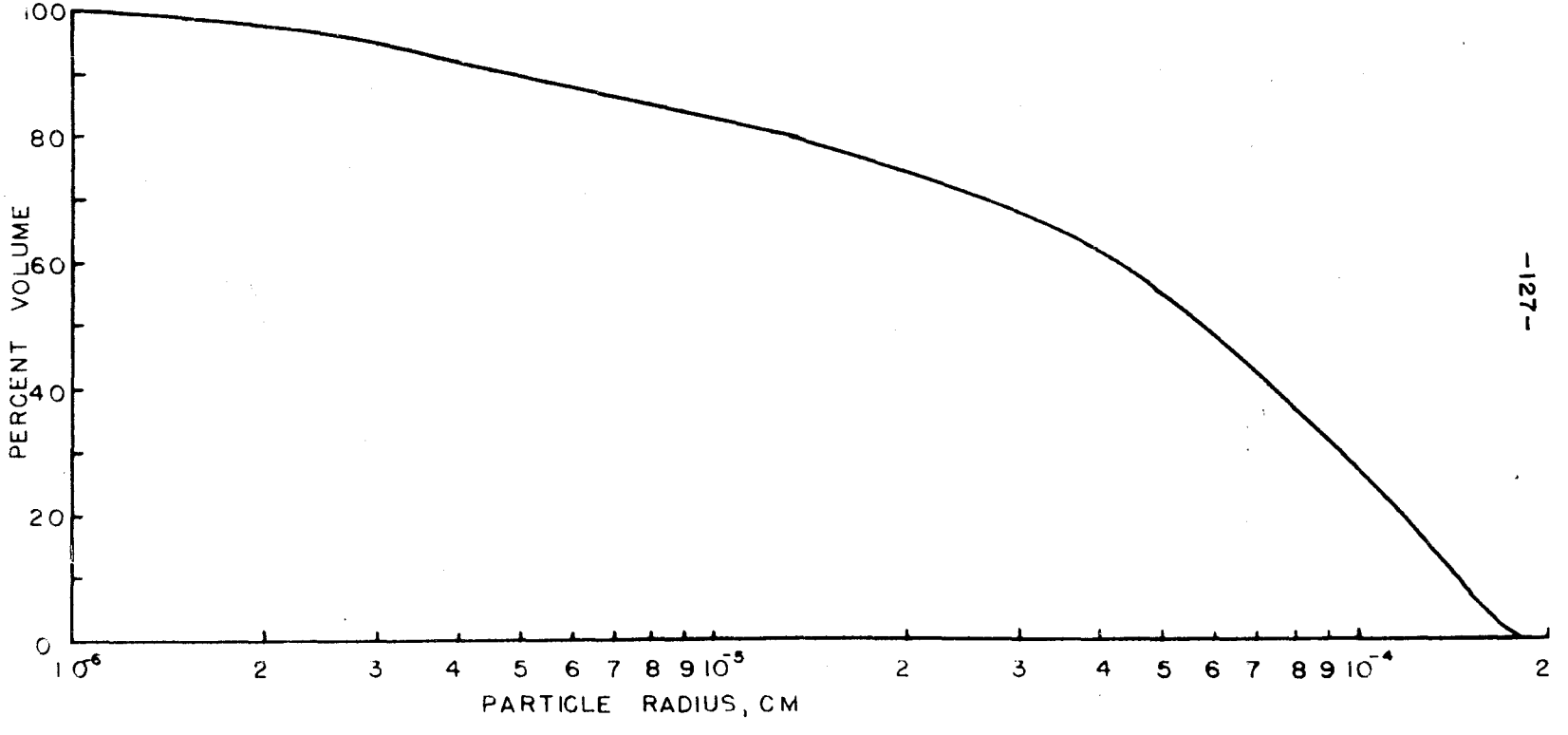

FIGURE 42 CUMULATIVE VOLUME VS PARTICLE SIZE FROM SOLIDIFICATION CURVE

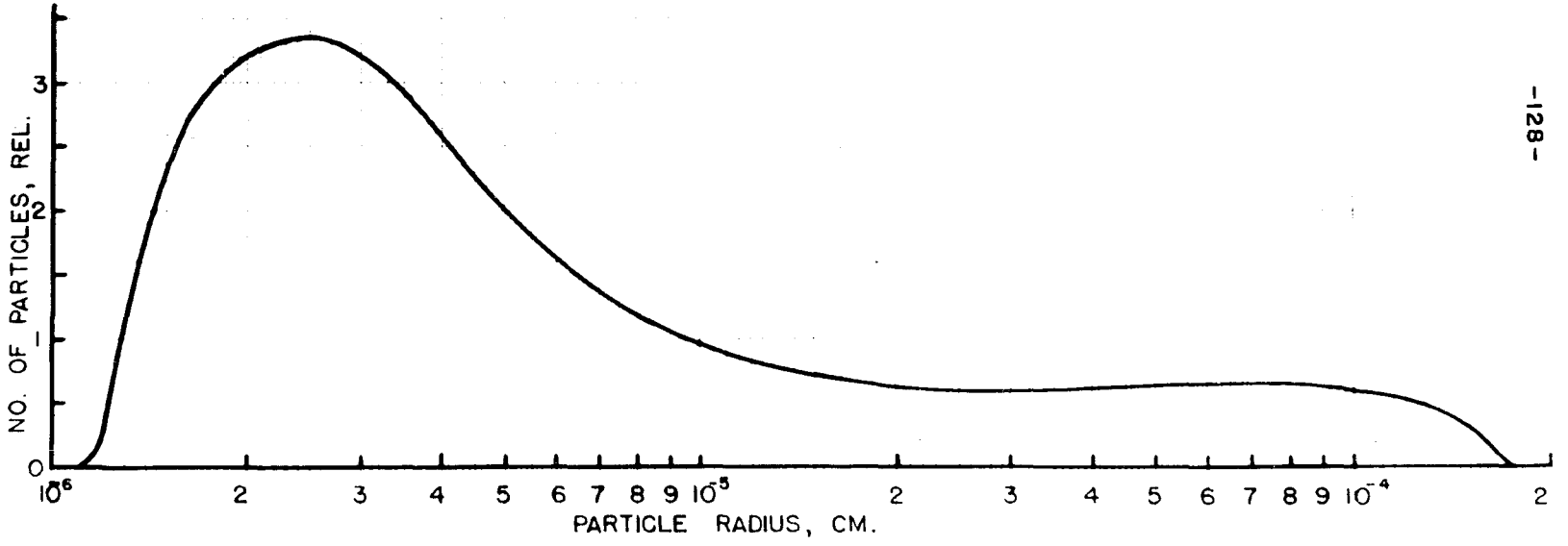

FIGURE 43. PARTICLE SIZE DISTRIBUTION IN THE SAMPLE.

V CONCLUSIONS AND RECOMMENDATIONS

The observations for both the melting and the solidification of the dispersed sample of sodium are explained by a particle size effect. Particle size distributions are obtained from the melting data and from the solidification data. These distribution curves are quite similar, but the curve from the melting data has a maximum at R equal to about 4×10^{-5} cm while the curve from the solidification data has a maximum at 2.5×10^{-5} cm. The melting curve predicts a smaller number of large particles than the solidification curve. Considering that the theories for both the lowering of the melting point and the lowering of the freezing point as a function of particle size are largely qualitative, the agreement between the melting data and the solidification data is to be considered satisfactory.

In addition to this some very important characteristics of the solidification of the sample have been observed. These characteristics may be summarized as follows: (1), there is an undercooling which depends to some extent on the rate of cooling, (2), over part of the range of solidification the transformation is non-isothermal, but if the temperature is raised from a low value to a higher one, the transformation will, in time, proceed isothermally, (3), the transformation is reversible over part of its range, though there is hysteresis in the reversibility, and,

(4), the transformation exhibits a "stabilization" effect.

To the knowledge of the author, there is no reference in the literature which lists the above characteristics, except that of undercooling, for a liquid-solid transformation. It is believed that the small particle size in the sample is responsible for the non-isothermal character of the transformation as explained in Section IV, and the heterogeneous nature of the nucleation process is responsible for the reversibility and "stabilization" of the transformation.

The effect of the nucleation catalyst may be explained as follows. If the sodium forms coherently on the NaOH as it solidifies, the sodium droplet will be strained because of the disregistry between the lattice of the NaOH and the sodium lattice. This strain contributes to the energy of the droplet and if the particle size is small enough, the strain energy per atom will be an appreciable part of the total energy. So when the solidification is interrupted and the temperature raised, the strain energy is sufficient that the particles can remelt at a temperature very much below the normal melting point. However, if the temperature is lowered sufficiently, the sodium lattice loses its strain, either at the expense of the NaOH or by an annealing process, so that now the temperature must be raised to the normal melting point before

any melting takes place.

The "stabilization" is explained on the basis that as the temperature is falling the tendency for the nucleus to form coherently on the NaOH layer contributes to the energy to the system. If the cooling is stopped and the temperature held constant for a period of time, this energy is given up, and now the temperature must be lowered more to produce a given effect, than if the temperature had fallen continuously.

The results of the experiments described in this dissertation indicate that further studies of the effect of particle size on the solidification of a sample by heterogeneous and by homogeneous nucleation would contribute significantly to the understanding of the process of phase transformations. A separate determination of the particle size distribution in the sample used in these experiments would be of great value in determining the relative importance of the various energy terms in the expression for ΔG^*.

The observation of the progress of the transformation with x-rays, using a proportional counter x-ray detector, is both convenient and accurate and very well suited for this type of study.

APPENDIX I

An estimate of the temperature difference across the face of the sample may be obtained by considering the simple case of one dimensional heat flow. The equation for one dimensional heat flow is

$$\partial T/\partial t = \alpha^2 \partial^2 T/\partial x^2, \tag{1}$$

where $\alpha^2 = k/c\rho$, k the thermal conductivity, c the specific heat and ρ the density of the material. This equation is solved by separating the variables. The solution is

$$T = (\exp(-\alpha^2\beta^2 t))(\sin\beta x + \cos\beta x), \tag{2}$$

where β is a constant. The boundary and initial conditions are: at $t = 0$, $T(x) = T_o$, a constant, and at all times, T at $x = 0$ and $x = l$ is zero. This latter condition rules out the cosine term in Equation (2) and requires that $\beta = n\pi/l$, where n is an integer and l is the length of the sample. To apply the first condition the solution is assumed to be a series,

$$T = \sum_{n=1}^{\infty} a_n(\exp(-\alpha^2\beta^2 t))\sin(n\pi x/l), \tag{3}$$

with

$$a_n = (2/l)\int_0^l T_o \sin(n\pi x/l)dx. \tag{4}$$

Integration of Equation (4) gives the value of $a_n = 0$ for n even, and $a_n = 4T_o/n\pi$ for n odd. The temperature at any point along the bar is then,

$$T = (4/\pi)T_o\{\exp[-(\alpha\pi/l)^2 t]\sin(\pi x/l) + (1/3)\exp[-(3\alpha\pi/l)^2 t]\sin(3\pi x/l) + \ldots\} \quad (5)$$

The temperature at the center of the bar is the lowest, and therefore is of most interest. This is given by

$$T = (4/\pi)T_o\{\exp[-(\alpha\pi/l)^2 t] - (1/3)\exp[-(3\alpha\pi/l)^2 t] + \ldots\} \quad (6)$$

To calculate α we assume that the heat conductivity of the oil-sodium dispersion is negligible compared to the beryllium windows, but that the heat capacity of the sample is the total of the beryllium windows and the dispersion. Table IA shows the heat capacity, heat conductivity and density of sodium, oil and beryllium. Using these values, $\alpha^2 = 0.26$, and for $l = 0.6$ cm, $(\alpha\pi/l)^2 = 7$. At the end of one second the temperature at the center is equal to $10^{-3}\ T_o$. So temperature equilibrium is established instantaneously across the face of the sample.

The temperature difference through the sample may be estimated in a similar manner, if the heat conductivity of the sample is considered to be limited by the oil. Then, $\alpha^2 = 0.0005$ and for $l = 0.05$ cm $(\alpha\pi/l)^2 = 7$. From Equation

Appendix Table IA

Thermal Properties of Sodium, Oil and Beryllium*

	Density	Specific Heat (cal per ^{o}C gm)	Thermal Conductivity (cal per sec cm ^{o}C)
Sodium	0.97	0.296	0.322
Oil	0.92	0.43	0.00035
Beryllium	1.82	0.425	0.385

*Smithell's Metals Reference Book, Interscience, New York (1949).

(5), at the end of one second the temperature in the center of the sample is 10^{-3} T_o. So equilibrium in this direction is reached instantaneously.

When the sample is melting, an effective specific heat may be calculated since the melting occurs over a range of temperatures. From Figure 27, fifty percent of the sample melts over a range of 0.044° C. The effective specific heat is then approximately 720 cal per °C per gm, and $\alpha^2 = 5.7 \times 10^{-6}$. The maximum temperature difference through the sample can now be calculated from Equation (5). At t = 60 seconds the temperature at the center of the sample is $T = 0.67\ T_o$, and at t = 300 seconds, $T = 0.08\ T_o$. So that equilibrium is established much more slowly than when the sample is not melting, but still fast enough so that the temperature lag in the center of the sample is small.

APPENDIX II

A calculation may be made to determine if the sample will completely melt if it has a perfectly sharp melting point, and if the temperature of the sample is at the melting point and the temperature of the container is 0.01° C above this, with no heat entering or leaving the system. This condition is approached in the run described on page 60 and shown in Figure 28.

The weight of copper in the oil bath is calculated to be 1100 gm and the weight of the oil is 138 gm. The specific heat of copper is 0.93 and of the oil is 0.43 cal per $^{\circ}$C per gm, so that the heat capacity of the copper is 100 cal per $^{\circ}$C and of the oil is 60 cal per $^{\circ}$C, a total of 160 cal per $^{\circ}$C.

The weight of sodium in the sample is calculated to be approximately 0.007 gm, and its latent heat of fusion is 31.7 cal per gm. So the heat necessary to completely melt the sample is 0.23 cal. If the temperature of the container is 0.01 $^{\circ}$C above the temperature of the sample which is at its melting point, then there is 1.6 cal of heat available to melt the sample. This is seven times that necessary. It is concluded then, that the entire melting curve represents particle size effects on the melting temperature.

APPENDIX III

The width of the x-ray diffraction line can be used to estimate the size of the scattering particle. Scherrer[1] developed an expression for the particle size as a function of the width of the line, thus,

$$D = (K\lambda/\beta)\cos\theta \qquad (1)$$

where D is the mean size of the crystallites, K, a constant depending on the definition of the width of the line β, and the particle shape, λ is the wavelength and θ the Bragg angle. If β is taken as the angular-width at the points of half-intensity, K is 0.9[2]. For application to x-ray diffraction patterns, the half-width must be corrected for the instrumental broadening of the line. Jones[3] has developed an expression for correcting the observed width of the line for instrumental effects. His results are presented in graphical form, and relate the ratio of true-width to the observed-width for small particles to the ratio of the

[1] Scherrer, P., Göttinger Nochrichten, 2, 98(1918).

[2] Klug, H. P. and Alexander, L. E., X-Ray Diffraction Procedures, p. 512, Wiley, New York(1954).

[3] Jones, F. W., Proc. Roy. Soc., (London), 166A, 16(1938).

observed-width for large particles to the observed-width for small particles. In practice, the unknown sample may be mixed with a sample of a different material of known particle size and the diffraction pattern of both materials taken simultaneously. Thus, the ratio of the widths of the lines of the two materials can be directly determined. The accuracy with which the Scherrer equation can be applied is limited by the success with which β can be deduced from the experimentally observed breadth. The method becomes more accurate as the particle size decreases. Generally the ratio of the measured line-width for large particle size (2 micron) to the measured line-width for the small particle size must be of the order 0.7 or less, before the method becomes accurate. From the observed line-width for the sodium particles, it is calculated that particle sizes less than 200 Å would cause this amount of broadening.

In the experiments described here, there was no noticeable broadening observed in the width of the line as the sample melted or as it solidified. This fact together with the appearance of the sample when observed under a microscope has led to the assumption that 90 percent of the volume of the sample consists of particles with diameters greater than 10^{-5} cm.

BIBLIOGRAPHY

Alexopolus, K. and Euthymion, P., Phil. Mag., 45, 1132(1954).

Avrami, M., J. Chem. Phys., 7, 1103(1939).

Becker, R., Ann. d. Physik, 32, 128(1938).

Becker, R. and Döring, W., Ann. d. Physik, 5-24, 719(1935).

Benedict, M., Rev. Sci. Instr., 8, 252(1937).

Bidwell, C. C., Phys. Rev., 23, 357(1924).

Bidwell, C. C., Phys. Rev., 27, 381(1926).

Born, M., J. Chem. Phys., 7, 591(1939).

Born, M., et al, Proc. Cambridge Phil. Soc., 36, 160, 173, 454, 466(1940).

Born, M., et al, Proc. Cambridge Phil. Soc., 37, 34, 177, (1941).

Born, M., et al, Proc. Cambridge Phil. Soc., 38, 61, 67, 82(1942).

Born, M., et al, Proc. Cambridge Phil. Soc., 39, 101, 104, 113(1943).

Born, M., et al, Proc. Cambridge Phil. Soc., 40, 151(1944).

Brillouin, L., Ann. d. Physik, 17, 88(1922).

Brooks, H., Metal Interfaces, Am. Soc. Metals, Cleveland (1952).

Carpenter, L. G., J. Chem. Phys., 21, 2244(1953).

Carpenter, L. G., Harle, T. F., and Steward, C. J., Nature, 141, 1015(1938).

Carpenter, L. G. and Steward, C. J., Phil. Mag., 27, 551(1939).

Chibula, A., J. Inst. Metals, 80, 1(1951).

Cohen, M., Phase Transformations in Solids, Wiley, New York (1951).

Collenge, J. P., Thesis, M. S., Ohio State University(1949).

Compton, A. H. and Allison, S. K., X-Rays in Theory and Experiment, Van Nostrand, New York(1939).

Darwin, C. G., Phil. Mag., 6-27, 675(1914).

Debye, P., Ann. d. Physik, 39, 789(1912).

Debye, P., Ann. d. Physik, 43, 49(1914).

Eborall, M. D., J. Inst. Metals, 76, 321(1949).

Einstein, A., Ann. d. Physik, 33, 1275(1910).

Faxen, H., Ann. d. Physik, 17, 615(1918).

Faxen, H., Zeit. f. Physik, 17, 266(1923).

Fisher, J. C., Holloman, J. H. and Leschen, J. G., Ind. Eng. Chem., 44, 1324(1952).

Frank, F. C. and Van der Merwe, J. H., Proc. Roy. Soc. (London), 198A, 216(1949).

Glasstone, S., Laidler, K. J. and Eyring, H., The Theory of Rate Processes, McGraw-Hill, New York(1941).

Guinier, A., European Scientific Notes, 6, 295(1952).

Harbury, L., J. Phys. and Colloid Chem., 50, 190(1946).

Herzfeld, K. and Goeppert Mayer, M., Phys. Rev., 46, 995 (1934).

Hinshelwood, C. N. and Hartley, H., Phil. Mag., 6-43, 78 (1922).

Holloman, J. H. and Turnbull, D., Progress in Metal Physics, 4, 333(1953).

Hüttig and Bradkart, Z. Anorg. Chem., 161, 256(1927).

International Tables for the Determination of Crystal Structures, Gebrüder Borntraeger, Berlin(1935).

Jones, F. W., Proc. Roy. Soc., (London), 166A, 16(1938).

Kantrowitz, A., J. Chem. Phys., 19, 1097(1951).

Kirkwood, J. G. and Monroe, E., J. Chem. Phys., 9, 514 (1941).

Kirkwood, J. G. and Buff, F. P., J. Chem. Phys., 17, 338 (1949).

Kirkwood, J. G. and Buff, F. P., J. Chem. Phys., 18, 991 (1950).

Klug, H. P. and Alexander, L. E., X-Ray Diffraction Procedures, New York(1954).

Korff, S. A., Nucleonics, 6, 1(June, 1950).

Korff, S. A., Nucleonics, 7, 46(Nov., 1950).

Korff, S. A., Nucleonics, 8, 38(Jan., 1951).

Kossel, W., Die Molekularen Vorgänge beim Kristallwachstum, Leipzig(1928).

LaMer, V. K., Ind. Eng. Chem., 44, 1269(1952).

Laue, M. v., Ann. d. Physik, 81, 877(1926).

LeMieux, A. F. and Beeman, W. W., Rev. Sci. Instr., 17, 130(1944).

Lennard-Jones, J. E. and Devonshire, A. F., Proc. Roy. Soc. (London), 169A, 317(1939).

Lindemann, F., Physik. Zeit., 11, 609(1910).

Loeb, L. B., Kinetic Theory of Gases, McGraw-Hill, New York (1927).

Mayer, J. E., J. Chem. Phys., 15, 187(1947).

Mellor's Modern Inorganic Chemistry, Longmon's, Green and Co., New York(1939).

Mott, N. F. and Gurney, R. W., Electronic Processes in Ionic Crystals, The Clarendon Press, Oxford(1948).

Pavlov, J., J. Russ. Phys. Chem. Soc., XL, 1022(1908).

Pepinsky, R. and Jermotz, P., Rev. Sci. Instr., 19, 247(1948).

Pound, G. M., Ind. Eng. Chem., 44, 1278(1952).

Pound, G. M. and LaMer, V. K., J. Chem. Phys., 74, 2323 (1952).

Preckshot, G. W. and Brown, G. G., Ind. Eng. Chem., 44, 1314(1952).

Probstein, R. F., J. Chem. Phys., 19, 619(1951).

Raschewsky, N. v., Zeit. f. Physik, 40, 214(1927).

Reiss, H. J., J. Chem. Phys., 20, 1216(1952).

Reynolds, J. A. and Tottle, C. R., J. Inst. Metals, 80, 93(1951).

Rie, E., Zeit. f. Phys. Chem., 104, 354(1923).

Rodebush, W. H., Ind. Eng. Chem., 44, 1289(1952).

Scherrer, P., Göttinger Nochrichten, 2, 98(1918).

Schroedinger, E., Physik. Zeit., 15, 79(1914).

Seitz, F., The Modern Theory of Solids, McGraw-Hill, New York(1940).

Shillaber, C. P., Photomicrography, Wiley, New York(1949).

Smithell's Metals Reference Book, Interscience, New York (1949).

Smoluchowski, M., Ann. d. Physik, 25, 205(1908).

Smoluchowski, R., Phase Transformations in Solids, Wiley, New York(1951).

Smoluchowski, R., Ind. Eng. Chem., 44, 1321(1952).

Structure Reports, Vol. 13, OOSTHOEK-UTRECHT(1950).

Tolman, R. C., J. Chem. Phys., 17, 333(1949).

Turnbull, D., J. Chem. Phys., 18, 198(1950).

Turnbull, D., J. Appl. Phys., 21, 1022(1950).

Turnbull, D., J. Chem. Phys., 20, 411(1952).

Turnbull, D. and Ceck, R. E., J. Appl. Phys., 21, 804 (1950).

Turnbull, D. and Fisher, J. C., J. Chem. Phys., 17, 71 (1949).

Turnbull, D. and Vonnegut, B., Ind. Eng. Chem., 44, 1292 (1952).

Van der Merwe, J. H., Proc. Phys. Soc., 63A, 616(1950).

Volmer, M., Zeit. f. Elektrochem., 35, 555(1929).

Volmer, M. and Flood, H. Z., Zeit. f. Phys. Chem., 170A, 273(1934).

Volmer, M. and Weber, A., Zeit. f. Phys. Chem., 119, 227 (1925).

Vonnegut, B., J. Appl. Phys., 18, 593(1947).

Waller, I., Zeit. f. Physik, 17, 389(1923).

Waller, I., Zeit. f. Physik, 51, 213(1928).

Waller, I., Ann. d. Physik, 79, 261(1926).

Waller, I., Ann. d. Physik, 83, 154(1927).

Wilchinsky, Z. W., Acta Cryst., 4, 1(1951).

Wyckoff, R. W. G., Crystal Structures, Interscience, New York(1951).

Zeldowich, J. B., Acta Physiochim, USSR, 18, 1(1943).

Zener, C. and Jauncey, G. E. M., Phys. Rev., 49, 17(1936).

AUTOBIOGRAPHY

I, Bernard Andrew Kulp, was born in Columbus, Ohio, August 3, 1923. I received my secondary school education at St. Charles High School in Columbus. My undergraduate training was obtained at The Ohio State University and The University of Minnesota, in Minneapolis. I received the degree of Bachelor of Electrical Engineering, with high distinction, in 1946 from the latter university. I received the degree of Master of Science in Physics from The Ohio State University in 1947. From 1947 to 1950, I was employed as Research Engineer at the Carnegie-Illinois Steel Corporation, Chicago, and Battelle Memorial Institute in Columbus. I returned to The Ohio State University in 1950 to continue my studies toward the degree Doctor of Philosophy. I remained at Battelle on a part time basis while completing the requirements for the latter degree.